PanScales parton showers for hadron collisions: formulation and fixed-order studies

Melissa van Beekveld,[a] **Silvia Ferrario Ravasio,**[a] **Gavin P. Salam,**[a,b]
Alba Soto-Ontoso,[c] **Gregory Soyez**[c] **and Rob Verheyen**[d]

[a]*Rudolf Peierls Centre for Theoretical Physics, Clarendon Laboratory,*
Parks Road, University of Oxford, Oxford OX1 3PU, U.K.

[b]*All Souls College,*
Oxford OX1 4AL, U.K.

[c]*Université Paris-Saclay, CNRS, CEA, Institut de physique théorique,*
91191, Gif-sur-Yvette, France

[d]*Department of Physics and Astronomy, University College London,*
London, WC1E 6BT, U.K.

E-mail: mcbeekveld@gmail.com, silvia.ferrario.ravasio@cern.ch,
gavin.salam@physics.ox.ac.uk, alba.soto@ipht.fr,
gregory.soyez@ipht.fr, r.verheyen@ucl.ac.uk

ABSTRACT: We formulate PanScales parton showers for hadron collisions so as to achieve next-to-leading logarithmic (NLL) accuracy across a broad set of observables. We do so specifically for colour singlet production. Relative to the existing PanScales final-state showers, the main new question is that of how to redistribute momentum imbalances from initial-state branching across the remainder of the event. We present tests of the showers at fixed order, including the treatment of full colour for soft-collinear emissions and of spin correlations in both the soft and collinear domains. We also include comparisons to a formulation of a standard dipole shower, the current leading-logarithmic state of the art. A forthcoming companion paper [1] will explore all-order tests of the new showers.

Contents

1 Introduction

One of the major achievements of CERN's Large Hadron Collider (LHC) programme is the remarkable accuracy being achieved across a broad range of measurements. To maximally exploit the potential of the data, it is essential for theoretical predictions to match that high accuracy, notably as concerns the tools that can fully simulate the final state of hadron collisions, i.e. general purpose Monte Carlo (GPMC) event generators. These tools play a crucial role both in the interpretation of measurements and in the extraction of those measurements from the raw experimental data.

Two major components of GPMCs are under control in perturbative Quantum Chromodynamics (QCD): the hard scattering process, and the parton shower, which simulates radiation from the hard scattering scale down to the hadronic scale. Over the past two decades major advances have been made in improving the accuracy of the hard scattering description [2] and its matching to parton showers, both for next-to-leading order (NLO) calculations [3–5] and, more recently, for (N)NNLO computations [6–11]. Alternatively, multi-leg matrix elements can be merged with parton shower simulations up to NLO accuracy [12–25].

Improvement of the accuracy of the hard scattering process is not the only requirement for precision LHC phenomenology. In particular parton showers are crucial for a correct physical description of many of the features of events that are essential in experimental measurements, such as the pattern of energy sharing between particles, or the transverse momentum distribution of colour-singlet objects such as a Drell-Yan (DY) pair or a Higgs boson and correlations with final-state energy flow. Since parton showers span disparate momentum scales, one natural way of viewing their theoretical role is that they should account for perturbative contributions that are enhanced by logarithms of the ratios of those disparate scales.

All dipole-shower algorithms [26–31] available in the commonly-used general purpose Monte Carlo event generators [26, 32–36] reach leading-logarithmic (LL) accuracy, i.e. they are correct in the limit where emissions are strongly ordered both in energy and angle.[1] The focus of this paper is to design a next-to-leading logarithmic (NLL) accurate shower for hadron-hadron collisions, which represents a key milestone in the PanScales programme [42–46] of developing parton showers with controlled logarithmic accuracy. To achieve this, we use the guiding principles introduced in refs. [42, 43] to assess the logarithmic accuracy of a shower. From the PanScales perspective, a shower can be said to be NLL if it satisfies two types of condition:

- Fixed-order: upon characterisation of the phase space of an emissions in terms of its transverse momentum, k_t, and rapidity η, the shower must reproduce the exact

---

[1]Another class of shower is represented by the angular-ordered showers, as used in the `Herwig7` program [33, 34]. They are based on the coherent branching formalism [37], that reproduces full-colour NLL accuracy for double logarithmic global observables [38, 39]. Note that angular ordering is known [40] to lead to an incomplete treatment of the soft single (NLL) logarithms that affect non-global observables [41], though the numerical impact is modest in many circumstances.

matrix element in the limit where every pair of emissions is well separated in at least one of the phase space variables, e.g. k_t or η are strongly ordered across emissions.

- All-orders: the shower must reproduce analytic resummation results for a broad range of observables, including global event shapes, subjet multiplicity and non-global observables.

These principles were used in ref. [43] to design the basic structure for several NLL-accurate dipole final-state parton showers, including tests across a wide range of observables. Full NLL accuracy for these showers (including full-colour (FC) at LL) was subsequently achieved with the addition of soft-collinear subleading colour corrections [44], and of spin correlations [45, 46].

Several other groups have also been investigating the logarithmic accuracy of showers. Refs. [47, 48] showed that a careful treatment of the kinematic map is necessary in angular-ordered showers, for both final and initial state radiation. Ref. [49] introduced a shower algorithm shown analytically to reproduce the NLL results for the e^+e^- thrust distribution and the subjet multiplicity (with soft-collinear subleading colour effects in ref. [50]). Ref. [51] showed that the so-called Λ-ordered (effectively time-ordered) Deductor shower reproduces the NLL thrust distribution in e^+e^- collisions [51].

Almost all of the above work has focused on the accuracy of final-state showers. In this work, we show how to extend and adapt the PanScales showers to include initial-state radiation, concentrating on the case of colour-singlet production, i.e. $q\bar{q} \to Z^0$ and $gg \to H$ at hadron colliders. Aside from the many hadronic observables that have already been tested in the final state, a particularly important observable in hadron-hadron collisions is the transverse momentum of the colour singlet system, whose resummation is well established [52, 53]. The approaches that we develop build on observations both from the PanScales work and from earlier parton-shower work that specifically considered the question of colour-singlet transverse momentum recoil in a shower [29–31, 54].

This paper is organised as follows. In section 2 we provide the basic building blocks for designing a dipole shower in hadronic collisions and give an explicit example of a transverse-momentum ordered shower based on the standard colour dipole approach, which we dub "Dipole-k_t". In section 3 we review the general methodology for performing a fixed-order study of a dipole shower in the limit of interest for NLL accuracy. We show that Dipole-k_t, variants of which are currently available in all the major Monte Carlo event generators, fails to reproduce the correct soft radiation pattern already at the two emissions level. Building on this knowledge, in section 4 we introduce two families of PanScales showers for hadronic collisions, one with a local and another with global recoil schemes. The choice of the ordering variable and the recoil scheme are crucial to satisfy the fixed-order shower requirement. In section 5, we adapt the subleading-colour prescriptions of ref. [44] to address initial-state radiation, and show a number of associated matrix-element tests. The inclusion of spin correlations following refs. [45, 46] is explained in section 6. We conclude in section 7. The appendices contain details on the splitting functions we use (appendix A), the kinematic mappings (appendix B), the analytic expectations for our colour tests (appendix C) and the derivation of the spin branching amplitudes (appendix D). The validation of our ap-

proach at all-orders across many observables and a presentation of the associated all-order testing methodology are to be found in a separate publication [1].
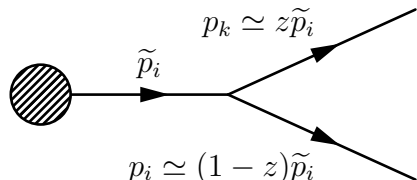
2 Basics of hadron-collision dipole showers

In this section we will highlight common features of dipole showers and formulate a generic standard dipole shower, which will be used as a convenient reference for a LL-accurate shower throughout this work and our companion article [1]. We will concentrate on colour-singlet production in proton-proton collisions, specifically $q\bar{q} \to Z$ and $gg \to H$, with a hadron-hadron centre-of-mass energy $\sqrt{s}$ and a colour-singlet Born four-momentum Q^μ.

2.1 Generic formulation of a hadron-collider shower

Standard dipole showers and the PanScales hadron-collider showers that we develop later in section 4 have a number of characteristics in common. These include the final and initial-state splitting probabilities, as well as the generic structure of recoil for emission of a parton from a dipole. In this work, all partons are considered to be massless and we will often refer to the colour singlet as the "hard system".

First, we consider a final-state parent parton $\tilde{\imath}$ that radiates a collinear emission k. The post-branching momentum of the parent is denoted by i. The phase-space of the emission k is parameterised by its transverse momentum $k_\perp$, its longitudinal momentum fraction z (relative to the pre-branching parent) and its azimuthal angle φ. In the collinear limit $(\theta_{ik} \ll 1)$, the differential branching probability then reads
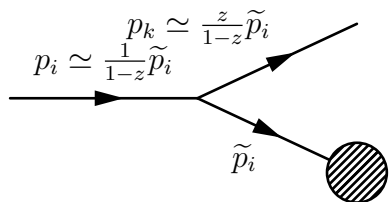

$$\to \quad \mathrm{d}\mathcal{P}^{\mathrm{FS}}_{\tilde{\imath} \to ik} = \frac{\alpha_s(k_\perp^2)}{2\pi} \frac{\mathrm{d}k_\perp^2}{k_\perp^2} \frac{\mathrm{d}z}{z} \frac{\mathrm{d}\varphi}{2\pi} N^{\mathrm{sym}}_{ik} [z P_{\tilde{\imath} \to ik}(z)],$$

(2.1)

with α_s the strong coupling and N^{sym}_{ik} a symmetry factor that is equal to $1/2$ for $g \to gg$ splittings, and 1 otherwise. We use symbols with a tilde to indicate pre-branching partons and their momenta, and symbols without any decoration to indicate post-branching partons. The DGLAP splitting functions $P_{\tilde{\imath} \to ik}$ are provided in appendix A. A well-known feature of eq. (2.1) is its singular behaviour in the soft $(z \to 0)$ collinear limit for flavour-conserving emissions (i.e. $P_{g \to gg}$ and $P_{q \to qg}$), and in the hard $(z \sim 1)$ collinear limit for every type of emission. The soft and collinear singularities compensate the smallness of α_s in the corresponding regions of phase space, resulting in the large logarithms that the shower resums.

In hadronic collisions, final-state radiation is to be supplemented with emissions from the incoming partons. Over three decades ago, it was realised that a backwards evolution from the hard scale Q^2 down to the hadronic scale $(\mathcal{O}(1)\,\mathrm{GeV})$ provides an efficient way of

simulating such initial-state radiation [55]. Defining z as the longitudinal momentum fraction carried by the emission relative to the post-branching incoming parton, the differential collinear branching probability is given by

$$\rightarrow \quad \mathrm{d}\mathcal{P}^{\mathrm{IS}}_{i \to \tilde{\imath}k} = \frac{\alpha_s(k_\perp^2)}{2\pi} \frac{\mathrm{d}k_\perp^2}{k_\perp^2} \frac{\mathrm{d}z}{z} \frac{d\varphi}{2\pi} z P_{i \to \tilde{\imath}k}(z) \frac{x_i f_i(x_i, k_\perp^2)}{\tilde{x}_i f_{\tilde{\imath}}(\tilde{x}_i, k_\perp^2)}.$$

(2.2)

The main difference with respect to eq. (2.1) is the additional presence of a ratio of parton distribution functions (PDFs) $f_i(x_i, k_\perp^2)$, denoting the density per unit momentum fraction of partons of flavour i, carrying a momentum fraction x_i inside a proton, at a factorisation scale $k_\perp$. Its inclusion follows directly from the DGLAP evolution equation with evolution variable $k_\perp^2$, and accounts for the change in the hadronic momentum fraction from $\tilde{x}_i$ to $x_i \equiv \tilde{x}_i/(1-z)$.

The branching probabilities given by eqs. (2.1) and (2.2) describe $1 \to 2$ collinear branchings. In this paper we will work with dipole showers in which the fundamental building block is instead a $2 \to 3$ branching kernel [56]. In the limit where the number of colours (N_{C}) is large, dipole showers make it straightforward to reproduce the matrix element for an arbitrary number of emissions in the soft wide-angle limit, and to achieve the associated resummation of non-global logarithms. In dipole showers, the particle that branches, $\tilde{\imath}$, is associated with a colour-connected spectator $\tilde{\jmath}$, such that the branching is $\tilde{\imath}\tilde{\jmath} \to ijk$, where i and j are the post-branching counterparts of $\tilde{\imath}$ and $\tilde{\jmath}$ respectively, and k is the radiated parton. Each of the dipole legs can be either an initial (I) or a final (F) state particle. As such, four types of dipoles exist: II, IF, FI and FF. By symmetrising eqs. (2.1) and (2.2) we obtain a generic dipole differential splitting probability[2]

$$\mathrm{d}\mathcal{P}_{\tilde{\imath}\tilde{\jmath} \to ijk} = \frac{\alpha_s(\mu_{\mathrm{R}}^2)}{2\pi} \left(1 + \frac{\alpha_s(\mu_{\mathrm{R}}^2)K}{2\pi}\right) \frac{\mathrm{d}v^2}{v^2} \mathrm{d}\bar{\eta} \frac{\mathrm{d}\varphi}{2\pi} \times$$
$$\times \frac{x_i f_i(x_i, \mu_{\mathrm{F}}^2)}{\tilde{x}_i f_{\tilde{\imath}}(\tilde{x}_i, \mu_{\mathrm{F}}^2)} \frac{x_j f_j(x_j, \mu_{\mathrm{F}}^2)}{\tilde{x}_j f_{\tilde{\jmath}}(\tilde{x}_j, \mu_{\mathrm{F}}^2)} \left[g(\bar{\eta}) z_i P_{ik}^{\mathrm{IS/FS}}(z_i) + g(-\bar{\eta}) z_j P_{jk}^{\mathrm{IS/FS}}(z_j)\right].$$

(2.3)

We will consider two standard approaches to generating the kinematics associated with the branching: so-called "dipole" showers and "antenna" showers. In the former, the two terms in square brackets are associated with distinct kinematic maps. In the latter one uses a common kinematic map for both terms.[3] The phase-space has been transformed to

---

[2]This specific form of the branching probability is not unique. Non-singular terms may be added, and the assignment of the soft singularity to different dipole ends (achieved by $g(\bar{\eta})$) may be accomplished in various ways.

[3]Eq. (2.3) suggests a natural way of assigning branching to one end or other of the dipole. In antenna showers, while this division does not affect the kinematics of the branching, it can affect the subsequent choice of splitting channel and associated spin correlations, e.g. concerning the choice of $g \to gg$ v. $g \to q\bar{q}$,

two specific shower variables: an evolution scale v and a pseudo-rapidity-like variable $\bar{\eta}$.[4] The exact relation between $(v, \bar{\eta})$ and $(z, k_\perp)$ is shower-dependent, and we thus postpone its discussion. However, in this work the following relation is always satisfied

$$\frac{\mathrm{d}k_\perp^2}{k_\perp^2} \frac{\mathrm{d}z}{z} = \frac{\mathrm{d}v^2}{v^2} \times \begin{cases} \mathrm{d}\bar{\eta} & \text{(final state)}, \\ (1-z)\ \mathrm{d}\bar{\eta} & \text{(initial state)}, \end{cases} \tag{2.4}$$

such that we can use the compact notation

$$P_{ik}^{\mathrm{IS}}(z) = (1-z)P_{i \to \tilde{i}k}(z), \qquad P_{ik}^{\mathrm{FS}}(z) = P_{i \to ik}(z), \tag{2.5}$$

for initial-state (IS) and final-state (FS) splittings, respectively. As in eq. (2.2), a PDF ratio for each of the dipole legs enters as a multiplicative factor. For final-state branchings the x and $\tilde{x}$ values are either identically equal, or very close to each other, so the ratio tends to one. There is limited freedom in choosing the factorisation and renormalisation scales, μ_{F} and μ_{R}. For a hard-collinear initial-state branching, μ_{F} should be commensurate with the emission transverse momentum. As concerns the evaluation of the coupling, the requirement of achieving NLL accuracy brings several constraints, notably for soft-collinear emissions: the running of the coupling should be performed at two loops or higher, and with μ_{R} chosen to coincide with the emission transverse momentum, the soft-collinear gluon emission probability must include an $\alpha_s K/(2\pi)$ correction term with $K = (67/18 - \pi^2/6)C_A - 5n_f/9$. As usual we have $C_A = 3$, $T_R = 1/2$ and we will work with $n_f = 5$ light flavours. Finally, the function $g(\bar{\eta})$ partitions the soft singularity among the two contributions of the dipole, avoiding any double counting. This function, which we will specify below, needs to satisfy three main requisites: (i) $0 \leq g(\bar{\eta}) \leq 1$, (ii) $g(\bar{\eta}) + g(-\bar{\eta}) = 1$ and (iii) $g(\bar{\eta}) = 0$ (1) for very negative (positive) $\bar{\eta}$.

Every time an emission is generated according to eq. (2.3), momentum conservation has to be restored through a choice of a suitable recoil scheme. We will explore two classes of shower, one where the kinematic map conserves momentum locally within the dipole that is branching and another that performs an overall global momentum-conservation procedure. Both share the feature that the emission's momentum p_k may be Sudakov-decomposed in terms of the parent dipole momenta $(\tilde{p}_i, \tilde{p}_j)$ and a transverse component:

$$p_k^\mu = a_k \tilde{p}_i^\mu + b_k \tilde{p}_j^\mu + k_\perp^\mu, \tag{2.6}$$

Within a given shower, the a_k, b_k and $|k_\perp|$ magnitudes are fixed by the value of the shower ordering variable (which may, for example, directly set the value of $|k_\perp|$), by a

which in the context, say, of a gq dipole might occur only at one end. In the implementations of antenna showers used here and in our companion work [1], the division is slightly different in a region where one of the z_i or z_j is not soft and additionally $g(\bar{\eta})$ differs substantially from 0 or 1. This region affects logarithmic accuracy only for terms that are beyond NLL, and will be re-examined in future work when considering higher logarithmic accuracy.

[4]Note that we use the notation $\bar{\eta}, k_\perp$ to denote shower variables, whereas η and k_t are reserved to denote the physical pseudorapidity and transverse momentum measured with respect to the incoming hadron beams.

longitudinal variable (i.e. $\bar{\eta}$ in eq. (2.3)) and by requiring eq. (2.6) to be on the mass shell, $|k_\perp|^2 = 2a_k b_k \, \tilde{p}_i \cdot \tilde{p}_j \equiv a_k b_k \tilde{s}_{ij}$, where $\tilde{s}_{ij}$ is the dipole mass. The direction of the transverse component is given by

$$k_\perp^\mu = |k_\perp|(\hat{n}_1^\mu \sin \varphi + \hat{n}_2^\mu \cos \varphi), \tag{2.7}$$

where $\hat{n}_{1,2}^2 = -1$, $\hat{n}_1 \cdot \hat{n}_2 = 0$ and $\hat{n}_{1,2} \cdot \tilde{p}_{i,j} = 0$.

Local recoil schemes. The momentum map is generically given by

$$\bar{p}_i^\mu = a_i \tilde{p}_i^\mu + b_i \tilde{p}_j^\mu \pm f k_\perp^\mu \tag{2.8a}$$

$$\bar{p}_j^\mu = a_j \tilde{p}_i^\mu + b_j \tilde{p}_j^\mu \pm (1 - f) k_\perp^\mu \tag{2.8b}$$

$$\bar{p}_k^\mu = a_k \tilde{p}_i^\mu + b_k \tilde{p}_j^\mu + k_\perp^\mu \,, \tag{2.8c}$$

where for each of i and j we use a plus (minus) sign for the transverse component if that particle is in the initial (final) state. The coefficients $(a_{i,j}, b_{i,j})$ can be determined as a function of a_k and b_k by imposing longitudinal momentum conservation plus on-shell conditions.

The function f in eq. (2.8) determines how transverse recoil is shared between the two parent legs of the dipole. In the case of dipole showers, one assigns a dedicated "emitter" and "spectator" parton, corresponding to setting $f = 1(0)$ if $p_i(_j)$ is the emitter. The $g(\bar{\eta})$ function in eq. (2.3) determines the relative weight for one end or other of the dipole to be the emitter. Following ref. [43] we take

$$g(\bar{\eta}) = g^{\text{dip.}}(\bar{\eta}) \equiv \begin{cases} 0 & \text{if } \eta < -1 \\ \frac{15}{16}\left(\frac{\bar{\eta}^5}{5} - \frac{2\bar{\eta}^3}{3} + \bar{\eta} + \frac{8}{15}\right) & \text{if } -1 < \bar{\eta} < 1 \\ 1 & \text{if } \bar{\eta} > 1. \end{cases} \tag{2.9}$$

Conversely, antenna showers do not identify a dedicated emitter and spectator (i.e. $f \neq 1, 0$ in general). Instead, they use a smooth function for f, so as to assign an $\bar{\eta}$-dependent fraction of the transverse momentum to each of the dipole legs. We choose to make the function for f coincide with the $g(\bar{\eta})$ that we use in eq. (2.3), and set both of them as follows:

$$f(\bar{\eta}) = g(\bar{\eta}) = g^{\text{ant.}}(\bar{\eta}) \equiv \frac{e^{\bar{\eta}}}{e^{\bar{\eta}} + e^{-\bar{\eta}}} = \frac{e^{2\bar{\eta}}}{e^{2\bar{\eta}} + 1}. \tag{2.10}$$

For the splitting of a final-final dipole, the above equations are sufficient and we write the ultimate post-branching momenta as $p_{i,j,k} = \bar{p}_{i,j,k}$. When one or other of the pre-branching momenta is in the initial state, the resulting $\bar{p}$ will no longer be aligned with the beam axis. Therefore, one needs a Lorentz transformation, $\Lambda^{\mu\nu}$, to realign it after the splitting. This transformation consists of a boost and a rotation, but is an under-constrained system, whose precise form we will discuss later on. It is applied to all particles in the event:

$$p_a^\mu = \Lambda^{\mu\nu} \bar{p}_{\nu,a} \quad \forall a \in i, j, k, \qquad p_a^\mu = \Lambda^{\mu\nu} \tilde{p}_{\nu,a} \quad \forall a \notin i, j, k. \tag{2.11}$$

Global recoil schemes. We explore also global recoil schemes in which the transverse-momentum imbalance is shared among a subset of the particles in the event. The global kinematic map for the particles in the dipole reads

$$\bar{p}_i^\mu = a_i \tilde{p}_i^\mu \,, \tag{2.12a}$$

$$\bar{p}_j^\mu = b_j \tilde{p}_j^\mu \,, \tag{2.12b}$$

$$\bar{p}_k^\mu = a_k \tilde{p}_i^\mu + b_k \tilde{p}_j^\mu + k_\perp^\mu \,. \tag{2.12c}$$

The details of which event particles' momenta are subsequently modified to achieve overall momentum conservation are shower specific.

Recall that we distinguish $k_\perp$, a transverse momentum used in the mapping and defined relative to the parent dipole, and k_t, a transverse momentum defined with respect to the beam directions. In general, the two do not coincide. Furthermore, across both local and global recoil prescriptions, the boosts and rotations that we perform to realign initial-state particles and achieve global momentum conservation may alter the transverse momentum (k_t) of the emission relative to the beam directions.

To sum up this section, designing a dipole shower for hadronic collisions involves: (i) the definition of a branching kernel, see eq. (2.3), (ii) a choice of ordering variable v, (iii) a prescription on how to partition the dipole, i.e. the definition of $\bar{\eta}$ in eqs. (2.3) and (2.9), and (iv) a recoil scheme, see eqs. (2.8), (2.12). The choices made for each of the four ingredients affect the logarithmic accuracy of the shower, as was shown in refs. [42] for final-state showers.

2.2 A standard transverse-momentum-ordered dipole shower

To provide a reference for our discussions of logarithmic accuracy, it is useful to introduce two concrete realisations of "standard" dipole showers for hadronic collisions, which we generically call "Dipole-k_t". All modern dipole showers are based on the pioneering ideas set out in refs. [56, 57]. The specific shower that we use takes the ordering variable and kinematic maps of the Dire-v1 shower [30] and partitions the two halves of the dipole according to eq. (2.3), with the midpoint between the two halves, $\bar{\eta} \equiv \bar{\eta}_{\text{dip}} = 0$, corresponding to zero rapidity in the dipole centre of mass frame. The resulting shower shares substantial similarities with the showers available in all major Monte Carlo event generators, such as Pythia [31, 58],[5] Sherpa [28] and Herwig [29]. It is also expected to give similar logarithmic structure to the Vincia shower [61, 62], even though the latter is antenna rather than dipole based.

All details of the shower are given in appendix B.1 and here we limit ourselves to outlining its main physical features. Its ordering variable v is transverse-momentum-like.

---

[5] Additional issues related to colour coherence have recently been raised regarding the standard Pythia shower [31, 59, 60] in the context of deep-inelastic scattering and vector-boson fusion, in its default option with global recoil for the space-like (initial-state) shower. While we do not explore this question here, it would deserve further study so as to understand whether it has implications for logarithmic accuracy more generally, especially as colour coherence issues can in some cases induce problems for leading logarithmic terms.

It is convenient to relate the longitudinal shower variable $\bar{\eta}_{\mathrm{dip}}$ used in eq. (2.3) to a collinear momentum fraction z carried by the emission p_k, defined relative to the pre-branching momentum, $\tilde{p}_i$, in the final-state case and the post-branching momentum, p_i, in the initial-state case. The relation reads

$$\bar{\eta} \equiv \bar{\eta}_{\mathrm{dip}} = \begin{cases} \frac{1}{2}\ln\frac{z^2\,\tilde{s}_{ij}}{v^2} & \text{(final state)}, \\ \frac{1}{2}\ln\frac{z^2\tilde{s}_{ij}}{(1-z)^2v^2} & \text{(initial state)}. \end{cases} \tag{2.13}$$

This makes it manifest that eq. (2.9) partitions the dipole in its rest frame, a property common to all widely-used dipole showers, and whose adverse consequences are expanded upon below.

The kinematic maps depend on the dipole type. In case both dipole constituents are in the final state (FF), we use a local recoil scheme, following the kinematic map given by eq. (2.8) with $f = 1$. This choice implies that all the other particles in the event, including the colour singlet, are not modified.

For an initial-initial (II) dipole, we use a global recoil scheme followed by a Lorentz transformation. The recoil scheme is as given by eq. (2.12) with $b_j = 1$, i.e. the spectator momentum is preserved. All other final-state particles (excluding p_k), are then boosted to achieve momentum conservation. Due to this boost, the transverse momentum of the colour singlet is modified. Several choices are possible as concerns the longitudinal component of the boost. A common prescription, which we adopt for our Dipole-k_t shower, is to preserve the longitudinal momentum fraction of the spectator parton, following the same logic as the use of $b_j = 1$ in eq. (2.12). Other options are, for example: (i) preserving the rapidity of the colour singlet, or (ii) preserving the longitudinal momentum of the colour singlet. We believe the specific choice is immaterial in terms of logarithmic accuracy, at least up to and including NLL, because the difference between them vanishes in the limit where the branching transverse momentum is small.

In the initial-final (IF) case two main options have been used in the literature. The simplest choice is a fully local map like eq. (2.8) with $f = 0$, i.e. transverse recoil is always assigned to the final-state dipole end. Taking $pp \to Z$ as an example, this has the consequence that after emission of a first gluon, no further transverse recoil is taken by the Z-boson. It was appreciated some time ago [29, 54] that this is unphysical (for example it is not expected to reproduce the structure of the Parisi-Petronzio Drell-Yan p_t resummation [52]). Still, such an option is available (or even default) in various public showers, and it is useful to include such an option in our studies. We refer to it as **"Dipole-k_t (local)"**.

Additionally, various authors have explored the possibility of a global map for IF dipoles [29, 30]. We therefore include such a shower in our studies here, named **"Dipole-k_t (global)"**. It is identical to the local variant with the exception of the IF kinematic map, which is given by

$$\begin{aligned} \bar{p}_i^\mu &= a_i\tilde{p}_i^\mu + b_i\tilde{p}_j^\mu + k_\perp^\mu \\ \bar{p}_j^\mu &= b_j\tilde{p}_j^\mu \\ \bar{p}_k^\mu &= a_k\tilde{p}_i^\mu + b_k\tilde{p}_j^\mu + k_\perp^\mu \,. \end{aligned} \tag{2.14}$$

Note that this global map differs from the generic one given by eq. (2.12) since the initial-state leg acquires a $k_\perp$ component. Momentum conservation is then achieved by performing a boost and a rotation on the entire event. The longitudinal degree of freedom of the boost is constrained by imposing that the momentum of the other incoming parton that does not participate in the splitting is unchanged. This Lorentz transformation is provided in appendix B.1. Lastly, the FI mapping follows a local recoil scheme as in eq. (2.8) with $f = 1$.

3 Methodology for fixed-order tests

Eq. (2.3) provides the correct singular limit for a single emission. Within the context of our NLL shower requirements, however, we require a shower to be able to reproduce the squared matrix element for producing multiple emissions whenever each emission is well-separated from all others in a Lund diagram [63]. Specifically, for a separation by some increasing distance d (e.g. the sum of the rapidity and of the $\ln k_t$ separations), we expect deviations from the true matrix element to vanish as a power of $e^{-|d|}$. One of the crucial characteristics of the full matrix elements is that when there is a large separation in rapidity between multiple soft-collinear emissions, all emitted from the Born partons, the squared matrix element and phase space for n emissions can be written as a product of n independent emission factors, schematically

$$ d\mathcal{P}_{\text{Born}+n} = d\mathcal{P}_{\text{Born}} \times \frac{1}{n!} \prod_{j=1}^{n} \frac{2C\alpha_s}{\pi} \frac{dk_{tj}}{k_{tj}} \frac{d\phi_j}{2\pi} d\eta_j \,. \tag{3.1} $$

Most showers effectively implement that structure of the matrix elements, generating momenta one at a time. As was observed in ref. [42], such a procedure only reproduces the matrix element of eq. (3.1) if each emission leaves all prior emissions' kinematics unchanged. To understand this requirement, consider the following sequence of steps. Firstly, emission 1 is generated with a certain momentum $\tilde{k}_1$ using a matrix element corresponding to that $\tilde{k}_1$. Then as a second step particle 2 is emitted, taking significant recoil from particle 1 such that the new momentum for particle 1, k_1, differs substantially from $\tilde{k}_1$. The result will be a configuration where the first emission has momentum k_1, but generated with a matrix element corresponding to $\tilde{k}_1$, i.e. that does not match the final kinematics. When this phenomenon occurs over a logarithmically enhanced region, it results in a failure to reproduce certain classes of NLL terms. This type of analysis leads to the PanScales condition that in order for a shower to correctly reproduce the matrix element, a given emission that is well separated (e.g. in rapidity) from other prior emissions should not alter the kinematics of those prior emissions. It is mainly this condition that we will be testing here and in section 4.

To verify this PanScales condition, it is useful to represent emission phase space on the Lund plane, i.e. in terms of the rapidity η and transverse momentum k_t of the emission, as shown in figure 1. Recall that η and k_t (as used in figure 1) are always defined with respect to the beam directions, while $\bar\eta$ and $k_\perp$ as used in eq. (2.3) and in the various kinematic maps are defined with respect to the dipole that is branching. Here, for illustration, we
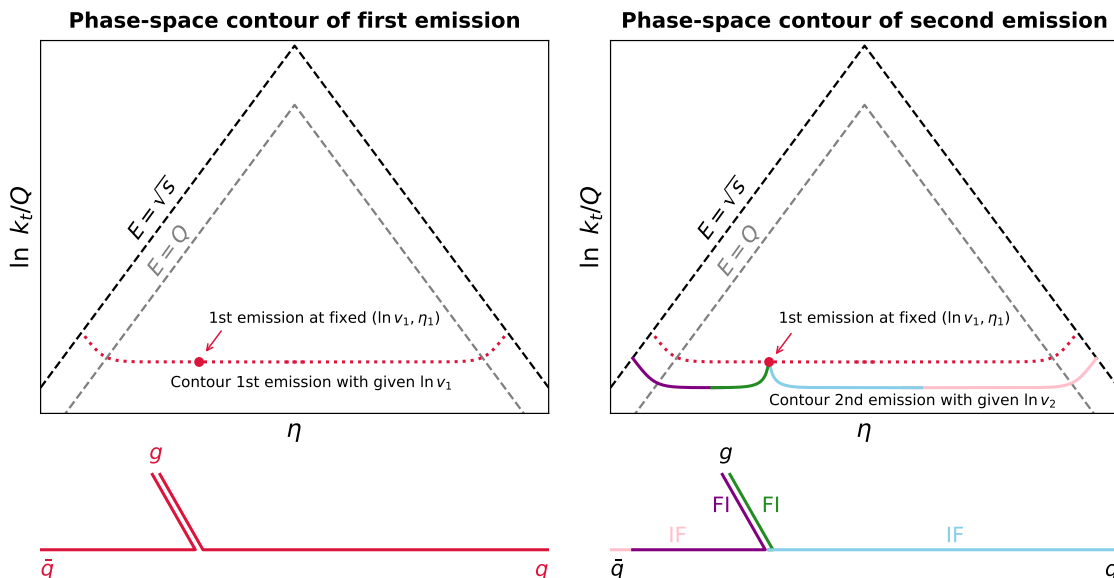
Figure 1. Illustration of the hadron-collider primary Lund plane, where the rapidity and transverse-momentum coordinates are defined with respect to the hadron beam directions. The left-hand plot shows the contour for the first emission from a Dipole-k_t shower for a fixed value v_1 of the ordering variable (local and global are identical here). The red point indicates the specific value of η_1 that is used in subsequent plots when adding a second emission. The right-hand plot additionally shows the contour for such a second emission at a fixed value of $v_2 < v_1$. The contour is colour-coded to roughly represent the partitioning of the two dipoles into IF and FI regions, as illustrated also below the plot. Note that the momentum of the second emission is shown as projected onto the primary Lund plane, to avoid having to represent the 3-dimensional secondary Lund plane. See text for further details.

choose the Dipole-k_t shower of section 2.2, which evolves following horizontal contours in the bulk of the Lund plane. We consider the process $q\bar{q} \to Z$, where Q is the Z-boson mass, $y_Z = 0$ is its rapidity and the proton-proton centre-of-mass energy is denoted by $\sqrt{s}$. The dashed black line illustrates the phase space boundary corresponding to the radiated parton having energy $\sqrt{s}$, while the grey one delineates an inner Lund plane where the maximum energy of the radiated parton is Q (the grey and black boundaries would coincide in the e^+e^- case). Had we chosen $y_Z \neq 0$, this would have led to a relative shift of the two planes. The phase space in between the two Lund planes corresponds to region where the PDF factors in eq. (2.2) can play a significant role in the branching probabilities.[6]

For our tests, we generate a first gluon emission from the (II) $q\bar{q}$ dipole at a fixed value of the evolution variable $\ln v_1$. Scanning over η_1 yields the dotted red contour shown in figure 1 left. Given an emitted momentum fraction z (relative to the post-branching

---

[6]When $\sqrt{s} \gg Q$, there can be additional logarithmic enhancements associated with so-called "small-x" terms $\alpha_s^n \ln^m s/Q^2$ for both t-channel gluon [64, 65] (BFKL) and quark [66] exchange. The inclusion of such terms in the context of a parton shower is a theoretically interesting question that has been explored by the CASCADE [67, 68] and HEJ [69–71] groups, but we do not consider these terms in our work here.

incoming momentum), the transverse momentum of the emission is given by

$$|k_{t,1}| = \frac{v_1}{\sqrt{1-z}} + \mathcal{O}\left(v_1^2/\sqrt{s_{ij}}\right) .\tag{3.2}$$

When the emission is soft $z \ll 1$, this means that the emitted transverse momentum coincides with v, while in the hard collinear regions the emitted transverse momentum curve bends upwards.

Going forwards, to keep the discussion relatively simple, we constrain the kinematics of the first emission, by fixing its rapidity to be in the soft-collinear region (here, $\eta_1 = -10$), as illustrated by the red dot. Note that we have also carried out tests with large-angle soft and hard-collinear choices for η_1, and we will highlight any relevant issues as they occur.

Next (figure 1 right), we consider a second gluon being emitted from either of the $\bar{q}g$ or qg dipoles at a commensurate scale, i.e. $\ln v_2 = \ln v_1 - \delta \ln v$, with $\delta \ln v$ a number of order 1. For a fixed value of the shower evolution variable $\ln v_2$, we show the emission contour, scanning over η_2. We choose a specific value of φ_2 such that the second emission is in the same plane as the first emission, and that it points in the same direction when far away in rapidity, though the issues that we will see below are relevant for essentially all values of φ_2. The 2nd-emission contour in figure 1 follows the shape of the 1st-emission contour except at rapidities close to the first emission, where the upwards bending reflects the fact that it takes momentum from that 1st emission. The fact that elsewhere the 2nd emission contours runs parallel to the first, at a distance of order $\delta \ln v$, ensures that the shower properly fills the double-logarithmic phase space. The contour is colour-coded to reflect the specific part (IF or FI) of the given dipole from which the 2nd emission is dominantly emitted, reflecting the use of the $g(\bar{\eta}_{\mathrm{dip}})$ function in eq. (2.3) to partition the dipole and the specific definition of $\bar{\eta}_{\mathrm{dip}}$ in eq. (2.13) for the Dipole-k_t showers.

Next we turn to figure 2, concentrating first on the left-hand plot, which is for the variant of Dipole-k_t with dipole-local recoil in IF dipoles. The upper panel is a zoomed-in version of figure 1 (right), but now showing contours for two different values of $\ln v_2$. The colour coding has changed and the intensity of the colour reflects the emission probability. The vanishing of the parton distribution function at large x causes the contours to fade in the hard collinear regions (the specific details of the PDF are not critical here).

The middle panel shows the logarithmic change in the first emission's momentum, which we write as $\ln k_{t,1}/\tilde{k}_{t,1}$. Recall our discussion at the beginning of this subsection where we emphasised that when the second emission is well separated in rapidity from the first (i.e. everywhere except the grey-shaded region), the first emission momentum should not change, otherwise we break the independent-emission picture of eq. (3.1). This condition is clearly violated in figure 2 (left). The reason is that $\vec{\tilde{k}}_{t,1}$ becomes $\vec{k}_{t,1} = \vec{\tilde{k}}_{t,1} - \vec{k}_{t,2}$ after the branching, as can be deduced from the kinematic map in eq. (2.8). This is worse than the analogous situation for final-state showers discussed in ref. [42], because the transverse-momentum recoil is *always* taken from the previous emission, rather than just half of the time.

In the case of initial-state branching, an alternative way of visualising the issue is given in the bottom panel, which shows the logarithmic deviation of the Z-boson transverse
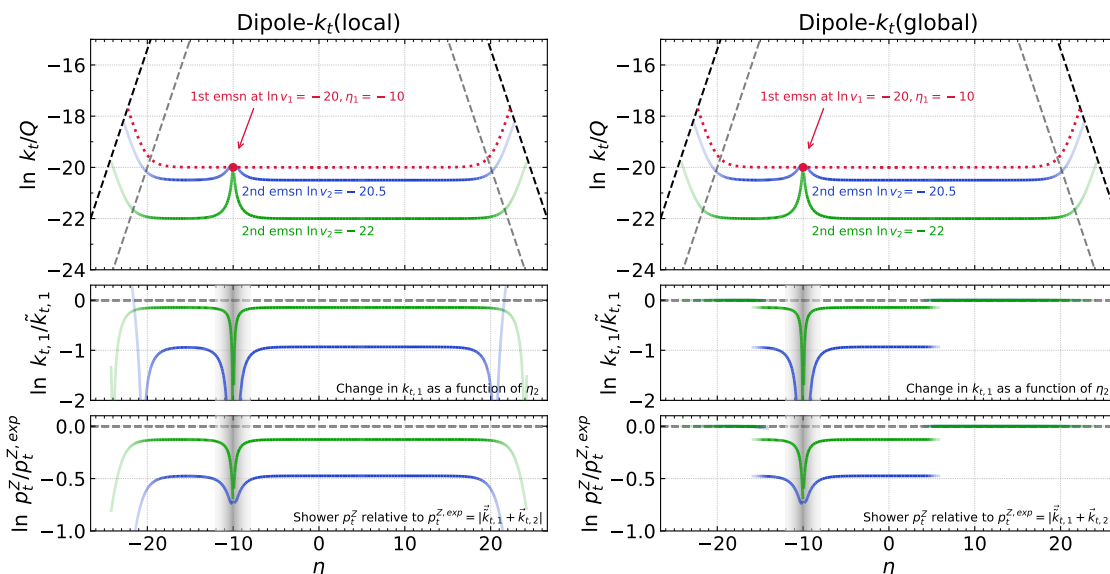
Figure 2. Double-emission contours for *Dipole-k_t (local)* (left) and *Dipole-k_t (global)* (right). The phase-space contours are shown as a function of $\ln k_t/Q$ and η. A red dot indicates the kinematics of the first emission which has $\eta_1 \approx -10$ and $\ln v_1/Q = -20$ (in the plot labels, values of v_i are always expressed in units of Q). For illustrative purposes, the contour of the first emission is shown with a red dotted line, whereas that of the second emission at $\ln v_2/Q = -20.5$ ($\ln v_2/Q = -22$) is drawn as a blue (green) solid line. The colour shading of the lines indicates the branching probability. In the middle panels we show the logarithm of the ratio between the transverse momentum of the first emission before ($k_{t,1}$) and after the second emission took place ($k'_{t,1}$), which is expected to be zero (dashed line) except when the two emissions are close in rapidity (shaded vertical band). The bottom panels show the ratio of the observed to the expected Z transverse momentum (where again, the expectation is valid when the two emissions are well separated in rapidity, i.e. well outside the grey vertical band).

momentum from the expectation $\vec{p}_t^Z = -\vec{\tilde{k}}_{t,1} - \vec{k}_{t,2}$. There is no location in rapidity where $k_{t,1}$ or the Z transverse momentum agrees with the physical expectation (which, again, is fundamental to obtaining NLL accuracy). Note that the NLL impact at $\alpha_s^2 L^2$ ($L = \ln m_Z/p_t^Z$, $Q \equiv m_Z$) is zero, owing to azimuthal averaging, as was found for the vector p_t sum in the final-state case, table 1 of ref. [42]. That same analysis identified a non-vanishing discrepancy from order $\alpha_s^3 L^3$ onwards. A further point to note is that in the Dipole-k_t (local) shower, the Z transverse momentum is always given by the transverse momentum of the first emission at the moment of its creation. This means that the mechanism for obtaining low Z transverse momenta identified long ago by Parisi and Petronzio [52], i.e. the vector cancellation between the momenta of subsequent emissions, is missing with local IF recoil. We will further explore the consequences of this in our companion paper [1].[7]

The right-hand plot shows analogous results for the Dipole-k_t shower in its variant where IF dipoles use global recoil. The main difference is that the unphysical shift in

---

[7]For gluon-fusion Higgs production, which involves two II dipoles, there can be independent emission from each of the II dipoles, and so the vector cancellation can still occur.

$\ln k_{t,1}$ and in $\ln p_t^Z$ is restricted to the rapidity region

$$\frac{1}{2}\left(\eta_1 + \ln\frac{k_{t,1}}{Q}\right) < \eta_2 < \frac{1}{2}\left(\eta_1 - \ln\frac{k_{t,1}}{Q}\right),\tag{3.3}$$

reflecting the fact that, inside this region, dipole-local recoil is used, while outside the region event-wide recoil is used (which implies that the transverse recoil is mainly assigned to the Z boson). Note that the rapidity extent, eq. (3.3), $\sim \ln Q/k_{t,1}$, of the region in which transverse recoil is incorrectly assigned is the same as for the pure final-state dipole showers discussed in ref. [42]. This suggests that the deviations from NLL accuracy will be the same as for those final-state showers. Concerning the vector cancellation of recoil for the Z transverse momentum, this can now occur in at least some of the phase space.

Overall, we have shown that the generic transverse-momentum ordered dipole showers of section 2.2 do not pass the fixed-order requirements needed to achieve NLL accuracy. In the next section, we propose a new family of showers that solve the observed issues.

4 The PanScales showers

As we have seen, the issues discussed in section 3 are qualitatively the same as those identified in final-state dipole showers in ref. [42]. As such it is natural to explore solutions similar to the PanScales e^+e^- showers of ref. [43]. There are, however certain important differences in initial-state showers. One concerns the choice of the conserved quantity during the shower: in the e^+e^- context it was essential to preserve the partonic centre of mass momentum; in contrast, an initial-state emission must induce a transverse recoil in the hard-system momentum in order to be consistent with momentum conservation (and, for multiple initial-state emissions, with Parisi-Petronzio resummation for the hard-system transverse momentum [52]). Another difference relates to the fact that with incoming beams an emission can be significantly more energetic than any of the pre-existing partons in the event. We will address these issues below, as they arise.

4.1 Aspects common to all showers

The PanScales showers need a reference momentum Q^μ, which defines a centre-of-mass frame. We set it equal to the four-momentum (p_x, p_y, p_z, E) of the hard system prior to showering,

$$Q^\mu = m_X(0, 0, \sinh y_X, \cosh y_X),\tag{4.1}$$

where X is a colour-singlet hard system (for example a Z or a Higgs boson), y_X is the hard-system rapidity, and $m_X^2 \equiv Q^2 = (\tilde{p}_a + \tilde{p}_b)^2$, where $(\tilde{p}_a, \tilde{p}_b)$ are the initial four-momenta of the incoming partons. We will make the choice to keep Q^μ fixed during the shower evolution, even as the momentum of the hard system evolves, for example by acquiring a transverse momentum recoil.[8] As in the final-state PanScales showers, we will consider a family of ordering variables parametrised by a variable $0 \leq \beta_{\mathrm{PS}} < 1$. Our ordering variable

---

will be labelled v. We will design our kinematic map such that, in a frame where Q^μ is at rest, for a soft-collinear emission at an angle θ and with a transverse momentum $k_\perp$ relative to the emitter, we will have

$$v \simeq k_\perp (\theta/2)^{\beta_{\rm PS}}. \tag{4.2}$$

Using an auxiliary longitudinal variable $\bar{\eta}_Q$, and a transverse momentum scale for emissions $\kappa_\perp$, this will be achieved by adopting the following definitions

$$\kappa_\perp \equiv \rho v e^{\beta_{\rm PS}|\bar{\eta}_Q|}, \tag{4.3}$$

with

$$\rho = \left(\frac{\tilde{s}_i \tilde{s}_j}{\tilde{s}_{ij} Q^2}\right)^{\beta_{\rm PS}/2}, \quad \tilde{s}_i = 2\tilde{p}_i \cdot Q, \quad \tilde{s}_j = 2\tilde{p}_j \cdot Q, \quad \tilde{s}_{ij} = 2\tilde{p}_i \cdot \tilde{p}_j. \tag{4.4}$$

Setting $\beta_{\rm PS} = 0$ corresponds to a transverse-momentum ordered shower. The choice $\beta_{\rm PS} = 1$ would result in a time-ordered shower, but as we shall explain below for the showers that we consider, that choice is not consistent with NLL accuracy.

Aside from the parametric form of the evolution variable v, the main novelty of the PanScales showers is the definition of an alternative pseudorapidity-like variable $\bar{\eta}_Q$ that enters the dipole partitioning function $g(\bar{\eta}_Q)$ in eq. (2.9). It represents the rapidity of the emission p_k with respect to the parent dipole, in the frame where the reference vector Q^μ is at rest, i.e.

$$\bar{\eta}_Q = \frac{1}{2} \ln \frac{p_k \cdot \tilde{p}_j}{p_k \cdot \tilde{p}_i} - \frac{1}{2} \ln \frac{\tilde{s}_j}{\tilde{s}_i}. \tag{4.5}$$

That is, $\bar{\eta}_Q = 0$ corresponds to a direction equidistant to $\tilde{p}_i$ and $\tilde{p}_j$ in the rest frame of Q^μ. This is an important difference when compared to the standard dipole showers which, as explained in the previous section, split the dipole in the dipole rest frame (see eq. (2.13)).

When formulating the kinematic maps, we find it useful to define intermediate variables

$$\alpha_k \equiv \sqrt{\frac{\tilde{s}_j}{\tilde{s}_{ij}\tilde{s}_i}} \kappa_\perp e^{\bar{\eta}_Q}, \qquad\qquad \beta_k \equiv \sqrt{\frac{\tilde{s}_i}{\tilde{s}_{ij}\tilde{s}_j}} \kappa_\perp e^{-\bar{\eta}_Q}. \tag{4.6}$$

The specific relation between α_k, β_k, and the a_k, b_k as used in Sudakov decomposition for the emitted momentum eq. (2.6) will depend on the shower. One common property for all our showers is that for emissions that are soft and collinear, $a_k = \alpha_k$ and $b_k = \beta_k$ (from which one can verify that eq. (4.2) is reproduced). A further common property is that for final-state branchings, the z values used in the splitting functions, eq. (2.3), are given by

$$z_i = \alpha_k, \qquad z_j = \beta_k, \qquad\qquad \text{(final state)}, \tag{4.7}$$

while for initial-state branchings they are

$$z_i = \frac{\alpha_k}{1 + \alpha_k}, \qquad z_j = \frac{\beta_k}{1 + \beta_k}, \qquad\qquad \text{(initial state)}. \tag{4.8}$$

Note that for initial-state branchings, α_k and β_k can grow larger than 1. Uniform generation of the $\bar{\eta}_Q$ variable ensures logarithmic sampling of both small z and small $1 - z$.

In what follows, we present two recoil schemes and show their fixed-order behaviour.

4.2 PanGlobal

The hadron-collider PanGlobal shower is an antenna shower. For the splitting probability, eq. (2.3), it uses $g(\bar{\eta}_Q) = g^{\text{ant.}}(\bar{\eta}_Q)$ (cf. eq. (2.10)). Its kinematic map can be viewed as follows:

1. Apply the "global" dipole map of eq. (2.12) with $a_k = \alpha_k$ and $b_k = \beta_k$ as defined in eq. (4.6).

2. The preceding step breaks momentum conservation for the event as a whole. First the component that is transverse to the beams is restored by applying a boost to the hard system such that the hard system rapidity remains unchanged and that the sum of the transverse momenta (with respect to the beams) of the boosted hard system and all final-state particles adds up to zero.

3. To restore conservation of the components of momentum that are longitudinal with respect to the beams, evaluate the sum of the light-cone ($p_+ = E + p_z$ and $p_- = E - p_z$) momenta of all final-state particles including the boosted hard system. Set the momentum of the incoming parton on side a to be $p_+/2$ and that on side b to be $p_-/2$.

Note that step 3 affects the momenta of the incoming partons regardless of whether the dipole is II, IF, FI or FF. In cases where one end of the dipole is in the initial state, it causes the incoming momentum to differ from that of the global map in eq. (2.12). Detailed equations for all steps are given in appendix B.2.

As compared to the e^+e^- PanGlobal shower [43] there are both points in common and differences. The use of the global map, eq. (2.12), is for example very similar. However the way in which we restore momentum conservation after that map is different: in particular the e^+e^- shower balances the momentum across all final-state particles, while the hadron-collider shower defined above leaves all final-state particles untouched (unless they belong to the hard system) and relies on adjusting the incoming particle momenta to conserve energy.[9]

4.2.1 Tests for $\beta_{\text{ps}} = 0$ and $1/2$

In figure 3, we perform the same fixed-order analysis as in figure 2 for the PanGlobal shower using $\beta_{\text{PS}} = 0$ (left) and $\beta_{\text{PS}} = 1/2$ (right). Let us first consider the situation where the second emission is far in rapidity from the first. Step 1 of the PanGlobal recoil scheme leaves an overall momentum imbalance in the direction transverse to the (IF) dipole. It can be shown that a unit vector transverse to any IF dipole ($\hat{n}_{1,2}$ in eq. (2.7)) has a unit component

---

[9]We also explored options in which all final-state particles get boosted. However, such options are delicate. Specifically, a transverse boost that modifies the hard-system transverse momentum by an amount of order k_t also modifies any energetic but collinear initial-state emissions by a comparable amount. This introduces long-distance correlations between soft-collinear and hard-collinear initial-state emissions, in violation of the PanScales conditions outlined in section 3. Such problems have also been commented upon in the context of the Deductor work, which introduces a specific Lorentz transformation to work around the issue [54].
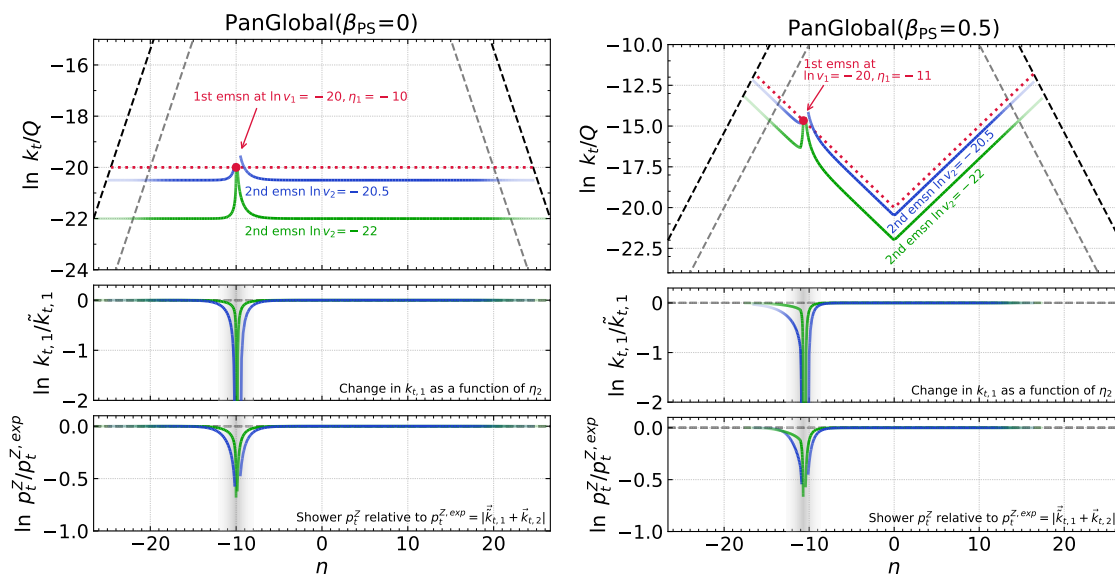
Figure 3. Same as figure 2, but for PanGlobal with $\beta_{\mathrm{PS}} = 0$ (left) and $\beta_{\mathrm{PS}} = 0.5$ (right).

transverse to the beam. As a result, step 2 assigns the shower transverse momentum to the hard system, i.e. the Z boson, as is physically correct, thus reproducing the pattern needed for NLL accuracy. When the 2nd emission is close in rapidity to the first, it is arguably less physically correct to take the transverse recoil from the Z boson. However, the assignment of transverse recoil only has a significant impact when $k_{\perp,2} \sim k_{\perp,1}$, and the region of commensurate rapidity and commensurate transverse momentum only affects terms at NNLL accuracy, the correct treatment of which would in any case require the inclusion of the full double-soft matrix element.[10] A similar discussion can be extended to subsequent emissions. Our conclusion, therefore, is that the PanGlobal showers with $\beta = 0$ and $\beta = 1/2$ satisfy the fixed-order NLL accuracy requirement.

4.2.2 Discussion of $\beta_{\mathbf{ps}} = 1$ case (time ordering)

We close our discussion of the PanGlobal shower with an explanation of why that shower requires $\beta_{\mathrm{PS}} < 1$ and an illustration of the issues that arise with $\beta_{\mathrm{PS}} = 1$. The choice of $\beta_{\mathrm{PS}} = 1$ is of interest because, physically, it corresponds roughly to a time ordering. This can be relevant, for example, in a heavy-ion context where one may wish to relate individual steps of the shower with the time-dependent evolution of a quark-gluon plasma. That $\beta_{\mathrm{PS}} = 1$ corresponds roughly to time-ordering can be seen as follows. Firstly, consider a soft large-angle emission with transverse momentum $k_\perp$ with respect to the parent dipole. The uncertainty principle tells us that the formation time is roughly $1/k_\perp$. Next, observe that a soft-collinear emission, with energy E and transverse momentum $k_\perp$ is equivalent to a soft emission that has been boosted along the parent dipole direction. The boost factor is roughly $E/k_\perp$ and so the formation time acquires a Lorentz dilation by that same factor,

---

[10]Note that $k_{t,1}$ is also affected by recoil that is longitudinal with respect to the dipole when emission 2 is collinear to 1. This is not the case for p_t^Z.
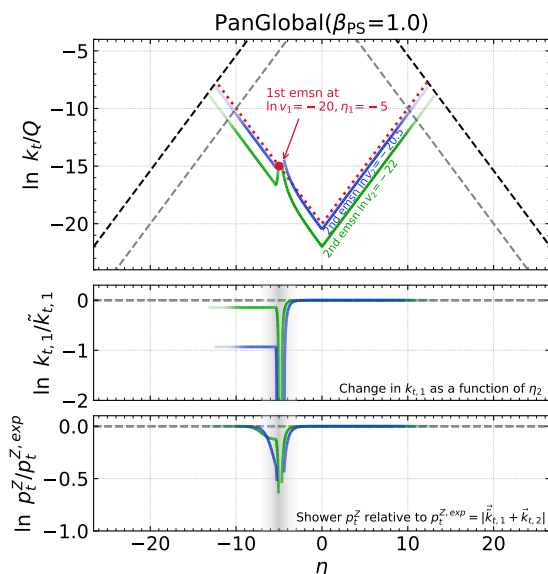
Figure 4. Same as figure 2, but for PanGlobal with $\beta_{\rm PS} = 1$ and $\eta_1 = -5$.

giving a net formation time of order $t \sim E/k_\perp^2 \sim 1/(k_\perp \theta)$, where θ is the emission angle. Inspecting eq. (4.2), one sees that with $\beta_{\rm PS} = 1$, $t \sim 1/v$.

Figure 4 repeats the analysis of figure 3 for PanGlobal with the "time-ordered" $\beta_{\rm PS} = 1$ choice. Contrary to the $\beta_{\rm PS} = 0$ and $\beta_{\rm PS} = 1/2$ cases, we see that the second emission modifies the transverse momentum of the first when that second emission is in the same hemisphere and at more forward rapidities than the first. One way of understanding why $\beta_{\rm PS} = 1$ might cause problems is to observe that, for $v_2 \simeq v_1$, the second emission is created close to the kinematic boundary of its parent dipole (recall that kinematic boundaries have slope ± 1 in the soft-collinear region of the Lund plane). Close to that kinematic boundary, it is almost inevitable that the parent dipole momenta will be substantially modified.

To obtain a more analytic understanding of our observations, let us consider a sequence of two soft-collinear emissions with commensurate $\ln v$ values, working with a general value of $\beta_{\rm PS}$. We start with an $a-b$ initial state, where particle a's momentum, p_a, has a negative z component. Since both emissions will be soft and collinear, the momenta of a and b will not be affected by those emissions and we need not worry about distinctions between their pre- and post-branching momenta (i.e. we will never write tildes over p_a and p_b). We place a first soft-collinear emission at negative physical rapidity, which, given a's negative z momentum, is obtained by choosing a large positive $\bar{\eta}_{Q,1}$,

$$\tilde{p}_1^\mu = a_1 p_a^\mu + b_1 p_b^\mu + k_{\perp,1}^\mu \,, \tag{4.9}$$

where, using eqs. (4.3)–(4.6), $a_1 = \alpha_1$, $b_1 = \beta_1$, and $s_{ab} = s_a = s_b = Q^2$, we have

$$a_1 = \frac{v_1}{Q} e^{(\beta_{\rm PS}+1)\bar{\eta}_{Q,1}} \,, \qquad b_1 = \frac{v_1}{Q} e^{(\beta_{\rm PS}-1)\bar{\eta}_{Q,1}} \,, \qquad (\bar{\eta}_{Q,1} > 0) \,. \tag{4.10}$$

Note that we have written the momentum of gluon 1 as $\tilde{p}_1^\mu$, i.e. with a tilde, in anticipation of a second soft-collinear emission to come.

For that second emission, we first consider the case where it comes from the $a-1$ IF dipole, with v_2 only moderately smaller than v_1, but a large positive value of $\bar{\eta}_{Q,2}$. The latter choice causes emission 2 to be substantially more forward than emission 1 (i.e. at a more negative physical rapidity). The global map, eq. (2.12), with $i = a$, $j = 1$ and $k = 2$ for this IF dipole, results in a change in the momentum of particle 1,

$$p_1^\mu = (1 - b_2)\tilde{p}_1^\mu, \qquad b_2 = \frac{s_a}{s_{1a}Q}\left(\frac{s_a s_1}{s_{1a}Q^2}\right)^{\frac{\beta_{\rm PS}-1}{2}} v_2\, {\rm e}^{(\beta_{\rm PS}-1)\bar{\eta}_{Q,2}}, \qquad (\bar{\eta}_{Q,2} > 0). \qquad (4.11)$$

Using

$$s_a = Q^2, \qquad s_1 = (a_1 + b_1)Q^2, \qquad s_{1a} = b_1 Q^2. \qquad (4.12)$$

Exploiting our assumption of a large value of $\bar{\eta}_{Q,1}$ so that $b_1 \ll a_1$, we have

$$b_2 = \frac{1}{b_1}\left(\frac{a_1}{b_1}\right)^{\frac{\beta_{\rm PS}-1}{2}}\frac{v_2}{Q}{\rm e}^{(\beta_{\rm PS}-1)\bar{\eta}_{Q,2}} = \frac{v_2}{v_1}{\rm e}^{(\beta_{\rm PS}-1)\bar{\eta}_{Q,2}}. \qquad (4.13)$$

We observe that for $\beta_{\rm PS} = 1$, b_2 is just given by v_2/v_1, independently of $\bar{\eta}_{Q,2}$, i.e.

$$p_1^\mu = \left(1 - \frac{v_2}{v_1}\right)\tilde{p}_1^\mu, \qquad (\beta_{\rm PS} = 1), \qquad (4.14)$$

no matter how far in rapidity emission 2 is from emission 1. Note that this scaling of the momentum gluon 1 changes its transverse momentum as measured with relative to the beam. This is a long-distance side effect of emission 2 on the momentum of emission 1, which prevents the shower from being NLL accurate.[11] The change in transverse momenta of the first emission after the second splitting (eq. (4.14)) is precisely what is observed in the ratio plot of figure 4. One can carry out a similar analysis for an emission from the $b-2$ dipole, and the findings are consistent with figure 4. The main further point that one observes is that if emission 1 is at large angles, then it is affected by a second soft-collinear emission regardless of which hemisphere that second emission is in.

To conclude, we have shown that using $\beta_{\rm PS} = 1$ for our ordering variable, we introduce a longitudinal rescaling of the first-emitted parton after emitting a second one. This rescaling alters the transverse momentum of the first-emitted parton in the event frame, even when the two emissions are well separated in rapidity. Therefore, the PanGlobal shower with $\beta_{\rm PS} = 1$ does not satisfy our fixed-order logarithmic accuracy requirement. It is reasonable to suppose that this behaviour of $\beta_{\rm PS} = 1$ showers can be cured by assigning the recoil only to the side of the dipole that is emitting.[12] This would require another form of the boost. We will leave further modifications and tests of the $\beta_{\rm PS} = 1$ showers for future work.

It is useful to be aware that $\beta_{\rm PS} = 1$ ordering differs from virtuality ordering in the sense of ref. [72]. Working in a frame where the fixed reference vector Q^μ is at rest, for a soft-collinear emission k with energy E_k and angle θ from a parent with energy E_i, we

---

[11]Ref. [51] commented that a standard final-state dipole-local map with so-called Λ ordering, i.e. effectively time ordering, results in NLL violations for the thrust observable. We believe that the issue observed there is effectively identical to that discussed here.

[12]The maps of the showers proposed in refs. [54] and [49] indeed satisfy this requirement, though only the former has explored time ("Λ") ordering.

have $v_{\beta_{\rm ps}=1} \simeq E_k\theta^2/2$, independently of E_i, cf. eq. (4.2). Virtuality, as defined in ref. [72] for Vincia, specifically the m_D^2 variable, corresponds to $2E_iE_k\theta^2$ in the soft-collinear limit, which does depend on E_i. Since one should consider a broad range of (soft and hard) parent energies E_i, ordering in $v_{\beta_{\rm ps}=1}$ is not the same as virtuality ordering. On the other hand, the ordering $v_{\beta_{\rm ps}=1}$ is similar to what is referred to as virtuality-based ordering in Deductor [73, 74], where, in our notation, the ordering variable is $\Lambda^2 \sim \frac{2p_i.p_k}{2\tilde{p}_i.Q}Q^2 \simeq E_k\theta^2Q/2$ (for Q^μ at rest), i.e. independent of E_i. Note that our conclusions about logarithmic accuracy still do not apply to Deductor. Their recoil treatment differs from ours, and it is our understanding that this is crucial to their observation of NLL accuracy for thrust [51].

4.3 PanLocal dipole and antenna

Here we consider two closely related variants of local shower, one of the dipole type, the other of antenna type, both intended to be used with an ordering choice $0 < \beta_{\rm PS} < 1$. The two non-trivial choices that we need to make in order to obtain showers that have NLL accuracy concern the kinematic map and the generation variables in the hard-collinear initial-state region. Let us start with the former:

1. For all dipole types (FF, II, etc.), we apply a dipole-local map eq. (2.8). The relation that we use to obtain a_k and b_k from α_k and β_k depends on the type of dipole and will be discussed below. When the dipole involves one or more initial-state particles, and at least one of them is assigned transverse recoil from the map, the local map results in the new incoming particle acquiring a transverse momentum.

2. When an initial-state particle acquires transverse momentum, we perform a Lorentz transformation (boost and a rotation) to all event particles, outgoing and incoming, so as to realign the initial-state parton with the original beam axes. The Lorentz transformation is constrained by the following requirements: after its application, both incoming particles should be aligned along the original beam axes, and the rapidity of the hard system, as defined with respect to the proton beams, should coincide with the pre-splitting hard-system rapidity.

The functional form of the transformation, together with the mapping coefficients, are provided in appendix B.3. The choice to boost all particles in the case of initial-state splittings differs from that of the Dipole-k_t algorithm (recall that for II dipoles, it boosts all final-state particles *except* for the new emission).

Our choice of Lorentz transformation leads to an important subtlety for hard-collinear initial-state branchings, notably as concerns the relation between the generated transverse momentum, $k_\perp$, and the final emission transverse momentum with respect to the beam, k_t.[13] Let us consider such a branching, concentrating just on the part of the dipole close

---

[13]The argument that follows is based on a physical picture of the angles involved in the branching. Some readers may instead prefer to consider a Lorentz-invariant definition of the transverse momentum with respect to reference directions a and b, $k_{ti}^2 = \frac{2(p_a.p_k)(p_b.p_k)}{p_a.p_b}$, and to use the explicit kinematic map in eq. (2.8) to derive the result that is shown below in eq. (4.16).

the initial-state emitter $\tilde{\imath}$, which emits a particle k and produces a new incoming particle i. Representing the angles as follows

$$\text{(4.15)}$$
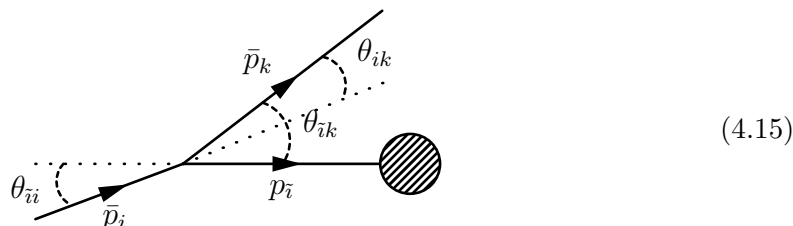
we note that the generated transverse momentum, defined with respect to the $\tilde{\imath}$ direction, is given by $k_\perp \simeq E_k \theta_{\tilde{\imath}k}$, where E_k is the energy of k. To determine the transverse momentum, k_t, of the emission with respect to the beam, note that in the limit where the ordering variable is small, the boost component of the Lorentz transformation is also small, and it essentially preserves the angles between all particles. As a result, we can write $k_t \simeq E_k \theta_{ik}$. Keeping in mind that $E_i \theta_{\tilde{\imath}i} = E_k \theta_{\tilde{\imath}k}$ (by conservation of transverse momentum), $\theta_{ik} = \theta_{\tilde{\imath}k} - \theta_{\tilde{\imath}i}$, $E_k = a_k E_{\tilde{\imath}}$ and $E_i = (1 + a_k) E_{\tilde{\imath}}$ (with a_k as in the kinematic map, eq. (2.8)), one has the following relation between the generated transverse momentum $k_\perp$ and the final transverse momentum with respect to the beam, k_t:

$$k_t = \frac{k_\perp}{1 + a_k} \, . \tag{4.16}$$

The critical feature to note is that k_t becomes much smaller than $k_\perp$ when $a_k \gg 1$. Physically this is a consequence of the fact that, in that limit, $E_k \simeq E_i$ and so the angles $\theta_{\tilde{\imath}i}$ and $\theta_{\tilde{\imath}k}$ almost coincide, resulting in a small value of the difference between them, θ_{ik}, which is the angle relevant for calculation the transverse momentum with respect to the beam.

A degree of freedom that we have in the kinematic map is the relation between the generation v and $\bar{\eta}$ (or equivalently α_k and β_k in eqs. (4.6)) and the variables a_k and b_k of the kinematic map. At first sight, the simplest choice would appear to be to use $a_k = \alpha_k$ and $b_k = \beta_k$, as we did for the PanGlobal shower. Considering the ordering parameter $\beta_{\mathrm{PS}} = 0.5$, we obtain the contours shown in figure 5 (left). Observe that in the soft-collinear region, i.e. the inner Lund triangle, the (red-dotted) contour for the first emission slopes upwards as one moves out from central rapidities, as expected for $\beta_{\mathrm{PS}} = 0.5$. However, beyond the edge of the inner-Lund triangle, where $a_k = \alpha_k$ becomes much larger than 1, the behaviour changes and the first emission contours bends down, a consequence of the $1 + a_k$ denominator in eq. (4.16). Next, we fix the first emission to be hard and at negative rapidities (red dot) and examine a second emission at v_2 slightly smaller than v_1, shown by the blue contour. When the second emission, k_2, satisfies $\eta_1 \lesssim \eta_2 \lesssim 0$, it is emitted from the FI dipole that stretches between emission 1 and the right-going beam, and so takes its transverse recoil from emission 1. When $k_{t2} \gtrsim k_{t1}$, this induces a significant recoil on particle 1, as is visible from the middle panel of that figure. How problematic is this? Strictly it only matters when the first emission has $\alpha_{k_1} \gg 1$, because only then is there a substantial region part of the inner Lund plane (i.e. soft and collinear region)
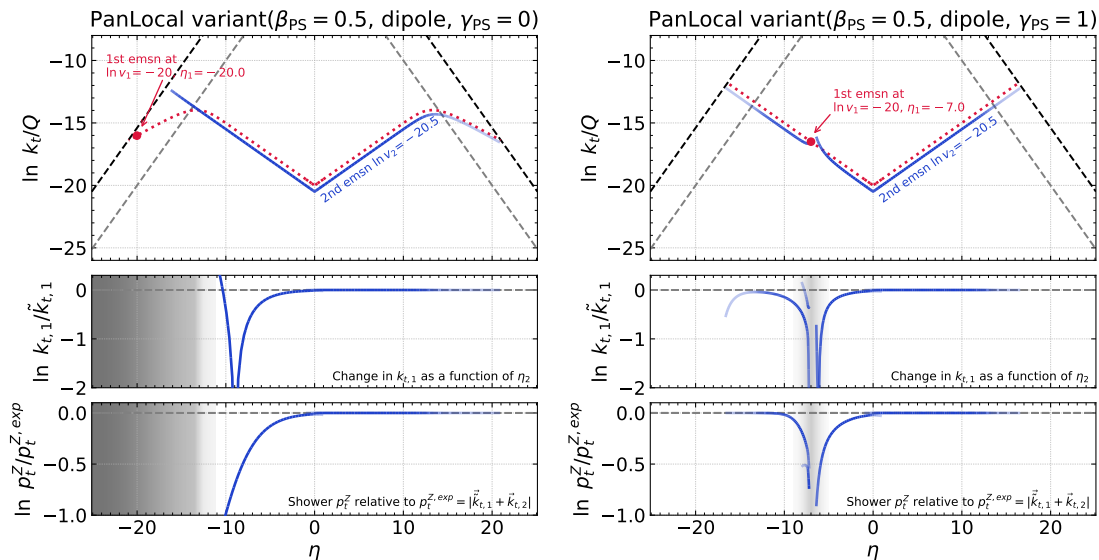
Figure 5. As in figure 2, showing non-default PanLocal variants with (left) the choice $b_k = \beta_k$ (corresponding to $\gamma = 0$ in eq. (4.17)) and (right) the choice $\gamma = 1$.

with $k_{t2} \gtrsim k_{t1}$. In practice the region $\alpha_{k_1} \gg 1$ is suppressed by the PDF ratio in eq. (2.2). From a logarithmic point of view it is relevant only to small-x resummations, which are beyond what we aim to control. Still, one might argue it would not be within the spirit of our overall approach to have a long-distance correlation between hard and soft-collinear emissions.

To address this concern, we consider a generalisation of the relation between the coefficients in the kinematic map and the ordering and auxiliary variables. Specifically, if the emitter is an initial-state particle, we maintain $a_k = \alpha_k$, but replace the $b_k = \beta_k$ relation with

$$b_k = \beta_k(1 + \alpha_k)^{2\gamma} \,, \tag{4.17}$$

where γ is a parameter to be chosen. This has a substantial effect when $\alpha_k \gg 1$, and in that region one finds

$$\ln k_t = \left(\gamma - \frac{1}{1 + \beta_{\mathrm{PS}}}\right) \ln \alpha_k + \left(\frac{1}{1 + \beta_{\mathrm{PS}}}\right) \ln v + \mathcal{O}\left(1\right). \tag{4.18}$$

If we are to prevent the contour from decreasing in k_t outside the inner Lund plane, then we need

$$\gamma \geq \frac{1}{1 + \beta_{\mathrm{PS}}} \,. \tag{4.19}$$

This requirement ensures that a soft-collinear emission does not affect a prior hard-collinear, even when that hard collinear one has large α_k.

A second consideration concerns the effect of a hard-collinear emission on a prior soft-collinear emission. Let us examine what happens if we take $\gamma = 1$. Such a choice has the effect of cancelling the denominator in eq. (4.16) so that k_t coincides with $\kappa_\perp$ in eq. (4.3). As can be seen in figure 5 (right), it gives a straight contour for the first emission. Next,

we fix the first emission to be soft and collinear (as represented with the red dot) and examine how its momentum is modified by a second emission, as a function of the rapidity of that second emission, η_2. We see from the middle panel of the figure that, sufficiently far into the left hard-collinear region, the transverse momentum of the first emission receives a large modification.[14] The origin of this problem requires an examination of the detailed kinematic map, as given in appendix B.3. Concentrating on the left-hand part of the plot, with $\eta_2 < \eta_1 < 0$, consider the b_j coefficient in eq. (B.56c) for an IF dipole with the initial-state parton as the emitter ($f = 1$),

$$b_j = 1 - \frac{b_k}{1 + a_k} \,. \tag{4.20}$$

The essential point to understand is that the large-α_k enhancement of b_k that we introduce with $\gamma = 1$ in eq. (4.17) can cause b_k to become commensurate with a_k, which results in a substantial modification of b_j. Considering the limit $a_k = \alpha_k \gg 1$, this occurs when b_k/a_k, given by

$$\frac{b_k}{a_k} \sim \alpha_k^{2\gamma - \frac{2}{1+\beta_{\mathrm{PS}}}} z_1^{\frac{2}{1+\beta_{\mathrm{PS}}} - 1} \left(\frac{v_2}{v_1}\right)^{\frac{2}{1+\beta_{\mathrm{PS}}}} \,, \qquad \text{valid for } \alpha_k \gg 1,\, z_1 \ll 1, \tag{4.21}$$

becomes of order 1. Since we started with a first soft-collinear emission, $z_1 \ll 1$, and since $v_2 < v_1$, by construction, the ratio in eq. (4.21) is guaranteed to be smaller than one if

$$\gamma \leq \frac{1}{1 + \beta_{\mathrm{PS}}} \,. \tag{4.22}$$

In particular, this shows that if we are to avoid non-trivial cross-talk between hard-collinear and soft-collinear emissions, $\gamma = 1$ is not suitable for any $\beta_{\mathrm{PS}} > 0$. Taken together, eqs. (4.19) and (4.22) tell us that there is only one value of γ in eq. (4.17) that enables us to avoid such cross-talk, specifically

$$\gamma = \frac{1}{1 + \beta_{\mathrm{PS}}} \,. \tag{4.23}$$

Figure 6 shows the contour plots as obtained with this choice. There can still be non-trivial side effects of the second emission on the first one, but only in the region where both emissions are hard and collinear (left), or close in rapidity (right). In particular, the problems seen in figure 5 are absent with the choice for γ in eq. (4.23). We make this the default choice for our PanLocal dipole shower.

The antenna variant of PanLocal is broadly similar in construction. The guiding principle is that for any dipole end that can be involved in a hard-collinear initial-state branching, the mapping coefficient for the light-cone component associated with the effective "spectator" end should have an enhancement as in eqs. (4.17) and (4.23). The details are given in appendix B.3.2. The contour plots, which we omit for brevity, are very similar to figure 6.

To close this section, we note that $\beta_{\mathrm{PS}} = 1$ for the PanLocal showers suffers from the same problem as $\beta_{\mathrm{PS}} = 1$ PanGlobal showers, i.e. a substantial effect of spectator

---

[14]With sufficiently large $\sqrt{s}/Q$ such an effect would be visible also in the right-hand collinear region.
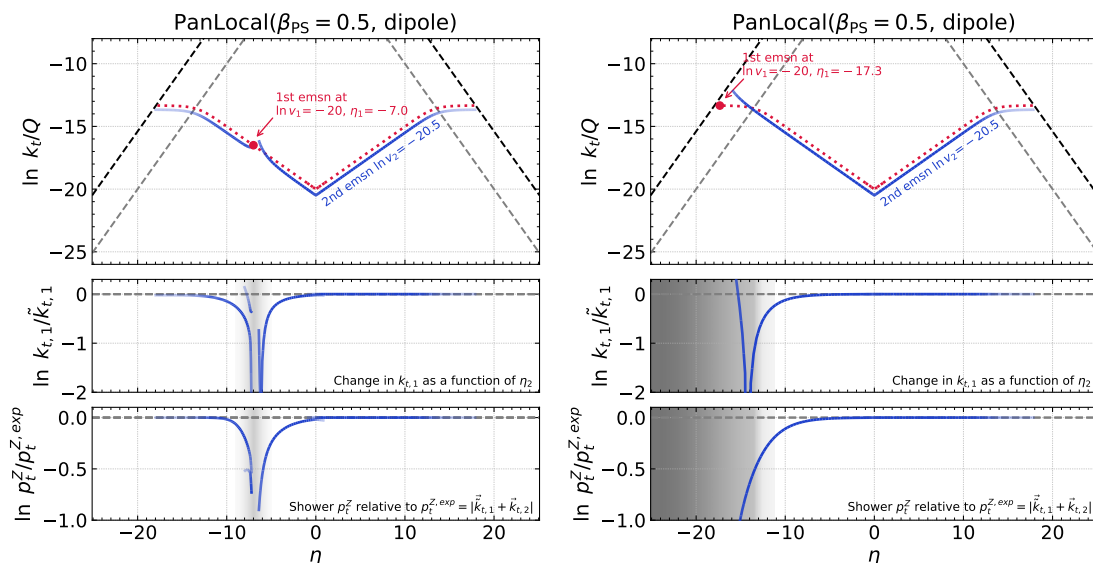
Figure 6. PanLocal contours for two first-emission configurations similar to those of figure 5, but with our default choice of the parameter $\gamma = 1/(1 + \beta_{\mathrm{PS}})$.

longitudinal recoil when two emissions are in the same hemisphere, v_2 is commensurate with v_1 and $|\eta_2| > |\eta_1|$. Additionally, PanLocal showers have issues of incorrect transverse recoil for $\beta_{\mathrm{PS}} = 0$, as in the final state case, cf. figure 7. In particular for $\eta_1 < 0$, the transverse momentum recoil from an emission from the $g_1 q$ dipole is taken by the gluon when $\eta_1 < \eta_2 < 0$ even if $\eta_2 - \eta_1 \gg 1$. Requiring $\beta_{\mathrm{PS}} > 0$ solves this problem: emissions with commensurate k_t values are ordered so that smaller-angle emissions are generated later. Then, the use of $g(\bar{\eta}_Q)$ to partition the dipole ensures that when the smaller-angle emission is in the primary Lund plane, the recoil is taken from the initial-state particle and so, after the boost, effectively from the hard system.

5 Subleading colour at LL accuracy and beyond

Dipole showers naturally achieve the large-N_{C} limit of QCD. It is common practice for dipole showers to adopt a modification of the large-N_{C} limit in which one uses a C_F colour factor for a quark or anti-quark end of a dipole and a $C_A/2$ colour factor for an end that corresponds to a gluon (we refer to this as the colour-factor-from-emitter scheme, CFFE). It has long been known [75] that such a choice is inconsistent with colour coherence. Ref. [42] pointed out that, for quite a range of observables, this results in the wrong subleading-N_{C} contributions at LL accuracy. Insofar as one views $1/N_{\mathrm{C}}^2$ as being comparable with α_s, subleading-N_{C} LL corrections are comparable to a leading-colour NLL terms and so should, arguably, be addressed on a par with such leading-colour NLL terms.

In this section, we extend the two efficient colour schemes introduced [44] for the final-state PanScales showers to the initial-state case. Section 5.1 summarises and extends the so-called segment colour scheme, section 5.2 does the same for the nested-ordered-double-soft (NODS) colour scheme, and section 5.3 shows the results of various fixed-order
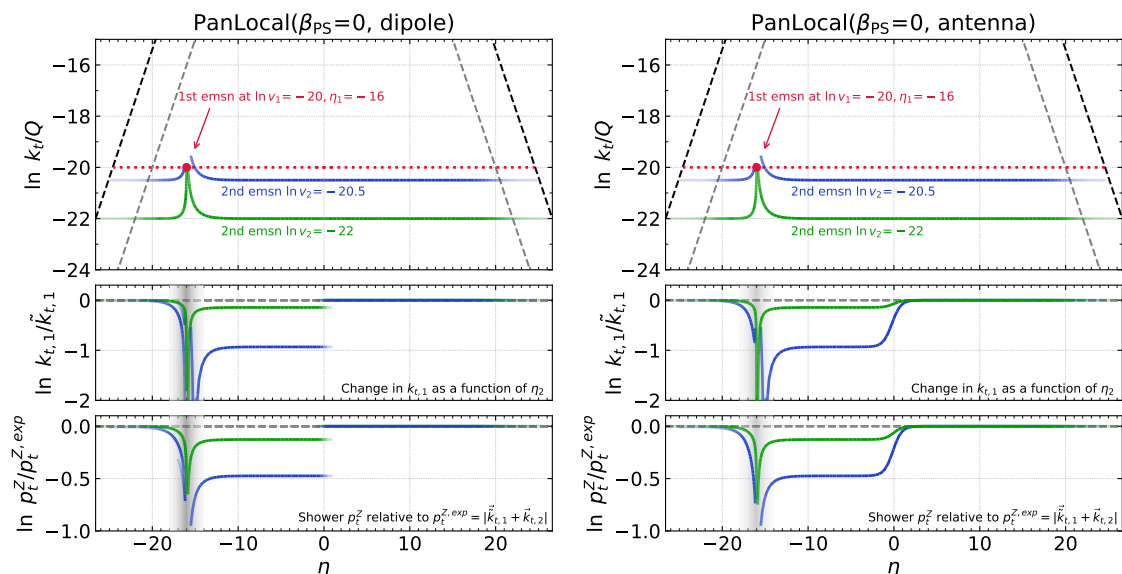
Figure 7. Same as figure 2, but for PanLocal, dipole (left) and antenna (right) with $\beta_{\mathrm{PS}} = 0$.

validation tests. These schemes achieve full-colour accuracy not just for LL terms but also for NLL terms in the case of global event-shape type observables [76], and for next-to-double-logarithms (NDLs) for jet multiplicities. Related schemes, adequate for full-colour LL accuracy have been explored also by other authors [50, 77].[15]

5.1 Adaption of segment scheme to initial-state splittings

The segment colour scheme divides each dipole into distinct segments in the underlying $\bar{\eta}$ generation variable, with some segments having a $C_F = (N_{\mathrm{C}}^2 - 1)/(2N_{\mathrm{C}})$ colour factor and the others having a $C_A/2 = N_{\mathrm{C}}/2$ colour factor. The guiding principle for the assignment is colour coherence. More concretely, consider the example of a $q\bar{q} \to Z$ event in which the incoming q backwards evolves by emitting a final-state gluon g_1, i.e. $q_I \to q_I g_1$. For this first emission, the colour factor is unequivocally C_F since it is emitted from a quark-like leg. Next, a second gluon g_2 is emitted. Let θ_i be the angle between g_i and the beam direction, and θ_{12} the angle between the two gluons. If $\theta_{12} \ll \theta_1$ then the segment method assigns a $C_A/2$ colour factor, while if $\theta_2 \ll \theta_1$ or $\theta_2 \gg \theta_1$ a C_F colour factor is assigned. In the region where the angles are commensurate, the correct emission intensity cannot be

---

[15]There has also been extensive work towards the inclusion of subleading-colour effects through amplitude-level evolution [78–82] and other schemes [83–85]. Note that amplitude evolution also has the potential to induce coherence-violating effects [86, 87] (sometimes called super-leading logarithms), terms specific to hadron colliders, whose all-order impact has recently started to be evaluated [88, 89]. The impact of coherence-violating terms on logarithmic accuracy depends on the observable [90, 91], though the quantitative understanding of this question remains to be elucidated. In this context, one may wish to keep in mind observations concerning spurious super-leading logarithms generated by long-distance shower-recoil effects [43], specifically terms $\alpha_s^n L^{2n-3}$ for the thrust. Their sum was found to vanish as $\alpha_s \to 0$ for fixed $\alpha_s L$, a behaviour that would be expected from NNLL terms or beyond. These questions clearly deserve further study. For now, when we refer to the full-colour NLL accuracy of our shower, this is to be understood as applying to terms of coherent origin.

reproduced by simply using one of C_F or $C_A/2$ but the segment method still uses a discrete choice between them, engineered so as to reproduce NDL accuracy for observables such as the multiplicity (or equivalently the correct integrated rate of emission of g_2 when it has an energy or k_t much lower than that of g_1).

The segment colour scheme implements this reasoning throughout the shower evolution. A dipole can have any number of alternating C_F and $C_A/2$ colour segments. We represent the segments with the notation

$$_{\bar{3}}[-\infty, C_A, \eta_1, C_F, \eta_2, C_A, \ldots, \infty]_3 \,, \tag{5.1}$$

This indicates that for all gluon emission rapidities (as defined below) between $-\infty$ and η_1, one uses a $C_A/2$ colour factor,[16] for emissions between η_1 and η_2, one uses a C_F colour factor, etc. Negative rapidity is always associated with the end of the dipole that has outgoing anti-triplet colour. In our notation we always refer to the effective outgoing colour-flow, so, for example, an initial-state quark is to be thought of as having outgoing anti-triplet colour. We establish where an emission k is positioned in the sequence of eq. (5.1) based on a specific approximate determination of its rapidity, which for PanScales showers and a parent dipole ij reads

$$\eta_{\text{approx}} \equiv \begin{cases} \bar{\eta}_Q - \frac{1}{2}\ln\left(\frac{1-\cos\theta_{ij}}{2}\right), & \bar{\eta}_Q > 0\,, \\ \bar{\eta}_Q + \frac{1}{2}\ln\left(\frac{1-\cos\theta_{ij}}{2}\right), & \bar{\eta}_Q < 0\,. \end{cases} \tag{5.2}$$

In the soft and collinear limit, this variable coincides with the physical rapidity of the emission with respect to the closer of i and j (in this section, all angles are evaluated in the frame where Q^μ is at rest). The sign of $\bar{\eta}_Q$ (and η_{approx}) is such that emission from the triplet (anti-triplet) end of a dipole has positive (negative) $\bar{\eta}_Q$.

After an emission, one needs to update the set of segments on the dipoles involved in the splitting. Returning to our earlier example of $q_I\bar{q}_I \to Z$, the initial-state q_I is at the $\bar{3}$-end of the dipole, and the starting dipole segment structure is

$$_{q_I}[-\infty, C_F, \infty]_{\bar{q}_I} \,. \tag{5.3}$$

When we radiate a gluon from this $q_I\bar{q}_I$ dipole, we obtain two new dipoles $q_I g_F$ and $g_F\bar{q}_I$, each of which now has a C_F and a C_A region.

$$_{q_I}[-\infty, C_F, \eta^L_{g_F}, C_A, \infty]_{g_F} + {}_{g_F}[-\infty, C_A, \eta^R_{g_F}, C_F, \infty]_{\bar{q}_I} \,. \tag{5.4}$$

For a gluon emission k, the new transition points are given by

$$\eta^L_k = \max(0, \eta_k)\,, \quad \eta^R_k = \min(0, \eta_k)\,. \tag{5.5}$$

To determine η_k, we evaluate the angle of the emission θ_k, with respect to the triplet (anti-triplet) end of the dipole if $\eta_{\text{approx}} > 0$ (< 0) and then take $\eta_k = \pm|\ln\tan\theta_k/2|$, where a positive (negative) sign is used when $\eta_{\text{approx}} > 0$ (< 0).

So far, the discussion has largely followed that of the final-state case in ref. [44]. We now summarise the non-trivial extensions needed for the new radiation channels that open up in hadron collisions:

---

[16]In the list of segments, it is labelled C_A rather than $C_A/2$ for ease of notation.

- $g_I \to q_I \bar{q}_F$: the backwards evolution of an initial-state quark q_I to an initial-state gluon g_I and a final-state anti-quark $\bar{q}_F$ results in the following configuration of segments

$$_{q_I}[-\infty, C_F, \dots]_{\dots} \to {}_{g_I}\left[-\infty, C_A, \eta_{\bar{q}_F}^R, C_F, \dots\right]_{\dots} + {}_{\bar{q}_F}\left[-\infty, C_F, \eta_{\bar{q}_F}^L, C_A, \infty\right]_{g_I} \quad (5.6)$$

The case in which $g_I \to \bar{q}_I q_F$ is similar. Relative to the default large-$N_{\rm c}$ splitting probability, no rejection factor needs to be applied because the splitting function involves a T_R colour factor (this is the same as for the treatment of a final state $g \to q\bar{q}$ splitting).

- $q_I \to g_I q_F$: the backwards evolution of an initial-state gluon g_I to an initial-state quark q_I and a final-state quark q_F is slightly more subtle. Two dipoles exist before the splitting: one with the C_A colour factor on the 3-end, and another on the $\bar{3}$-end, i.e.

$$_{g_I}[-\infty, C_A, \dots]_{\dots} + {}_{\dots}[\dots, C_A, \infty]_{g_I} . \quad (5.7)$$

After the evolution to an initial-state quark, which becomes the new $\bar{3}$-end of a dipole, both dipoles need to be updated to include a new C_F segment, resulting in

$$\begin{aligned}
_{g_I}[-\infty, C_A, \dots]_{\dots} &\to {}_{q_I}[-\infty, C_F, -|\eta_{q_I q_F}|, C_A, \dots]_{\dots} \\
_{\dots}[\dots, C_A, \infty]_{g_I} &\to {}_{\dots}[\dots, C_A, |\eta_{q_I q_F}|, C_F, \infty]_{q_F} ,
\end{aligned} \quad (5.8)$$

where $\eta_{q_I q_F} = -\ln \tan \theta_{q_I q_F}/2$. Instead, for the $\bar{q}_I \to g_I \bar{q}_F$ case one has

$$\begin{aligned}
_{g_I}[-\infty, C_A, \dots]_{\dots} &\to {}_{\bar{q}_F}[-\infty, C_F, -|\eta_{\bar{q}_I \bar{q}_F}|, C_A, \dots]_{\dots} \\
_{\dots}[\dots, C_A, \infty]_{g_I} &\to {}_{\dots}[\dots, C_A, |\eta_{\bar{q}_I \bar{q}_F}|, C_F, \infty]_{\bar{q}_I} .
\end{aligned} \quad (5.9)$$

Note that even though the emission is in a C_A segment, relative to the default dipole emission strength of $C_A/2$ one must apply a rejection factor of $(1-2C_F/C_A)$, because the underlying splitting function is $P_{q\to qg}$.

All other channels and the precise implementation of the algorithm are as discussed in ref. [44].

5.2 NODS

Despite capturing the dominant subleading-colour correction for the integrated rate of soft gluon emissions at NLL, as shown in ref. [44], the segment method fails in the limit where two soft and energy-ordered emissions occur at commensurate angles. Thus, a second method was explored in ref. [44], referred to as NODS. This method extends the segment method so as to provide the correct full-colour branching probability to produce any number of energy-ordered commensurate-angle pairs, as long as each pair is well separated in rapidity from all others ("NODS accuracy"). The method works by accepting a given emission with a colour acceptance probability that is the ratio of the full-colour soft matrix element, $|M^2|$, to the leading-colour one, $|M_{\rm LC}^2|$.

To illustrate the method, we again consider the case in which a gluon g_2 is emitted from a $q\bar{q}g_1$ system. The colour acceptance probability for emission of a softer gluon g_2 is given by

$$p^{\text{accept}} \equiv \frac{|M|^2}{|M_{\text{LC}}|^2} = 1 + \left(\frac{2C_F - C_A}{C_A}\right) \frac{(\bar{q}q)}{(\bar{q}g_1) + (g_1q)}, \quad (ab) \equiv \frac{p_a \cdot p_b}{(k \cdot p_a)(k \cdot p_b)}. \qquad (5.10)$$

This expression has full colour accuracy and one should recall that $(2C_F - C_A)/C_A = -1/N_C^2$. The discussion of ref. [44] showed how to generalise this formula so that it delivers the NODS accuracy for events with arbitrary numbers of gluons and quarks. If we remain with a single $\bar{q}q$ pair and an arbitrary number of gluons that are well-separated in rapidity, the correction factor relative to the large-N_C emission probability is given exactly by

$$p^{\text{accept}}(\bar{q}, 1, 2, \ldots, n, q) = 1 + \left(\frac{2C_F - C_A}{C_A}\right) \frac{(\bar{q}q)}{(\bar{q}1) + (12) + \cdots + (nq)}, \qquad (5.11)$$

which holds for each dipole. One of the observations of ref. [44] was that for a given individual large-N_C ij dipole, one can drop most of the terms in the denominator of eq. (5.11) and instead use $p^{\text{accept}}([\bar{a}], i, j, [a])$. In this context, $[\bar{a}]$ and $[a]$ are suitably chosen "auxiliary" momenta, which can in practice be any of the momenta along the $\bar{q}, 1, \ldots, q$ respectively to the left and right of ij. The auxiliaries are shown in square brackets, because if one or other of i and j is at the end of the dipole chain (with a resulting infinite extent of the C_F segment), there is no auxiliary momentum and the corresponding argument is omitted in p^{accept}.

One additional aspect of the full algorithm is the choice of what to do when there is more than one $\bar{q}q$ pair. Ref. [44] uses a product of p^{accept} factors, one for each C_F segment in the dipole (each finite extremity of a segment has an associated auxiliary momentum).[17] Another aspect is that of how to update the auxiliary momenta after a dipole branching. Suppose we have an ij dipole with a single C_F segment, whose auxiliaries are $\bar{a}$ and a. When a gluon k is emitted from that C_F segment, each of the two new dipoles, ik and kj, will inherit part of that C_F segment. Then the auxiliaries are updated so that the C_F segment of the ik dipole is assigned auxiliaries $\bar{a}$ and j, while the C_F segment of the kj dipole is assigned auxiliaries i and a. We represent this as
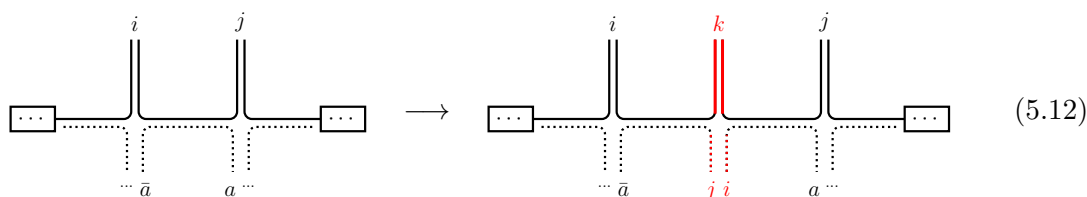
where the solid lines represent large-N_C dipoles and the dotted lines represent the relative $-1/N_C^2$ correction to the leading-N_C emission probability. Those dotted lines are labelled with the corresponding auxiliary momenta. If one or other of the $\bar{a}$ and a auxiliaries is absent from the parent dipole, it remains absent from the child dipoles.

---

[17]In practice, in NODS limit, i.e. where all pre-branching momenta are well separated in the rapidity direction in the Lund diagram, only one of the p^{accept} factors ever differs noticeably from 1.

For backwards evolution of an initial-state parton, there are some additional configurations to consider beyond those studied in ref. [44]. Backwards evolution of an initial-state quark into an initial-state quark and a final-state gluon behaves precisely as in eq. (5.12). Backwards evolution of an initial-state gluon into an initial-state quark and a final-state quark can be accounted for with the following update

$$(5.13)$$

where the dipoles associated with the initial and final-state quarks each acquire a new C_F segment, whose (single) auxiliary is given by the final and initial-state quark respectively. Finally we have the situation where an initial-state quark backwards evolves to give an initial-state gluon and a final-state anti-quark,

$$(5.14)$$

Here the existing C_F segment of the $q_I 1$ dipole is inherited by the $g_I 1$ dipole, with an additional auxiliary momentum $\bar{q}_F$, while the new $g_I \bar{q}_F$ dipole has a C_F segment with auxiliary 1.

5.3 Matrix-element tests

We perform two kinds of fixed-order tests of the colour schemes outlined above. Both involve configurations with a fixed number of energy-ordered branchings, at least one of which is an initial-state branching. In a first set of tests we fix the kinematics of a first emission and examine the branching probability for a second emission differentially in its rapidity and azimuth. In a second set of tests we consider several kinematic configurations for one or two soft emissions and verify that the integral over the rapidity and azimuth of an additional soft emission, at a fixed much smaller transverse momentum, reproduces the analytic expectation, as required for NDL accuracy for the observables such as the multiplicity. The analytic expectation coincides with the result that one would obtain by assuming an exact angular-ordered pattern for emissions. We show results just for the PanGlobal $\beta_{\rm PS} = 0$ (transverse-momentum ordered) shower, keeping in mind that the underlying implementation is common to all showers.

5.3.1 Differential tests

We fix the kinematics of a first emitted parton (which can be either a quark or a gluon) to be soft and collinear using

$$\ln \frac{v_1}{Q} = -10\,, \quad \bar{\eta}_{Q,1} = 5\,, \quad \varphi_1 = 0\,, \tag{5.15}$$

which corresponds to $z_1 = 6.69 \cdot 10^{-3}$, with a measured transverse momentum $\ln k_{t,1}/Q = -10$ and rapidity $\eta_1 = 5$. The second emission, a soft gluon, is emitted at $\ln v_2/Q = -60$, and we examine the shower branching probability differentially as a function of its direction, i.e. we sample over $\bar{\eta}_{Q,2}$ and φ_2.

Specifically, we sample over the generation variables $\bar{\eta}_Q$ and φ for emission 2. Then, we compute the angular separation between the two emissions

$$\Delta R_{12} = \sqrt{\Delta\eta_{12}^2 + \Delta\psi_{12}^2}\,, \tag{5.16}$$

where $\Delta\eta_{12}$ and $\Delta\psi_{12}$ are their difference in rapidity and azimuth. If $\Delta R_{12} > 1$, the second emission is considered to be primary, and we examine its distribution differentially in the rapidity η and azimuth ψ defined with respect to the beam direction. Otherwise it is secondary, i.e. emitted predominantly from the first emission, and we examine its distribution differential in a rapidity η and an azimuthal angle ψ defined with respect to emission 1. The relevant analytic expectations are provided in appendix C.

The results for the segment and NODS colour schemes are shown in the first two rows of figures 8 and 9, for $q\bar{q} \to Z$ and $gg \to H$ production respectively (the bottom two rows are discussed further below). We separate the cases in which the second emission is either primary (left-hand panels of each plot) or secondary (right-hand panels). Let us first focus on the ratio between the parton shower and the analytic LC result (obtained using $C_A = 2C_F = 3$, upper panels of each plot). In most regions, the value of this ratio for all cases is either 1, when the effective colour factor is $C_A/2$, or 8/9 if the emission occurs with an additional $2C_F/C_A$ relative weight. The other quantity that is displayed is the deviation between the shower and the analytic result at full colour (lower panels of each plot). The segment method fails to describe the colour pattern if the two emissions have commensurate angles. The size of the deviation depends on the azimuthal angle ψ. However, as we will see below, the deviation vanishes after integrating over angular phase space. The NODS scheme reproduces the exact full-colour matrix element in all double-emission configurations.

For completeness, in the bottom two rows, figures 8 and 9 also show results for the colour-factor-from-emitter (CFFE) approach. This scheme is implemented in standard dipole showers, and the colour factor that multiplies the splitting function is determined according to whether the emitter (as determined by the shower) is a (anti-)quark or a gluon. The results with the CFFE approach depend on how one decides which of the two dipole ends is the emitter, and so we show CFFE with both the PanGlobal shower (penultimate row) and the Dipole-k_t shower (last row), with the latter corresponding to the behaviour expected in standard dipole showers. Labelling the rapidity of the first final-state emission as η_1 (equal to 5), CFFE with the PanGlobal showers gives the wrong answer on the primary plane (left-hand panels) when the second emission has $0 \lesssim \eta \lesssim \eta_1$ (except in the $g_I g_I \to H g_F$ case). For a $q\bar{q}$ initial state, i.e. figure 8 (left), CFFE with the Dipole-k_t shower gives wrong answers in the logarithmically extended region

$$-2.5 = \frac{1}{2}\left(\eta_1 - \ln\frac{Q}{k_{t,1}}\right) < \eta < \frac{1}{2}\left(\eta_1 + \ln\frac{Q}{k_{t,1}}\right) = 7.5\,, \tag{5.17}$$
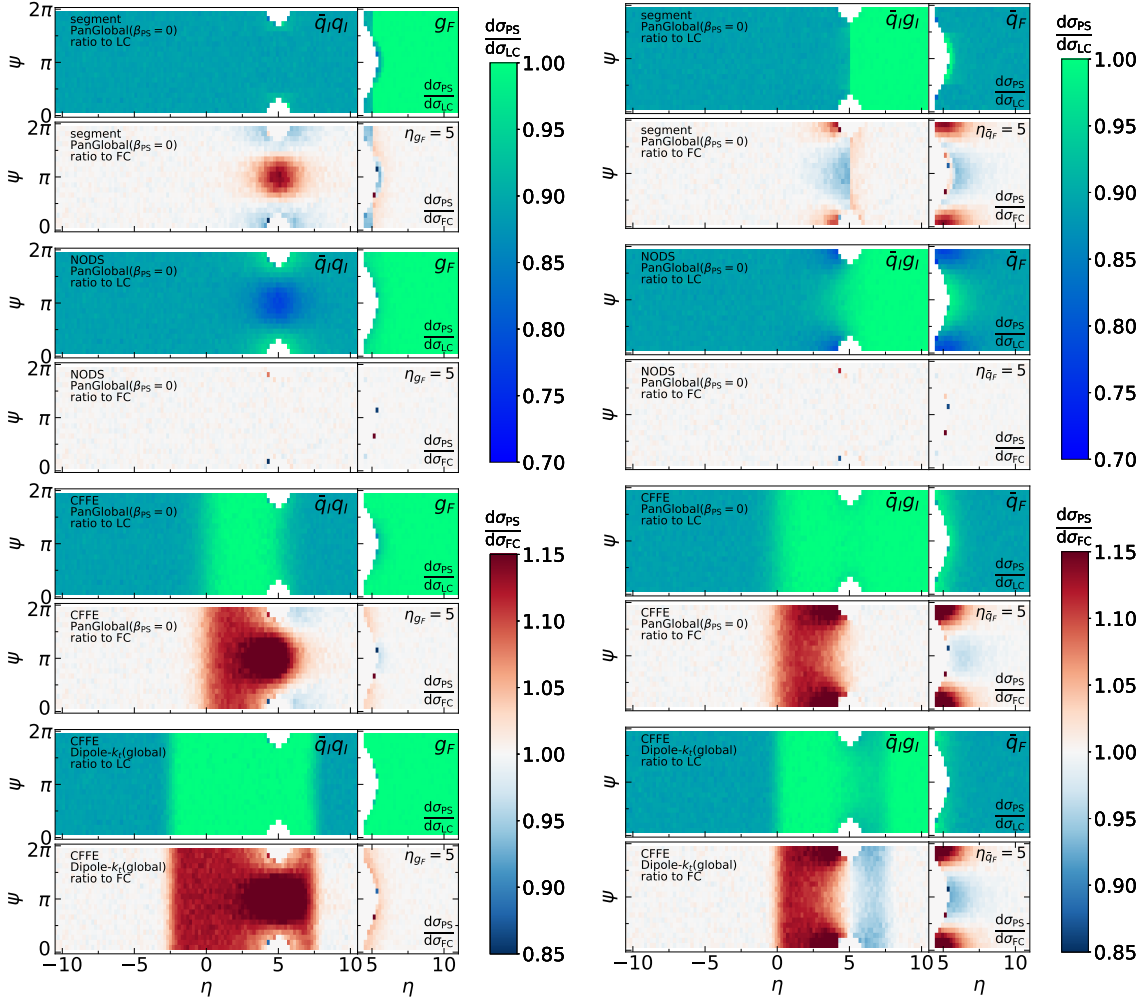
– 29 –

Figure 8. Density for the emission of a soft gluon from a $q_I \bar{q}_I \to Z g_F$ (left) or $g_I \bar{q}_I \to Z \bar{q}_F$ (right) system in the rapidity-azimuth plane. From top to bottom, the rows show the segment, NODS and CFFE methods with the PanGlobal shower, and the CFFE method with the Dipole-k_t shower. For each plot, the upper panels display the ratio between the parton shower differential cross section and the leading colour result, $d\sigma_{\mathrm{PS}}/d\sigma_{\mathrm{LC}}$. The LC parton-shower result is obtained setting $C_A = 2C_F = 3$, i.e. an emission strength $C_A/2 = 3/2$ for each dipole. The lower panels show the deviation from the FC differential matrix element, given in appendix C, $d\sigma_{\mathrm{PS}}/d\sigma_{\mathrm{FC}}$. For each plot, the left-hand panels correspond to emissions from the incoming partons (in the sense of a Cambridge/Aachen algorithm with jet radius $R = 1$ [92, 93]), whereas the right-hand panels correspond to emissions from the first emitted parton (either g_F or $\bar{q}_F$).
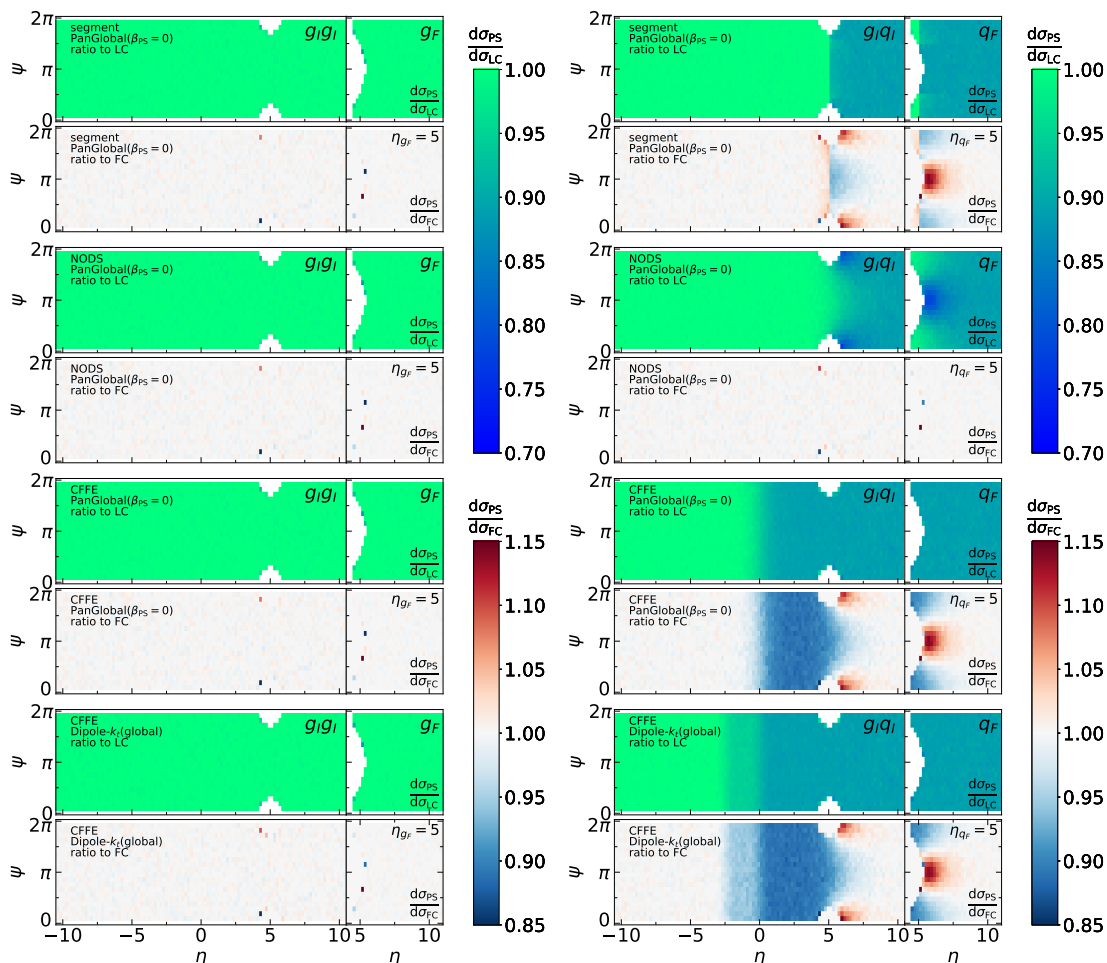
Figure 9. Same as figure 8 but for emission of a soft gluon from $g_I g_I \to H g_F$ (left) and $g_I q_I \to H q_F$ (right) systems.

as expected from the analysis in refs. [42, 44]. Note that this is the same region where recoil is misassigned for this configuration, cf. eq. (3.3). Where the initial state is $\bar{q}g$ or gq (the right-hand columns, respectively, of figures 8 and 9), there are rapidity regions with two dipoles simultaneously in play, each of which have different regions of incorrect colour, resulting in a more complex overall structure.

5.3.2 Integrated tests

Next, we integrate the differential cross section over the emission angles for the soft gluon to obtain the overall rate of emissions from the shower, I_{PS}. We compare the result to the analytic full-colour expectation, I_{FC}. We perform these comparisons for configurations where the first emission (whose direction is *not* integrated over) is either soft and collinear, hard and collinear, or soft and large-angle with respect to the initial-state emitting system.[18]

---

[18]Explicitly, we set $\ln v_1/Q = -10$ and take $\bar{\eta}_{Q,1} = 5$ (soft collinear), $\bar{\eta}_{Q,1} = 11.09861$ (hard collinear), and $\bar{\eta}_{Q,1} = 0$ (soft, large angle). The corresponding z_1, η_1 values are quoted in figure 10.
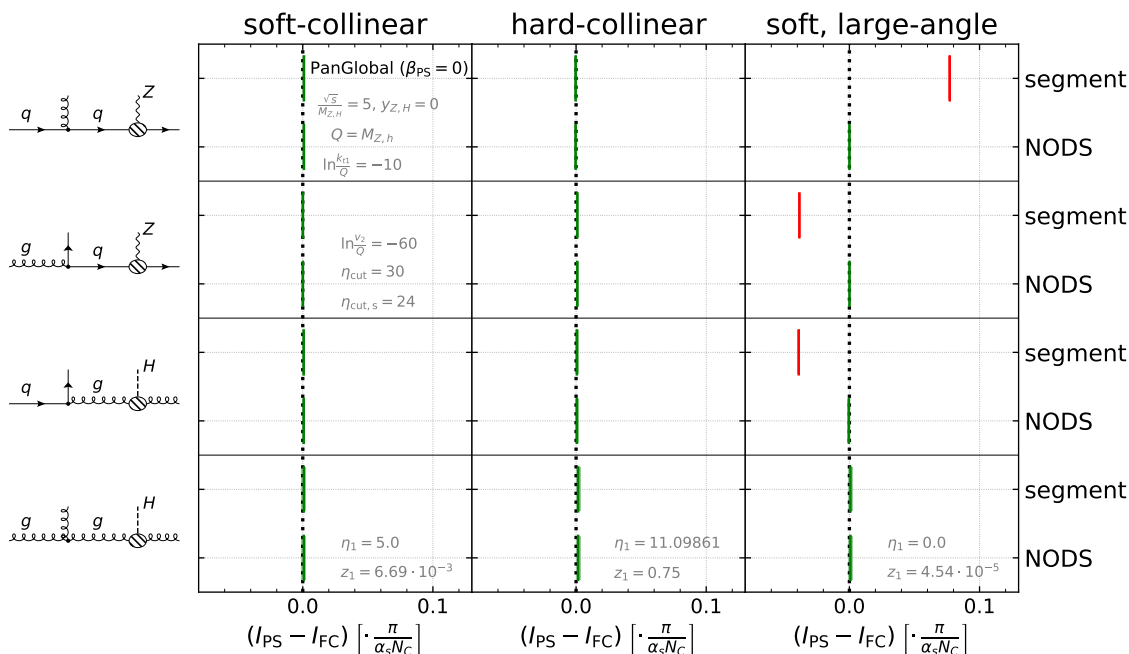
Figure 10. Normalised deviation of the integrated rate of a single soft emission (emission 2), as produced by the parton shower I_{PS} from the configurations in the left-hand column, relative to the exact analytic results I_{FC} quoted in appendix C. We show four configurations, two for the $q\bar{q} \to Z$ event, and one for the $gg \to H$ event, and only consider initial-state splittings (the results for final-state splittings may be found in ref. [44]). For each configuration, we show three kinematics regimes for the first emission, as labelled at the top of the plot (and detailed at the bottom). For each configuration and kinematic regime, we show results for both the segment and NODS colour schemes. The colours of the lines indicate whether the result is consistent with zero.

The second emission is radiated at a fixed $\ln v_2/Q = -60$ and we impose a collinear regulator that takes a different value depending on whether the emission is primary $\eta_{cut} = 30$ or secondary $\eta_{cut,s} = 24$.[19] The integrated rate is computed for all possible branching histories: starting with $q\bar{q} \to Z$, (i) the backwards evolution of a quark into a gluon while emitting a quark ($q_1 g$), (ii) the backwards evolution into a quark while emitting a gluon ($g_1 g$); and starting with $gg \to H$, (iii) the backwards evolution of a gluon into a gluon while emitting a gluon ($g_1 g$), and (iv) the backwards evolution into a quark while emitting a quark ($q_1 g$). The analytic expectations for I_{FC} are derived in appendix C.

We show the comparison between I_{PS} and I_{FC} in figure 10 where the specific values for the kinematics of the first emission, i.e. z_1 and η_1, are indicated on the plot. The NODS colour scheme reproduces the FC analytic integral in all cases. The segment method fails to describe the analytic result for the soft large-angle configuration except in the $g \to gg$ case, where there are no C_F segments. This failure was already observed for final-state splittings in ref. [44] and it is due to the discrepancy between the physical η and η_{approx},

---

[19]The reason for having two different regulators is to avoid any type of artificial cancellations that could lead to an apparent agreement between the shower and the analytics even if the implementation is not correct.
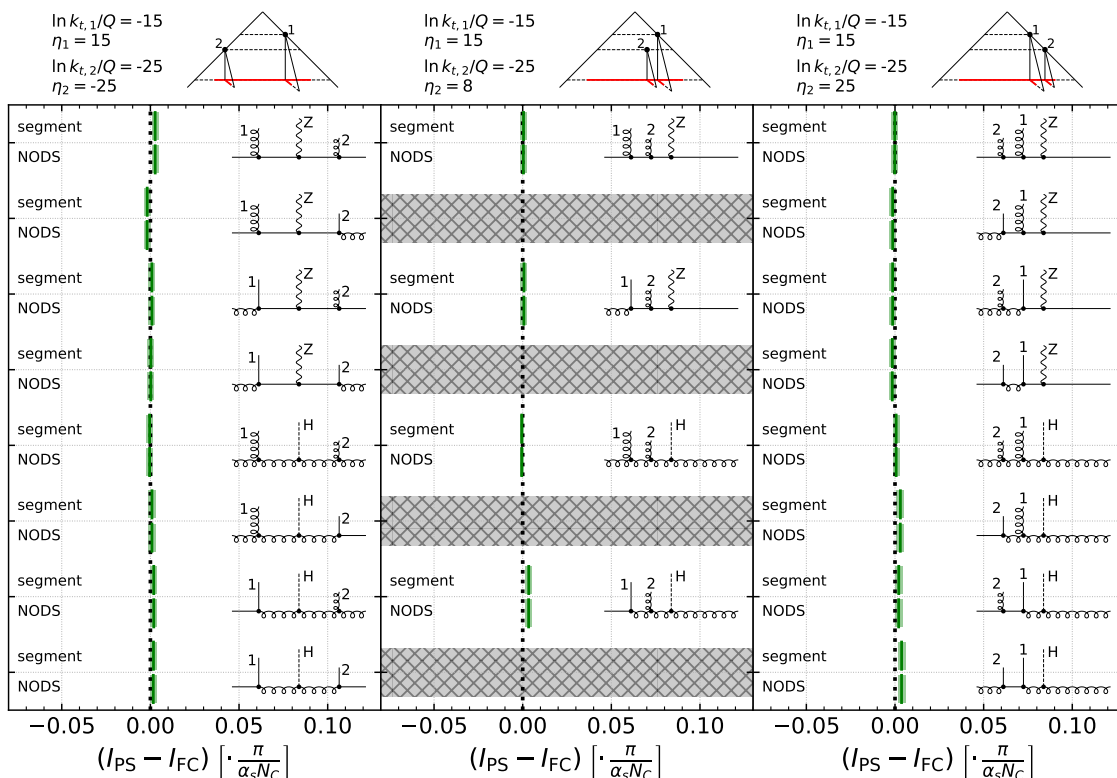
Figure 11. Similar to figure 10, but for soft emission from configurations with two prior initial-state emissions (well separated in rapidity, at least one of which is hard).

given by eq. (5.2), in the large-angle regime. The disagreement vanishes in the case of $g \to gg$ since in this case the leading and full-colour results are identical.

Our last colour test considers three emissions. We fix the first emission, which can be either a quark or a gluon, at

$$\ln \frac{v_1}{Q} = -15, \quad \bar{\eta}_{Q,1} = 15, \quad \varphi_1 = 0. \tag{5.18}$$

Then, the shower generates a second lower-$\ln v$ emission (quark or gluon) with $\ln v_2/Q = -25$ and $\varphi_2 = \pi/3$. To reduce the number of possibilities, we impose that this second emission is a primary one. We consider three kinematic configurations: (i) opposite hemisphere, i.e. $\bar{\eta}_{Q,2} < 0$, (ii) same hemisphere with $0 < \bar{\eta}_{Q,2} < \bar{\eta}_{Q,1}$, and (iii) same hemisphere with $0 < \bar{\eta}_{Q,1} < \bar{\eta}_{Q,2}$. At this stage, taking all the possible flavor combinations into account, each of the previous kinematic configurations correspond to a total of $8, 4$ and 8 cases, respectively.

The third emission is then fixed to be a soft-collinear gluon with $\ln v_3/Q = -45$, and arbitrary $\bar{\eta}_{Q,3}, \varphi_3$.

This gluon may effectively be a primary emission or radiated off either the first or second emission. As for the double-emission case, the third gluon contributes to the total integrated rate if it satisfies $\eta_3 < \eta_{\text{cut}}(\eta_{\text{cut,s}})$ depending on whether it is a primary or secondary emission. The analytic expectations are presented in appendix C. The difference

between the shower and the analytic result is shown in figure 11. We find a perfect agreement between the shower and the analytic calculation with either of the two colour schemes. Notice that the segment method satisfies this test in all cases since we are imposing that the first and second emissions are collinear. For the segment scheme, we would have encountered the same problem as in the double-emission case if either had been radiated at a large angle.

We have thus thoroughly tested the extension of both colour schemes to initial-state radiation, up to $\mathcal{O}\left(\alpha_s^3\right)$, and shown that they behave as expected.

6 Spin correlations

The last ingredient that we incorporate into our showers is an algorithm to include spin correlations. These are essential to correctly reproduce the azimuthal structure of strongly angular-ordered collinear splittings, and so achieve full NLL accuracy according to the matrix-element part of the PanScales conditions outlined on p. 1. In refs. [45, 46], spin correlations were included in the PanScales e^+e^- showers using an approach based on the Collins-Knowles algorithm [94–97]. While Collins [94] originally proposed an algorithm to include spin correlations for final-state showers, Knowles [95–97] extended the procedure to initial-state radiation and backwards evolution. In this work, we extend the PanScales spin-correlation implementation to hadron-hadron collisions, and validate it, as in the colour case, by comparison to analytic matrix elements up to $\mathcal{O}(\alpha_s^3)$. Relative to the Collins-Knowles algorithm, the PanScales spin-correlation algorithm also accounts for the (dominant) large-N_C part of the spin correlations in soft emissions [46].

6.1 Spin-correlation algorithm and extension to initial-state branching

The starting point is the procedure outlined in refs. [45], which successfully includes spin correlations in any dipole or antenna shower. The fundamental building blocks are the collinear branching amplitudes $\mathcal{M}_{i\to\tilde{i}k}^{\lambda_{\tilde{i}}\lambda_i\lambda_k}$, which can be written in terms of helicity-dependent splitting functions $\mathcal{F}_{i\to\tilde{i}k}^{\lambda_{\tilde{i}}\lambda_i\lambda_k}(z)$ and a spinor product $S_\tau(p_i, p_k)$, i.e.

$$\mathcal{M}_{i\to\tilde{i}k}^{\lambda_{\tilde{i}}\lambda_i\lambda_k} = \frac{1}{\sqrt{2}}\frac{g_s}{p_i \cdot p_k}\mathcal{F}_{i\to\tilde{i}k}^{\lambda_{\tilde{i}}\lambda_i\lambda_k}(z)\, S_\tau(p_i, p_k)\,. \tag{6.1}$$

The spin indices of the particles $i \to \tilde{i}k$ are denoted $\lambda_{\tilde{i},i,k} = \pm 1$. Note that in our convention, for initial-state splittings, the order of spin indices in the superscript of $\mathcal{M}_{i\to\tilde{i}k}^{\lambda_{\tilde{i}}\lambda_i\lambda_k}$ differs from that of particle indices in the subscript (similarly for $\mathcal{F}$). This choice facilitates re-use of code between our initial and final-state implementations of spin correlations. The label $\tau = \pm 1$ for the spinor product indicates the sign of the complex phase (following the convention of ref. [98]), with

$$\tau = \tilde{\lambda}_i + \tilde{\lambda}_k - \tilde{\lambda}_{\tilde{i}} \text{ where } \tilde{\lambda} = \begin{cases} \lambda/2 \text{ for a quark,} \\ \lambda \text{ for a gluon.} \end{cases} \tag{6.2}$$

A derivation of the branching amplitudes for final-state collinear splittings, $\mathcal{M}_{\tilde{i}\to ik}^{\lambda_{\tilde{i}}\lambda_i\lambda_k}$, was presented in ref. [45]. In appendix D of this work we extend this derivation to include

$\lambda_{\tilde{\imath}}$	λ_i	λ_k	$q_I \to \tilde{q}_I g_F$	$g_I \to \tilde{q}_I \bar{q}_F$	$g_I \to \tilde{g}_I g_F$	$q_I \to \tilde{g}_I q_F$
λ	λ	λ	$\dfrac{1}{\sqrt{z(1-z)}}$	0	$-\dfrac{1}{\sqrt{z(1-z)}}$	$-\dfrac{1}{1-z}$
λ	λ	$-\lambda$	$\sqrt{\dfrac{1-z}{z}}$	$\sqrt{1-z}$	$-\dfrac{1-z}{\sqrt{z}}$	0
λ	$-\lambda$	λ	0	0	0	0
λ	$-\lambda$	$-\lambda$	0	$-\dfrac{z}{\sqrt{1-z}}$	$-\dfrac{z^{3/2}}{1-z}$	$-\dfrac{z}{1-z}$

Table 1. The helicity-dependent Altarelli-Parisi splitting amplitudes $\mathcal{F}_{i\to\tilde{\imath}k}^{\lambda_{\tilde{\imath}}\lambda_i\lambda_k}(z)$ that appear in eq. (6.4), using the convention of eq. (2.2) where $\tilde{\imath}$ evolves backwards to i while emitting k such that $p_k = z/(1-z)\tilde{p}_i$, $p_i = 1/(1-z)\tilde{p}_i$. Aside from overall colour factors, the amplitudes satisfy the relation $(1-z)\sum_{\lambda_i,\lambda_k} |\mathcal{F}_{i\to\tilde{\imath}k}^{\lambda_{\tilde{\imath}}\lambda_i\lambda_k}(z)|^2 = P_{i\to\tilde{\imath}k}(z)$, with the $P_{i\to\tilde{\imath}k}(z)$ as given in eqs. (A.1).

initial-state collinear branchings. The resulting helicity-dependent splitting amplitudes $\mathcal{F}_{i\to\tilde{\imath}k}^{\lambda_{\tilde{\imath}}\lambda_i\lambda_k}(z)$ for backwards initial-state splittings are summarised in table 1.[20] The Collins-Knowles algorithm then makes use of these branching amplitudes to construct a binary tree following the shower history. This data structure facilitates the efficient computation of spin-density matrices for new shower branchings, which are used to sample the azimuthal distribution of that branching.[21]

The regime of validity of the Collins-Knowles algorithm is limited to collinear $1 \to 2$ branchings. An extension to correctly model the azimuthal distribution of soft large-angle branchings at leading colour was presented in ref. [46] for final-state branchings. The colour-stripped amplitude for the emission of a soft gluon from a colour dipole follows the eikonal approximation, and, for example for an initial-initial dipole, reads

$$\mathcal{M}_{ij\to\tilde{\imath}\tilde{\jmath}k}^{\lambda_k}(\ldots,p_i,p_j,p_k\ldots) = g_s \left(\frac{p_i \cdot \epsilon_{\lambda_k}^*(p_k)}{p_i \cdot p_k} - \frac{p_j \cdot \epsilon_{\lambda_k}^*(p_k)}{p_j \cdot p_k} \right) \mathcal{M}(\ldots,\tilde{p}_i,\tilde{p}_j,\ldots), \quad (6.3)$$

with $g_s \equiv \sqrt{4\pi\alpha_s}$ and an implicit constraint $\delta_{\lambda_{\tilde{\imath}}\lambda_i}\delta_{\lambda_{\tilde{\jmath}}\lambda_j}$. Note that helicity flips of the parent dipole partons are suppressed in the soft limit, and we do not account for them here.

Although formulated in terms of $1 \to 2$ kinematics, the Collins-Knowles algorithm can still be modified to account for soft wide-angle emission, because the eikonal approximation does not depend on the spin of the dipole legs i and k. The branching amplitudes of eq. (6.1) have to be modified such that the $i \to \tilde{\imath}k$ branching acquires a dependence on the kinematics of the $\tilde{\imath}$'s dipole partner $\tilde{\jmath}$. Eq. (6.3) can be rewritten as (see appendix D)

$$\mathcal{M}_{ij\to\tilde{\imath}\tilde{\jmath}k}^{\lambda_k}(\ldots,p_i,p_j,p_k\ldots) = \sqrt{2}g_s \frac{S_{-\lambda_k}(p_i,p_j)}{S_{-\lambda_k}(p_i,p_k)S_{-\lambda_k}(p_j,p_k)}\mathcal{M}(\ldots,\tilde{p}_i,\tilde{p}_j,\ldots). \quad (6.4)$$

This implies that soft corrections can be included in the collinear branching amplitudes in the case $\lambda_{\tilde{\imath}} = \lambda_i$, leading to

$$\mathcal{M}_{i\to\tilde{\imath}k}^{\lambda\lambda\lambda_k} = \sqrt{2}g_s\sqrt{z}\,\mathcal{F}_{i\to\tilde{\imath}k}^{\lambda\lambda\lambda_k}(z) \, \frac{S_{-\lambda_k}(p_i,p_j)}{S_{-\lambda_k}(p_i,p_k)S_{-\lambda_k}(p_j,p_k)}, \quad (6.5)$$

---

[20]These amplitudes coincide with the final-state ones in table 1 of ref. [45] after replacing $z \leftrightarrow (1 - z)$, including an overall factor of $\sqrt{z}$, exchanging $\lambda_{\tilde{\imath}} \leftrightarrow \lambda_i$ and, in the case of incoming gluons, accounting for a further factor of -1.

[21]In the case of an antenna shower, we use $g(\bar{\eta}_Q)$ to decide which dipole leg acts as the emitter.

One initial, then one final			
Primary splitting		Secondary splitting	
$q_I \to \tilde{q}_I g_F$	$A(z) = \frac{2(1-z)}{1+(1-z)^2}$	$g_F \to q_F \bar{q}_F$	$B(z) = \frac{-2z(1-z)}{1-2z(1-z)}$
$g_I \to \tilde{g}_I g_F$	$A(z) = \frac{(1-z)^2}{(1-z(1-z))^2}$	$g_F \to g_F g_F$	$B(z) = \frac{z^2(1-z)^2}{(1-z(1-z))^2}$

Two initial, same side			
Primary splitting		Secondary splitting	
$g_I \to \tilde{q}_I \bar{q}_F$	$A(z) = \frac{-2z(1-z)}{1-2z(1-z)}$	$q_I \to \tilde{g}_I q_F$	$B(z) = \frac{2z}{1+z^2}$
$g_I \to \tilde{g}_I g_F$	$A(z) = \frac{z^2(1-z)^2}{(1-z(1-z))^2}$	$g_I \to \tilde{g}_I g_F$	$B(z) = \frac{z^2}{(1-z(1-z))^2}$

Two initial, opposite side	
$q_I \to \tilde{g}_I q_F$	$A(z) = B(z) = \frac{2z}{1+z^2}$
$g_I \to \tilde{g}_I g_F$	$A(z) = B(z) = \frac{z^2}{(1-z(1-z))^2}$

Table 2. The coefficients $A(z)$ and $B(z)$ in eq. (6.6) for all possible sequences that involve at least one initial-state branching and non-zero spin correlations. The separate cases correspond with a final-state secondary branching (top), a same-side initial-state secondary branching (middle), and an opposite-side initial-state secondary branching (bottom). These results complement the corresponding final-state ones given in table 2 of ref. [45]

and analogously for initial-final and final-final dipoles. Note that the identification of a colour partner is only unambiguous in the large-N_C limit. Therefore, our results for soft-spin correlations are only correct at LC.[22] Collinear spin correlations are not affected by this. The spinor products are evaluated numerically using the techniques explained in appendix A of ref. [45], where special care is required in choosing a reference spinor direction in the soft limit, as is detailed in appendix C of ref. [46]. The algorithm itself remains unchanged when extended to the initial state, and details are given in section 2.2 of ref. [45].

6.2 Matrix-element tests

We validate our implementation of spin correlations at fixed order by comparing the shower weight to analytic results as a function of the azimuthal angle $\Delta\psi_{ij}$ between the planes spanned by emissions i and j. At $\mathcal{O}(\alpha_s^2)$, the differential cross section can be written as

$$\frac{d\sigma}{d\Delta\psi_{ij}} \propto a_0 \left(1 + \frac{a_2}{a_0}\cos(2\Delta\psi_{ij})\right) = a_0\left(1 + A(z_i)B(z_j)\cos(2\Delta\psi_{ij})\right),\qquad(6.6)$$

where the two non-zero Fourier coefficients a_0 and a_2 depend on the type of branching, and on the momentum fractions associated with the first (z_i) and second (z_j) splitting. The ratio a_2/a_0 is equal to 0 in the absence of spin correlations. The analytic expressions for

---

[22]Ref. [46] investigated the size of subleading colour effects in the soft spin case for e^+e^- collisions and they were never larger than a few percent.
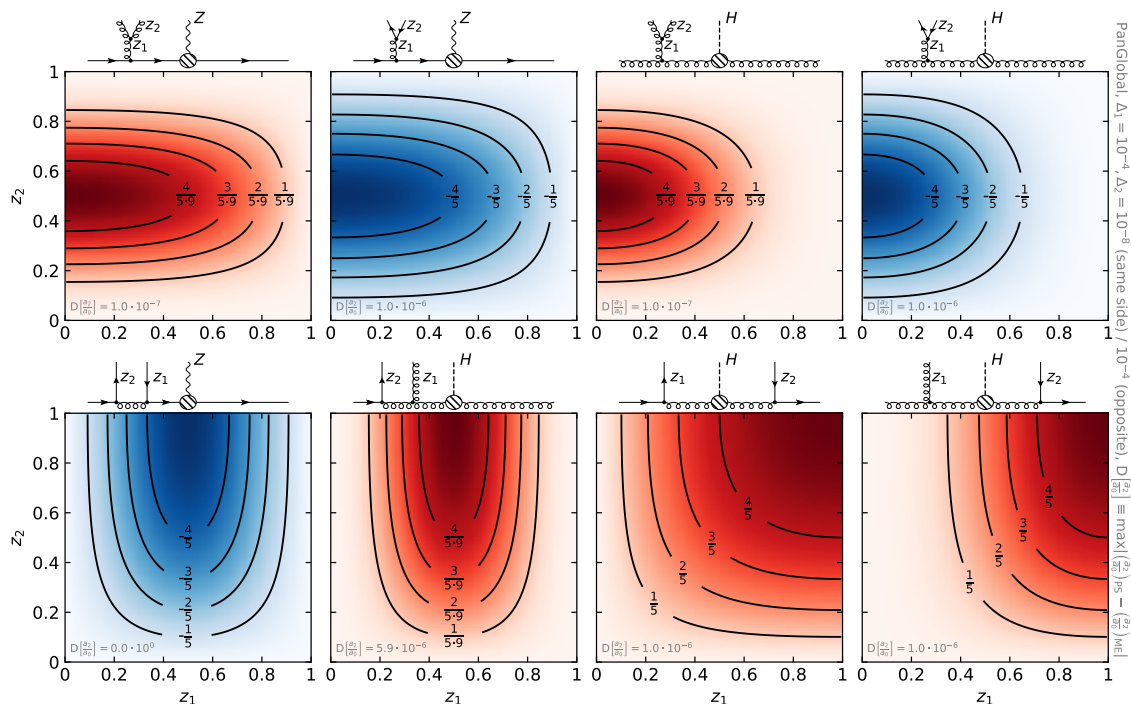
Figure 12. Size of the spin correlations a_2/a_0 at $\mathcal{O}(\alpha_s^2)$ for collinear splittings. The Feynman diagrams indicate the sequence of splittings under consideration. We study the azimuthal difference between the plane defined by the primary and secondary splittings with momentum fraction z_1 and z_2, respectively. The colour indicates the size of a_2/a_0 as predicted by the shower. Black lines indicate constant values for this ratio, and are obtained using the analytic predictions of table 2. The maximum deviation of the analytic prediction and the shower is given by $\mathrm{D}\left[\frac{a_2}{a_0}\right] \equiv \max\left|\left(\frac{a_2}{a_0}\right)_{\mathrm{PS}} - \left(\frac{a_2}{a_0}\right)_{\mathrm{ME}}\right|$, with $\left(\frac{a_2}{a_0}\right)_{\mathrm{PS}}$ the shower prediction and $\left(\frac{a_2}{a_0}\right)_{\mathrm{ME}}$ the analytic prediction for the matrix element.

$A_i(z_i)$ and $B_j(z_j)$ are given in table 2. As was the case for the colour tests, we only show results for the PanGlobal shower with $\beta_{\mathrm{PS}} = 0$, given that the implementation is largely identical across all showers.

To begin with, we consider purely collinear branchings at $\mathcal{O}(\alpha_s^2)$, where a first initial-state branching is followed by either (i) a final-state branching, (ii) another initial-state branching of the same parton, or (iii) another initial-state branching on the opposite site. The shower-to-analytics comparison of the a_2/a_0 ratio as a function of z_1 and z_2 across a number of branching sequences is shown in figure 12. The coloured background shows the shower result, while the black contour lines indicate the analytic expectation given by table 2. The largest absolute magnitude of the deviation between the shower and the analytic result, $\mathrm{D}[a_2/a_0]$, is indicated in the lower left corner of each panel.[23] No cases with intermediate quarks are shown, as they have vanishing spin correlations. The top row shows cases where an initial-state gluon emission is followed by a final-state splitting of that same gluon. The ratio a_2/a_0 is negative when the final-state gluon splits to a quark-anti-

---

[23]Small deviations are expected because the splittings angles that we use, while small, are not asymptotically so.

quark pair, and positive when it splits to a gluon-gluon pair. Spin correlations are maximal when $z_1 \to 0$ and $z_2 = 0.5$, i.e. the gluon is soft and the energy is shared equally between the final-state partons. This can be deduced from table 2. The spin correlations for the $g \to gg$ final-state splittings fall off more steeply as $z_2 \to 0$ or 1, and its absolute maximum size is smaller (1/9) than the $g \to q\bar{q}$ splittings (1). We also observe that spin-correlations as $z_1 \to 1$ decrease more rapidly for gluon backwards splittings than for quarks.

The two leftmost panels in the bottom row of figure 12 show the spin correlations resulting from two subsequent initial-state branchings on the same side. Splitting configurations with non-vanishing spin correlations occur in both Z and H production processes. For brevity, we only show the cases where an intermediate gluon is produced, which then backwards evolves into a quark. This time, spin correlations are maximal when $z_1 = 0.5$, $z_2 \to 1$, but vanish when $z_1 \to 0, 1$ and $z_2 \to 0$.[24]

Finally, the two rightmost panels in the bottom row of figure 12 show the spin correlations in opposite-side initial-state branchings. These peak at $z_1, z_2 \to 1$, i.e. the limit where the emitted partons are soft, and vanish for either $z_1 \to 0$ or $z_2 \to 0$. The case where both gluons backwards evolve into a quark is necessarily symmetric in the z_1, z_2 plane, whereas a backwards evolution into a gluon again leads to an enhanced reduction in a_2/a_0 as $z_1 \to 0$. The case where both gluons backwards evolve into a gluon is not shown in the figure. It behaves similarly to the case where both gluons backwards evolve into a quark, but with a stronger drop off as $z_1, z_2 \to 0$.

In figure 13 we repeat the same exercise as in figure 12, but with kinematic configurations in which one or more branchings are soft. In this case, the analytic calculation is obtained by crossing the relevant matrix elements in the soft limit, given in appendix A of ref. [45]. On the two leftmost plots, we examine configurations at $\mathcal{O}(\alpha_s^2)$, where a soft-wide angle gluon g_1 with energy fraction z_1 is emitted from the initial-state dipole $q\bar{q}$. This gluon then splits collinearly as $g_1 \to gg$ (first plot) or $g_1 \to q\bar{q}$ (second plot) with momentum fraction z_c. We scan over the rapidity y_1 of gluon g_1 relative to the $q\bar{q}$ system between $-2 < y_1 < 2$, and over the energy fraction z_c of the emitted parton (g or q). Spin correlations are in this case independent of the rapidity of the soft gluon.[25] The spin correlations are again maximal in absolute size when the energy fraction of the gluon is shared equally between the two final-state partons.

A more interesting pattern appears at $\mathcal{O}(\alpha_s^3)$ as displayed in the two rightmost panels of figure 13. In this case we study the azimuthal correlations between the first and third emission. The first gluon emission is now fixed at $y_1 = 1$ with an energy fraction $z_1 = 10^{-4}$, while we scan the rapidity of a second gluon emission between $-2 < y_2 < 2$ with $z_2 = 10^{-8}$, which then splits collinearly. The two soft gluons are emitted at different azimuthal angles, $\Delta\psi_{12} = 1$. Because we fix $\Delta\psi_{12}$, the analytical form for the azimuthal correlations needs

---

[24]There are two additional cases not shown, namely where the initial-state gluon backwards evolves into a new initial-state gluon and emits a final-state one, which carry the same sign and show the same behaviour, except that the spin correlations drop off more sharply as $z_1 \to 0, 1$ and $z_2 \to 0$.

[25]A purely collinear Collins-Knowles algorithm would in general not correctly reproduce this pattern [46].
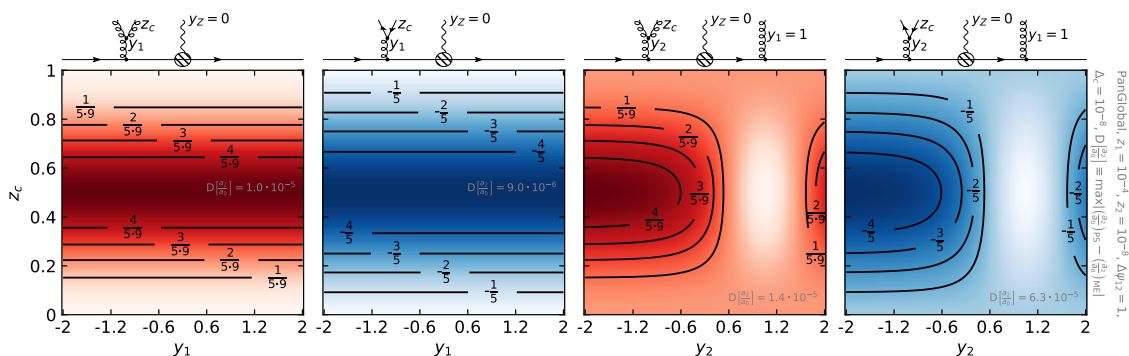
Figure 13. Size of the spin correlations for sequences that involve both soft and collinear splittings, showing a_2/a_0 at $\mathcal{O}(\alpha_s^2)$ (two left-hand plots) and $\mathcal{O}(\alpha_s^3)$ (two right-hand plots). The Feynman diagrams indicate the sequence of splittings under consideration for all cases. We consider the azimuthal difference between the plane defined by the primary soft splitting with momentum fraction z_1 (z_2), and the plane defined by the second (third) splitting with momentum fraction z_c. The colour indicates the size of a_2/a_0 as predicted by the shower. Black lines indicate constant values for this ratio, and are obtained by using crossing relations in the matrix elements calculated in ref. [45] for final-state configurations.

to be extended relative to eq. (6.6), and now reads

$$\frac{d\sigma}{d\Delta\psi_{13}} \propto a_0 \left(1 + \frac{a_2}{a_0} \cos(2\Delta\psi_{13}) + \frac{b_2}{a_0} \sin(2\Delta\psi_{13}) \right). \tag{6.7}$$

We plot just the ratio a_2/a_0 and see that it is enhanced when the second gluon is emitted with a larger rapidity difference with respect to the first gluon, and when its energy fraction is shared equally between the children ($z_c = 0.5$).

Finally, we also check the spin correlations at $\mathcal{O}(\alpha_s^3)$ for collinear splittings. We consider two configurations: (i) one backwards splitting followed by two final-state emissions, and (ii) two backwards splittings on opposite hemispheres followed by one final-state splitting. For case (i) we consider both $q\bar{q} \to Z$ and $gg \to H$, whereas for case (ii) we only consider $gg \to H$, as $q\bar{q} \to Z$ features no spin correlations due to the intermediate quark line. The azimuthal angle of the first emission is fixed to $\psi_1 = 0$. For the second emission we fix both the longitudinal momentum fraction $z_2 = 0.5$ and the azimuthal angle $\psi_2 = \pi/6$ (if emission 2 is secondary from 1, this is the angle between the $1-2$ plane and the beam-1 plane; if it is primary, it is the angle between the beam-2 plane and the beam-1 plane). Further, we fix the angles of these three collinear emissions with respect to the emitter at $\Delta_1 = 10^{-4}$, $\Delta_2 = 10^{-8}$, and $\Delta_3 = 10^{-12}$. Finally, we integrate over the azimuthal angle ψ_3 to obtain the Fourier coefficients in eq. (6.7) and scan over z_1 and z_3.

In figure 14, we also show the resulting ratio a_2/a_0 as a function of z_1 and z_3.[26] Overall, we find an excellent agreement between the shower and the analytic expectations.

---

[26]The z_2-dependence of $\Delta\psi_{13}$ is given as an overall normalisation, which reads

$$\frac{(1-z_2)^2}{(1-z_2+z_2^2)^2} \tag{6.8}$$

for a final-state splitting of a gluon into a gluon-gluon pair, relevant for the splittings considered for
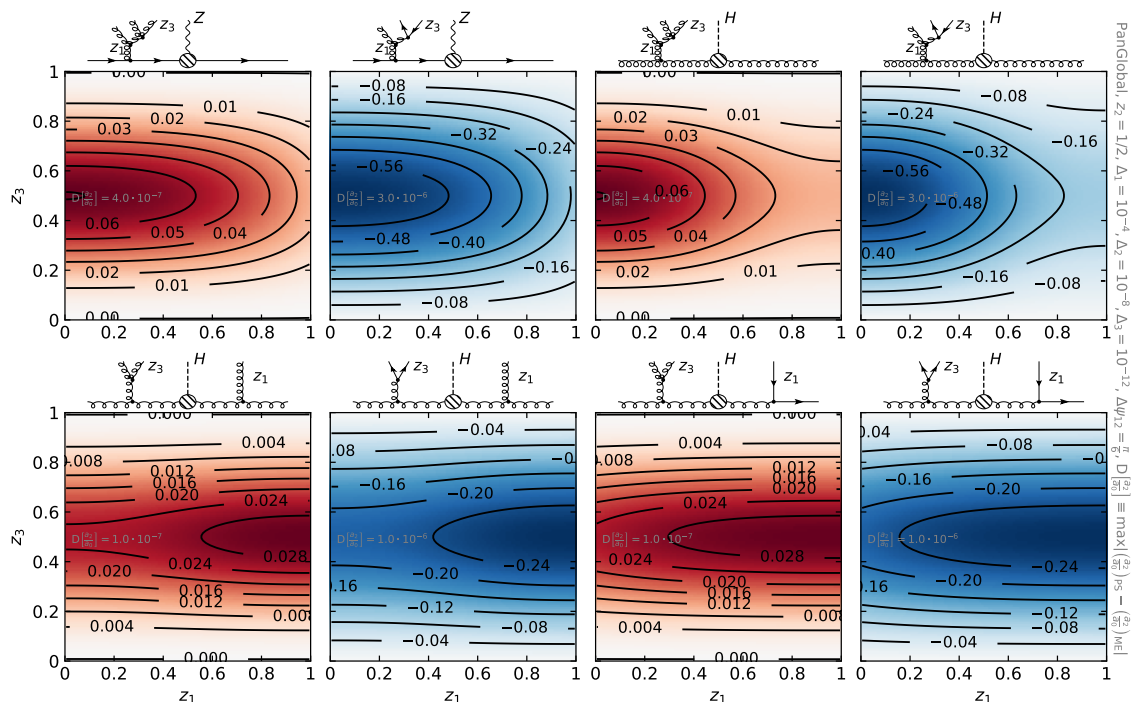
Figure 14. Analogue of figure 12, but for the spin correlations a_2/a_0 at $\mathcal{O}(\alpha_s^3)$ for three collinear splittings. The first splitting carries a longitudinal momentum fraction z_1, the third one z_3. We fix the longitudinal momentum fraction of the second emission to $z_2 = 0.5$, and its azimuthal angle such that $\Delta\psi_{12} = \pi/6$.

The shape and magnitude of the spin correlations are strongly dependent on ψ_2, and for reference, in figure 15 we show the spin correlations if we change ψ_2 to $\pi/2$.

The tests that we have shown in this section provide solid validation of the correctness of the spin-correlation implementation in the PanScales showers, also for initial-state branching.

7 Conclusions

In this work we have introduced new dipole showers applicable to colour-singlet production processes in hadronic collisions, extending earlier PanScales work on final-state showers [43].

The hadron-collider PanGlobal shower, section 4.2, shares the characteristic of the final-state case that the dipole map assigns only longitudinal recoil to the dipole parent particles. The detailed mechanism to ensure energy-momentum conservation differs, with

---

configuration (i) (upper row of figure 14), and

$$\frac{(1-z_2)^2 z_2^2}{(1-z_2+z_2^2)^2} \tag{6.9}$$

for the backwards splitting of an initial-state gluon into a final-state gluon and a new initial-state gluon, relevant for configuration (ii) (lower row of figure 14). For $z_2 = 0.5$, the overall normalisation of configurations (i) and (ii) is 4/9 and 1/9, respectively.
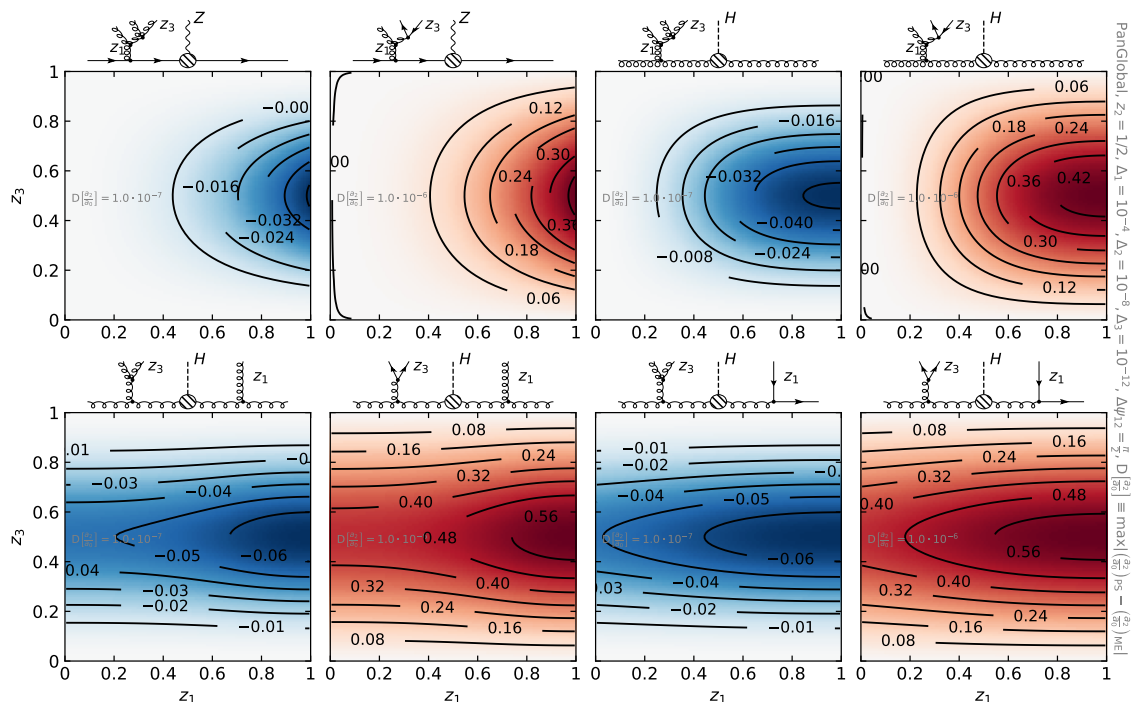
Figure 15. Same as figure 14 but with $\Delta\psi_{12} = \pi/2$.

recoil transverse to the beam being assigned to an explicit "hard system" (in the cases we have studied, the colour singlet) and energy and longitudinal momentum conservation ensured by rescaling the incoming momenta. As in the final-state case this shower can be used with transverse momentum ordering, $\beta_{\rm PS} = 0$ in eq. (4.3), and more generally for any $0 \leq \beta_{\rm PS} < 1$.

The hadron-collider PanLocal (dipole and antenna) family, section 4.2, as with the final-state case, assigns all recoil dipole locally within the dipole. For initial-state branchings this effectively results in a change in the direction of the incoming parton(s). The incoming parton(s) are then realigned with the original axis through a Lorentz transformation of the whole event, under the constraint that the rapidity of the hard system should remain unchanged relative to that before the branching. As in the final-state case, the PanLocal hadron-collider showers are expected to be NLL accurate for $0 < \beta_{\rm PS} < 1$, and the use of the hard-system momentum to provide a fixed reference frame is critical in order to correctly identify when to assign transverse recoil to one or other end of the dipole.

To provide a point of comparison, we have also formulated a "standard" transverse-momentum ordered dipole shower, Dipole-k_t, section 2.2, which shares similarities with existing widely used dipole showers.

We have carried out a number of "matrix-element" tests at fixed emission multiplicity, related to the conditions needed to achieve NLL accuracy. The core set of tests for the new showers has been to demonstrate that they satisfy the PanScales condition that emission in one region of phase space should not modify earlier emissions in logarithmi-

cally distant regions of phase space, an essential condition for accuracy beyond leading logarithms. Subtleties that are new in the initial-state case concern potential interplay between hard-collinear and soft-collinear emissions, in particular because the momentum of a post-branching initial-state particle can greatly exceed the pre-branching value. Examining this region led to specific choices for the kinematic maps and post-branching Lorentz transformations in the new showers, which while not critical for NLL accuracy (at least in a regime where $\ln s/m_Z^2$ remains finite), do help avoid unmotivated interplay between soft-collinear and hard-collinear branchings. Our tests also served to illustrate the way in which the PanScales logarithmic accuracy conditions fail to be respected by standard dipole shower schemes, as they do also for the $\beta_{\rm PS} = 1$ choice (and $\beta_{\rm PS} = 0$ for PanLocal) for current PanScales showers.

In addition to designing new hadron-collider showers, we have also extended the final-state schemes for subleading colour [44] as well as collinear and soft spin correlations [45, 46], introducing the new elements needed for initial-state radiation. These developments have been tested through comparisons to fixed-order matrix elements with up to three emissions.

Our companion work [1] will provide comparisons of the results of our showers to analytic all-order resummations, demonstrating that NLL accuracy has indeed been achieved for a wide range of observables. Future work will examine applications to processes beyond the colour-singlet hadro-production cases addressed here.

A Spin-averaged splitting functions

The DGLAP splitting functions $P_{i \to jk}$ are given by

$$P_{q \to qg}(z) = C_F \frac{1 + (1-z)^2}{z}\,, \tag{A.1a}$$

$$P_{g \to gg}(z) = 2C_A \left[\frac{z}{1-z} + \frac{1-z}{z} + z(1-z) \right]\,, \tag{A.1b}$$

$$P_{g \to q\bar{q}}(z) = T_R \left[z^2 + (1-z)^2 \right]\,. \tag{A.1c}$$

For final-state splitting in eq. (2.3), we employ

$$P^{\rm FS}_{\tilde{q}\to qg}(z) = P_{q\to qg}(z) = C_F \frac{1+(1-z)^2}{z}\,, \tag{A.2a}$$

$$P^{\rm FS}_{\tilde{g}\to gg}(z) = \frac{1}{2}P^{\rm asym}_{g\to gg}(z) = \frac{C_A}{2}\frac{1+(1-z)^3}{z}, \tag{A.2b}$$

$$P^{\rm FS}_{\tilde{g}\to q\bar{q}}(z) = \frac{1}{2}P^{\rm asym}_{g\to q\bar{q}}(z) = T_R(1-z)^2. \tag{A.2c}$$

The last two expressions include a factor of $1/2$ to compensate for the double counting due to the fact that a gluon belongs to two dipoles, with a further $1/2$ symmetry factor for identical particles in the final state in the case of $P_{\tilde{g}\to gg}$. One of the factors of $1/2$ is implemented by taking an asymmetric subset of the $z \leftrightarrow (1-z)$ symmetric terms. The use of the asymmetric kernels in eqs. (A.2b) and (A.2c) is possible due to the symmetry in the exchange of final-state particles. This symmetry does not hold anymore for an initial-state branching. In that case we use

$$P^{\rm IS}_{q\to\tilde{q}g}(z) = P_{q\to qg}(z) = C_F \frac{1+(1-z)^2}{z}\,, \tag{A.3a}$$

$$P^{\rm IS}_{q\to\tilde{g}q}(z) = \begin{cases} P_{q\to qg}(1-z) = C_F\frac{1+z^2}{1-z} & \text{if the gluon is the } \bar{3} \text{ end of the dipole,} \\ 0 & \text{if the gluon is the } 3 \text{ end of the dipole,} \end{cases} \tag{A.3b}$$

$$P^{\rm IS}_{\bar{q}\to\tilde{g}\bar{q}}(z) = \begin{cases} 0 & \text{if the gluon is the, } \bar{3} \text{ end of the dipole,} \\ P_{\bar{q}\to\bar{q}g}(1-z) = C_F\frac{1+z^2}{1-z} & \text{if the gluon is the, } 3 \text{ end of the dipole,} \end{cases} \tag{A.3c}$$

$$P^{\rm IS}_{g\to\tilde{g}g}(z) = \frac{1}{2}P_{g\to gg}(z) = C_A\left[\frac{z}{1-z} + \frac{1-z}{z} + z(1-z)\right], \tag{A.3d}$$

$$P^{\rm IS}_{g\to\tilde{q}\bar{q}}(z) = \frac{1}{2}P_{g\to q\bar{q}}(z) = \frac{1}{2}T_R\left[(1-z)^2 + z^2\right]. \tag{A.3e}$$

The choice in eqs. (A.3b) and (A.3c) to split only the $\bar{3}$ or the 3 end of the dipole is natural in terms of how the shower organises colour flows. For possible future extension beyond NLL accuracy (i.e. beyond LO splitting functions) one should keep in mind, however, that such a choice may introduce effective NLO splitting terms with a spurious difference between $q \to q' + X$ and $q \to \bar{q}' + X$. We leave the study of this question to future work.

B Shower mapping coefficients and scale choices

Here we provide the kinematic mappings associated with an $\tilde{i}\tilde{j} \to ijk$ dipole splitting. We denote by i and j the partons that descend from the parent dipole (and maintain their flavour in the case of gluon emission), while k is the newly emitted parton, whose transverse component, $k^\mu_\perp$, will always be given by eq. (2.7).

All of our shower implementations will share the factorisation scale choice

$$\ln\mu_F = \ln Q + \frac{1}{1+\beta_{\rm PS}}\ln\frac{v}{Q}\,, \tag{B.1}$$

where $\beta_{\rm PS}$ is taken to be zero for the Dipole-k_t shower family. In this work and in our companion paper [1], we restrict $v < Q$. The expression to be used for $\mu_{\rm R}$ in the shower branching probability, eq. (2.3), will be given separately for each shower.

B.1 Dipole-k_t

The kinematic maps that we use for the Dipole-k_t shower follow from the Catani-Seymour dipole subtraction formalism [57] and, unless otherwise specified, are as used in a number of dipole showers [28–30, 99]. The mapping coefficients and boosts expressions for each of the dipole types are as follows.

Initial-Initial: the dipole map is given by

$$p_i^\mu = a_i \tilde{p}_i^\mu \,, \tag{B.2a}$$

$$p_j^\mu = \tilde{p}_j^\mu \,, \tag{B.2b}$$

$$p_k^\mu = a_k \tilde{p}_i^\mu + b_k \tilde{p}_j^\mu - k_\perp^\mu \,, \tag{B.2c}$$

and the coefficients read

$$a_k = \frac{1-\zeta}{x_{jab}}, \ b_k = \frac{\kappa^2}{1-\zeta} \,, a_i = \frac{1}{x_{jab}}, \ |k_\perp|^2 = 2 a_k b_k \tilde{p}_i \cdot \tilde{p}_j, \tag{B.3}$$

where $\zeta = 1 - z$ with z as defined in eq. (2.13), and

$$\zeta = \frac{1}{1 + \kappa e^{\bar{\eta}_{\text{dip}}}} \,, \quad \kappa^2 = \frac{v^2}{\tilde{s}_{ij}} \,, \quad x_{jab} = \zeta - \frac{\kappa^2}{1-\zeta} \,. \tag{B.4}$$

The boost acts on all of the final-state particles except the newly created one (k), and takes their pre-branching total momentum $\tilde{F}^\mu = \tilde{p}_i^\mu + \tilde{p}_j^\mu$ to a new total momentum $F^\mu = p_i^\mu + p_j^\mu - p_k^\mu$ where $\tilde{F}^2 = F^2$. The boost reads

$$\Lambda^{\mu\nu}(F, \tilde{F}) = g^{\mu\nu} + \frac{2 F^\mu \tilde{F}^\nu}{\tilde{F}^2} - \frac{2(\tilde{F} + F)^\mu (\tilde{F} + F)^\nu}{(\tilde{F} + F)^2} \,. \tag{B.5}$$

To facilitate more precise numerical evaluation, the boost can be reformulated to be linear in terms of

$$F_{\text{diff}}^\mu = F^\mu - \tilde{F}^\mu = \left(\frac{\zeta}{x_{jab}} - 1\right) \tilde{p}_i^\mu - \frac{\kappa^2}{1-\zeta} \tilde{p}_j^\mu + k_\perp^\mu, \tag{B.6}$$

which can be evaluated accurately. We find

$$\Lambda^{\mu\nu}(F, \tilde{F}) = g^{\mu\nu} - 4 \frac{F^\mu}{F^2 F_{\text{sum}}^2} \left(F_{\text{diff}} \cdot F \, \tilde{F}^\nu + F^2 \, F_{\text{diff}}^\nu\right) + \frac{2}{F_{\text{sum}}^2} F_{\text{diff}}^\mu F_{\text{sum}}^\nu \tag{B.7}$$

where $F_{\text{sum}}^\mu = \tilde{F}^\mu + F^\mu$.

Initial-Final (local-recoil variant): the map is given by

$$p_i^\mu = a_i \tilde{p}_i^\mu, \tag{B.8a}$$

$$p_j^\mu = a_j \tilde{p}_i^\mu + b_j \tilde{p}_j^\mu + k_\perp^\mu, \tag{B.8b}$$

$$p_k^\mu = a_k \tilde{p}_i^\mu + b_k \tilde{p}_j^\mu - k_\perp^\mu \,, \tag{B.8c}$$

with

$$a_k = \frac{1 - \zeta - \kappa^2}{\zeta} \,, \qquad\qquad b_k = \frac{\kappa^2}{1 - \zeta} \,, \qquad\qquad \text{(B.9a)}$$

$$a_i = \frac{1}{\zeta} \,, \qquad\qquad\qquad\qquad\qquad\qquad\qquad \text{(B.9b)}$$

$$a_j = \frac{\kappa^2}{\zeta} \,, \qquad\qquad\qquad b_j = 1 - b_k \,, \qquad\qquad \text{(B.9c)}$$

and ζ, κ^2 defined as in eq. (B.4).

Initial-Final (global-recoil variant): we have [100, 101]

$$\bar{p}_i^\mu = a_i \tilde{p}_i^\mu + b_i \tilde{p}_j^\mu + k_\perp^\mu \,, \qquad\qquad \text{(B.10a)}$$

$$\bar{p}_j^\mu = b_j \tilde{p}_j^\mu \,, \qquad\qquad\qquad\qquad \text{(B.10b)}$$

$$\bar{p}_k^\mu = a_k \tilde{p}_i^\mu + b_k \tilde{p}_j^\mu + k_\perp^\mu \,, \qquad\qquad \text{(B.10c)}$$

with

$$a_k = \frac{1 - \zeta}{\zeta - u_j} \,, \qquad\qquad b_k = \frac{u_j}{\zeta} \frac{1 - u_j}{\zeta - u_j} \,, \qquad\qquad \text{(B.11a)}$$

$$a_i = \frac{1 - u_j}{\zeta - u_j} \,, \qquad\qquad b_i = \frac{u_j}{\zeta} \frac{1 - \zeta}{\zeta - u_j} \,, \qquad\qquad \text{(B.11b)}$$

$$b_j = 1 - \frac{u_j}{\zeta} \,, \qquad\qquad\qquad\qquad\qquad \text{(B.11c)}$$

where $u_j = \kappa^2/(1 - \zeta)$ and ζ, κ^2 are defined as in eq. (B.4). As one may observe, this map leaves the initial-state parton misaligned with the original beam direction. This is resolved, while ensuring momentum conservation, by performing a boost and rotation on the initial-state particle that partakes in the map and on all final-state particles, keeping the other initial-state particle untouched. Denoting $p_A^\mu \equiv \tilde{p}_i$ (the initial-state parton of the dipole), p_B^μ the other initial-state parton, and $p_a^\mu \equiv p_i$, the boost and rotation can be written as

$$B^{\mu\nu} = g^{\mu\nu} + \frac{p_B^\mu p_a^\nu - p_a^\mu p_B^\nu}{p_a \cdot p_B} + \frac{p_A^\mu p_B^\nu - p_B^\mu p_A^\nu}{p_A \cdot p_B} + \frac{p_A \cdot p_a}{(p_A \cdot p_B)(p_a \cdot p_B)} p_B^\mu p_B^\mu. \qquad \text{(B.12)}$$

To achieve a numerically stable version of eq. (B.12) we define

$$d_{AB} = p_A \cdot p_B, \quad d_{aB} = p_a \cdot p_B, \quad d_{aA} = p_a \cdot p_A \,, \qquad\qquad \text{(B.13)}$$

and decompose p_a^μ as

$$p_a^\mu = \frac{d_{aB}}{d_{AB}} p_A^\mu + \frac{d_{aA}}{d_{AB}} p_B^\mu + p_t^\mu, \qquad\qquad \text{(B.14)}$$

where p_t^μ is not the transverse momentum with respect to the dipole, but that with respect to the beams. In this form, the boost reduces to the remarkably simple form

$$B^{\mu\nu} = g^{\mu\nu} + \frac{1}{d_{aB}} (p_B^\mu p_t^\nu - p_t^\mu p_B^\nu) - \frac{1}{2} \frac{p_t^2}{d_{aB}^2} p_B^\mu p_B^\nu \,. \qquad\qquad \text{(B.15)}$$

Final-Initial: the map is given by

$$p_i^\mu = a_i\tilde{p}_i^\mu + b_i\tilde{p}_j^\mu + k_\perp^\mu\,, \tag{B.16a}$$

$$p_j^\mu = b_j\tilde{p}_j^\mu\,, \tag{B.16b}$$

$$p_k^\mu = a_k\tilde{p}_i^\mu + b_k\tilde{p}_j^\mu + k_\perp^\mu\,, \tag{B.16c}$$

and the coefficients read

$$a_k = z\,, \qquad\qquad b_k = (1-z)y\,, \tag{B.17a}$$

$$a_i = 1-z\,, \qquad\qquad b_i = zy\,, \tag{B.17b}$$

$$b_j = \frac{1}{x_{ija}}\,, \tag{B.17c}$$

with

$$z = \kappa e^{\bar{\eta}_\text{dip}}\,, \qquad\qquad \kappa^2 = \frac{v^2}{\tilde{s}_{ij}^2}\,, \tag{B.18}$$

$$x_{ija} = \frac{\kappa^2}{z}\,, \qquad\qquad y = \frac{1-x_{ija}}{x_{ija}}\,. \tag{B.19}$$

Final-Final: the map is given by

$$p_i^\mu = a_i\tilde{p}_i^\mu + b_i\tilde{p}_j^\mu + k_\perp^\mu\,, \tag{B.20a}$$

$$p_j^\mu = b_j\tilde{p}_j^\mu\,, \tag{B.20b}$$

$$p_k^\mu = a_k\tilde{p}_i^\mu + b_k\tilde{p}_j^\mu - k_\perp^\mu\,, \tag{B.20c}$$

where

$$a_k = 1-\tilde{z}\,, \qquad\qquad b_k = y_{ijk}\tilde{z}\,, \tag{B.21a}$$

$$a_i = \tilde{z}\,, \qquad\qquad b_i = y_{ijk}(1-\tilde{z})\,, \tag{B.21b}$$

$$b_j = 1 - y_{ijk}\,, \tag{B.21c}$$

with z and κ^2 as in eqs. (B.18) and

$$\tilde{z} = \frac{\kappa^2 - z(1-z)}{\kappa^2 - z}\,, \quad y_{ijk} = \frac{\kappa^2}{z}\,. \tag{B.22}$$

For all dipole kinds, the renormalisation scale in eq. (2.3) is taken to be

$$\mu_\text{R} = v\,. \tag{B.23}$$

B.2 PanGlobal

The kinematic map is given by eq. (2.12). The rescaling factors for the radiated particles are linked to the shower variables via eq. (4.6) where we take

$$a_k = \alpha_k\,, \qquad b_k = \beta_k\,. \tag{B.24}$$

As usual, the magnitude of the transverse momentum is obtained by imposing $p_k^2 = 0$. For convenience, in the mapping that we use below, we make use of a Sudakov decomposition of the momentum of the (pre-branching) hard system with the light-cone directions given by $\tilde{p}_a$ and $\tilde{p}_b$, i.e., the incoming partons,

$$\tilde{p}_H^\mu = a_H \tilde{p}_a^\mu + b_H \tilde{p}_b^\mu + \widetilde{H}_t^\mu . \tag{B.25}$$

with the coefficients given by

$$a_H = \frac{\tilde{p}_H \cdot \tilde{p}_b}{\tilde{p}_a \cdot \tilde{p}_b} , \quad b_H = \frac{\tilde{p}_H \cdot \tilde{p}_a}{\tilde{p}_a \cdot \tilde{p}_b} , \quad \widetilde{H}_t^\mu = \tilde{p}_H^\mu - a_H \tilde{p}_a^\mu - b_H \tilde{p}_b^\mu . \tag{B.26}$$

A common feature for all dipole types is that the hard system absorbs the part of the recoil that is transverse to the beam. For a hard system composed of more than one particle, this is to be achieved through a boost applied to all particles in the hard system. The boost takes the form $\Lambda(p_H, \tilde{p}_H)$, cf. eq. (B.5), with $\tilde{p}_H^\mu$ the pre-branching momentum of the hard system, and p_H^μ the momentum that the hard system should have after absorbing the transverse recoil.

Our renormalisation scale choice, common to all dipole kinds, is

$$\mu_{\mathrm{R}} = \kappa_\perp \equiv \rho v e^{\beta_{\mathrm{PS}} |\bar{\eta}_Q|} . \tag{B.27}$$

Initial-Initial: the mapping (and rescaling) takes the form

$$p_k^\mu = a_k \tilde{p}_a^\mu + b_k \tilde{p}_b^\mu + k_\perp^\mu , \tag{B.28a}$$

$$p_a^\mu = r_a \tilde{p}_a^\mu , \tag{B.28b}$$

$$p_b^\mu = r_b \tilde{p}_b^\mu . \tag{B.28c}$$

The momentum of the hard system after the rescaling plus boost can be computed (through momentum conservation), as the momentum of the 'rest of the event', i.e.

$$p_H^\mu = r_a \tilde{p}_a^\mu + r_b \tilde{p}_b^\mu - p_k^\mu = (r_a - a_k - 1)\tilde{p}_a^\mu + (r_b - b_k - 1)\tilde{p}_b^\mu - k_\perp^\mu + \tilde{p}_H^\mu . \tag{B.29}$$

To obtain the right-hand side we have used the map as well as momentum conservation for the pre-branching event. The coefficients r_a and r_b are obtained by requiring that p_H and $\tilde{p}_H$ have the same rapidity and invariant mass. Using the Sudakov decomposition given by eq. (B.25) we get

$$0 = (r_a - 1 - a_k)(r_b - 1 - b_k) + a_H(r_b - 1 - b_k) + b_H(r_a - 1 - a_k) - \frac{2\widetilde{H}_t \cdot k_\perp + k_\perp^2}{\tilde{s}_{ab}} , \tag{B.30a}$$

$$\frac{a_H}{b_H} = \frac{r_a - 1 - a_k + a_H}{r_b - 1 - b_k + b_H} . \tag{B.30b}$$

Solving this system of equations leads to

$$r_a = 1 + a_k + \omega a_H , \qquad r_a = 1 + b_k + \omega b_H , \tag{B.31}$$

with

$$\omega = \sqrt{1 + \frac{2\widetilde{H}_t \cdot k_\perp + k_\perp^2}{a_H b_H \tilde{s}_{ab}}} - 1 . \tag{B.32}$$

Initial-Final: In this case we have

$$p_k^\mu = a_k \tilde{p}_a^\mu + b_k \tilde{p}_j^\mu + k_\perp^\mu \,, \tag{B.33a}$$

$$p_a^\mu = r_a \tilde{p}_a^\mu \,, \tag{B.33b}$$

$$p_j^\mu = (1 - b_k)\tilde{p}_j^\mu \,, \tag{B.33c}$$

$$p_b^\mu = r_b \tilde{p}_b^\mu \,, \tag{B.33d}$$

where a denotes the incoming leg participating in the splitting, b is the other incoming leg, and j is the final-state colour partner of a. The rescaling factors r_a and r_b are determined imposing that the mass and the rapidity of the hard system is preserved

$$p_H^\mu = r_a \tilde{p}_a^\mu + r_b \tilde{p}_b^\mu - p_k^\mu - p_j^\mu - \sum_{l \neq j} \tilde{p}_l^\mu = (r_a - 1 - a_k)\tilde{p}_a^\mu + (r_b - 1)\tilde{p}_b^\mu - k_\perp^\mu + \tilde{p}_H^\mu \,, \tag{B.34}$$

where the sum runs over all final-state particles except the new emission. The virtuality and rapidity constraints can then be written as

$$0 = (r_a - 1 - a_k)(r_b - 1) + (a_H - c_b)(r_b - 1) + b_H(r_a - 1 - a_k) - (c + b_H c_b), \tag{B.35a}$$

$$\frac{a_H}{b_H} = \frac{r_a - 1 - a_k + a_H - c_b}{r_b - 1 + b_H}, \tag{B.35b}$$

with

$$c_b = \frac{2\tilde{p}_b \cdot k_\perp}{\tilde{s}_{ab}} \,, \qquad c = \frac{2\widetilde{H}_t \cdot k_\perp + k_\perp^2}{\tilde{s}_{ab}} \,. \tag{B.36}$$

This system admits the following solution (with ω as in eq. (B.32))

$$r_a = 1 + a_k + \omega a_H + \frac{2\tilde{p}_b \cdot k_\perp}{\tilde{s}_{ab}} \,, \qquad r_b = 1 + \omega b_H \,. \tag{B.37}$$

Since we are considering an antenna shower here, there is no need to have a separate treatment for an FI dipole.

Final-Final: we now have two final-state particles i and j that emit a parton k, for which the mapping is

$$p_k^\mu = a_k \tilde{p}_i^\mu + b_k \tilde{p}_j^\mu + k_\perp^\mu \,, \tag{B.38a}$$

$$p_i^\mu = (1 - a_k)\tilde{p}_i^\mu \,, \tag{B.38b}$$

$$p_j^\mu = (1 - b_k)\tilde{p}_j^\mu \,, \tag{B.38c}$$

$$p_a^\mu = r_a \tilde{p}_a^\mu \,, \tag{B.38d}$$

$$p_b^\mu = r_b \tilde{p}_b^\mu \,. \tag{B.38e}$$

We therefore have

$$p_H^\mu = r_a \tilde{p}_a^\mu + r_b \tilde{p}_b^\mu - p_k^\mu - p_j^\mu - p_i^\mu - \sum_{l \neq i,j,k;l} \tilde{p}_l^\mu = (r_a - 1)\tilde{p}_a^\mu + (r_b - 1)\tilde{p}_b^\mu - k_\perp^\mu + \tilde{p}_H^\mu. \tag{B.39}$$

The virtuality and rapidity constraints can then be written as

$$0 = (r_a - 1)(r_b - 1) + (a_H - c_b)(r_b - 1) + (b_H - c_a)(r_a - 1) - (a_H c_a + b_H c_b + c),$$

(B.40a)

$$\frac{a_H}{b_H} = \frac{r_a - 1 + a_H - c_b}{r_b - 1 + b_H - c_a},$$

(B.40b)

with

$$c_{a,b} = \frac{2\tilde{p}_{a,b} \cdot k_\perp}{\tilde{s}_{ab}}, \qquad c = \frac{2\widetilde{H}_t \cdot k_\perp + k_\perp^2}{\tilde{s}_{ab}}$$

(B.41)

which admit the following solution (again with ω as in eq. (B.32))

$$r_a = 1 + \omega a_H + \frac{2\tilde{p}_b \cdot k_\perp}{\tilde{s}_{ab}}, \qquad r_b = 1 + \omega b_H + \frac{2\tilde{p}_a \cdot k_\perp}{\tilde{s}_{ab}}.$$

(B.42)

B.3 PanLocal

Here we discuss both the dipole and antenna variants of the PanLocal shower. We start with the aspects that are common to both, in particular the boost and rotation that are to be applied to the event after any splitting that assigns transverse momentum to an initial-state particle, i.e. initial-initial and initial-final dipoles. As discussed in the main text, the boost and rotation realign the incoming partons with the beam axes. This transformation contains a longitudinal degree of freedom, which we exploit so as to conserve the rapidity y_H of the hard system H. We use $\tilde{p}_H$ for the pre-branching momentum of the hard system, $\bar{p}_H$ for the momentum after the emission occurred, and p_H is the final value after the boost has been performed. For colour-singlet production, we have $\bar{p}_H = \tilde{p}_H$, but we maintain the distinction in our notation to keep the discussion general (for example as concerns future extension to situations with coloured particles that are part of the hard system).

The first step to obtain the precise form of the boost is to determine the new momenta of the incoming partons, which we label with indices a and b. Using $p_{a,b}$ to refer to the momenta after the boost and rotation, we can write

$$\tilde{p}_{a,b} = \tilde{x}_{a,b} P_{a,b},$$

(B.43a)

$$p_{a,b} = x_{a,b} P_{a,b},$$

(B.43b)

where $P_{a,b} \equiv \widetilde{P}_{a,b}$ are the incoming hadron momenta. The hadron momenta must remain unchanged after the combination of kinematic map, boost and rotation. Thus to determine the boost we need to find the new values $x_{a,b}$ such that the rapidity of the hard system is unchanged (as defined with respect to the incoming hadron momenta). Before the splitting, we have

$$\tilde{y}_H = \frac{1}{2} \ln \frac{\tilde{p}_H \cdot P_b}{\tilde{p}_H \cdot P_a} = \frac{1}{2} \ln \frac{\tilde{p}_H \cdot \tilde{p}_b}{\tilde{p}_H \cdot \tilde{p}_a} + \frac{1}{2} \ln \frac{\tilde{x}_a}{\tilde{x}_b},$$

(B.44)

while after the emission

$$y_H \equiv \frac{1}{2} \ln \frac{p_H \cdot P_b}{p_H \cdot P_a} = \frac{1}{2} \ln \frac{p_H \cdot p_b}{p_H \cdot p_a} + \frac{1}{2} \ln \frac{x_a}{x_b}$$
$$= \frac{1}{2} \ln \frac{\bar{p}_H \cdot \bar{p}_b}{\bar{p}_H \cdot \bar{p}_a} + \frac{1}{2} \ln \frac{x_a}{x_b},$$

(B.45)

where in the last step we used the Lorentz invariance of the dot product. Equating eq. (B.44) and (B.45) we obtain

$$\frac{\tilde{x}_a}{x_a}\frac{x_b}{\tilde{x}_b} = \frac{\tilde{p}_H \cdot \tilde{p}_b}{\bar{p}_H \cdot \bar{p}_b}\frac{\bar{p}_H \cdot \bar{p}_a}{\tilde{p}_H \cdot \tilde{p}_a}. \tag{B.46}$$

Since the Lorentz transformation will preserve the invariant mass of the final-state system, we also have

$$2\bar{p}_a \cdot \bar{p}_b = 2p_a \cdot p_b = 2\tilde{p}_a \cdot \tilde{p}_b \frac{x_a x_b}{\tilde{x}_a \tilde{x}_b}. \tag{B.47}$$

Solving eqs. (B.46) and (B.47) for the new momentum fractions $x_{a,b}$ yields

$$x_a = \tilde{x}_a \sqrt{\frac{\bar{p}_a \cdot \bar{p}_b}{\tilde{p}_a \cdot \tilde{p}_b}\frac{\tilde{p}_H \cdot \tilde{p}_b}{\bar{p}_H \cdot \bar{p}_b}\frac{\bar{p}_H \cdot \bar{p}_a}{\tilde{p}_H \cdot \tilde{p}_a}}, \qquad x_b = \tilde{x}_b \sqrt{\frac{\bar{p}_a \cdot \bar{p}_b}{\tilde{p}_a \cdot \tilde{p}_b}\frac{\bar{p}_H \cdot \bar{p}_b}{\tilde{p}_H \cdot \tilde{p}_b}\frac{\tilde{p}_H \cdot \tilde{p}_a}{\bar{p}_H \cdot \bar{p}_a}}. \tag{B.48}$$

We are now in a position to carry out the boost. It is useful to introduce a notation for the total hadron-hadron four momentum before and after the boost as

$$\bar{P}^\mu = \frac{\bar{p}_a^\mu}{x_a} + \frac{\bar{p}_b^\mu}{x_b}, \qquad P^\mu \equiv \widetilde{P}^\mu = \widetilde{P}_a^\mu + \widetilde{P}_b^\mu. \tag{B.49}$$

Then every particle in the event is boosted as

$$p^\mu = \Lambda^{\mu\nu}(P,\bar{P})\bar{p}_\nu \tag{B.50}$$

with $\Lambda^{\mu\nu}$ as defined in eq. (B.5). This boost ensures that the new incoming momenta are back-to-back and have the correct energy, and we then perform a rotation so as to align them with the z axis.[27]

In practice, one also has the possibility to perform the boost (and the final rotation) only at the very end of the parton showering, provided that the values of the incoming partons energy fractions x are stored at each step of the shower evolution. These values are used to compute the beams' momenta in the unboosted frame

$$\bar{P}_{a,b}^\mu = \frac{\bar{p}_{a,b}^\mu}{x_{a,b}}. \tag{B.51}$$

Since to define $\bar{\eta} = \bar{\eta}_Q$ and ρ we use the scalar product with a reference vector Q^μ, we should apply the inverse rotation and the inverse boost to Q^μ. For colour-singlet production Q^μ is chosen to be

$$Q^\mu = e^y \frac{m}{S}\bar{P}_a^\mu + e^{-y}\frac{m}{S}\bar{P}_b^\mu, \tag{B.52}$$

where m and y are the mass and the rapidity of the colour singlet (in the original frame), while $S = (\bar{P}_a + \bar{P}_b)^2$ is the squared total centre of mass energy. Thus, in this case we can simply evaluate eq. (B.52) after we have recomputed the beam momenta according to eq. (B.51).

The renormalisation scale choice for the PanLocal showers is the same as for the PanGlobal shower, i.e. eq. (B.27).

---

[27]For this last step, we assume that the hadrons collide in their centre-of-mass frame, i.e. that P^μ's 3-momentum components are all zero.

B.3.1 PanLocal dipole

Initial-Initial: the map is given by

$$\bar{p}_i^\mu = a_i \tilde{p}_i^\mu + b_i \tilde{p}_j^\mu + k_\perp^\mu \,, \tag{B.53a}$$

$$\bar{p}_j^\mu = b_j \tilde{p}_j^\mu \,, \tag{B.53b}$$

$$\bar{p}_k^\mu = a_k \tilde{p}_i^\mu + b_k \tilde{p}_j^\mu + k_\perp^\mu \,, \tag{B.53c}$$

and the coefficients read

$$a_k = \alpha_k \,, \qquad\qquad b_k = \beta_k (1 + \alpha_k)^{\frac{2}{1+\beta_{\mathrm{PS}}}} \,, \tag{B.54a}$$

$$a_i = 1 + a_k \,, \qquad\qquad b_i = \frac{a_k b_k}{a_i} \,, \tag{B.54b}$$

$$b_j = 1 - \frac{b_k}{a_i} \,. \tag{B.54c}$$

Initial-Final: the map is given by

$$\bar{p}_i^\mu = a_i \tilde{p}_i^\mu + b_i \tilde{p}_j^\mu + k_\perp^\mu \,, \tag{B.55a}$$

$$\bar{p}_j^\mu = b_j \tilde{p}_j^\mu \,, \tag{B.55b}$$

$$\bar{p}_k^\mu = a_k \tilde{p}_i^\mu + b_k \tilde{p}_j^\mu + k_\perp^\mu \,, \tag{B.55c}$$

with

$$a_k = \alpha_k \,, \qquad\qquad b_k = \beta_k (1 + \alpha_k)^{\frac{2}{1+\beta_{\mathrm{PS}}}} \,, \tag{B.56a}$$

$$a_i = 1 + a_k \,, \qquad\qquad b_i = \frac{a_k b_k}{a_i} \,, \tag{B.56b}$$

$$b_j = 1 + \frac{b_k}{a_i} \,. \tag{B.56c}$$

Final-Initial: the map is given by

$$p_i^\mu = a_i \tilde{p}_i^\mu + b_i \tilde{p}_j^\mu - k_\perp^\mu \,, \tag{B.57a}$$

$$p_j^\mu = b_j \tilde{p}_j^\mu \,, \tag{B.57b}$$

$$p_k^\mu = a_k \tilde{p}_i^\mu + b_k \tilde{p}_j^\mu + k_\perp^\mu \,, \tag{B.57c}$$

and the coefficients read

$$a_k = \alpha_k \,, \qquad\qquad b_k = \beta_k \,, \tag{B.58a}$$

$$a_i = 1 - a_k \,, \qquad\qquad b_i = \frac{a_k b_k}{a_i} \,, \tag{B.58b}$$

$$b_j = 1 + \frac{b_k}{a_i} \,. \tag{B.58c}$$

Final-Final: the map is given by

$$p_i^\mu = a_i \tilde{p}_i^\mu + b_i \tilde{p}_j^\mu - k_\perp^\mu \,, \tag{B.59a}$$

$$p_j^\mu = b_j \tilde{p}_j^\mu \,, \tag{B.59b}$$

$$p_k^\mu = a_k \tilde{p}_i^\mu + b_k \tilde{p}_j^\mu + k_\perp^\mu \,, \tag{B.59c}$$

and the coefficients read

$$a_k = \alpha_k \,, \qquad\qquad b_k = \beta_k \,, \tag{B.60a}$$

$$a_i = 1 - a_k \,, \qquad\qquad b_i = \frac{a_k b_k}{a_i} \,, \tag{B.60b}$$

$$b_j = 1 - \frac{b_k}{a_i} \,. \tag{B.60c}$$

B.3.2 PanLocal antenna

Initial-Initial: the map is given by

$$\bar{p}_i^\mu = a_i \tilde{p}_i^\mu + b_i \tilde{p}_j^\mu + f k_\perp^\mu \,, \tag{B.61a}$$

$$\bar{p}_j^\mu = a_j \tilde{p}_i^\mu + b_j \tilde{p}_j^\mu + (1-f) k_\perp^\mu \,, \tag{B.61b}$$

$$\bar{p}_k^\mu = a_k \tilde{p}_i^\mu + b_k \tilde{p}_j^\mu + k_\perp^\mu \,, \tag{B.61c}$$

and the coefficients read

$$a_k = \alpha_k (1+\beta_k)^{\frac{2}{1+\beta_{\mathrm{PS}}}} \,, \qquad\qquad b_k = \beta_k (1+\alpha_k)^{\frac{2}{1+\beta_{\mathrm{PS}}}} \,, \tag{B.62a}$$

$$a_i = \frac{(\sqrt{\lambda_1}+\sqrt{\lambda_2})^2 + 4f^2 a_k b_k}{4(1+b_k)} \,, \qquad b_i = \frac{(\sqrt{\lambda_1}-\sqrt{\lambda_2})^2 + 4f^2 a_k b_k}{4(1+a_k)} \,, \tag{B.62b}$$

$$a_j = \frac{(\sqrt{\lambda_1}-\sqrt{\lambda_2})^2 + 4(1-f)^2 a_k b_k}{4(1+b_k)} \,, \quad b_j = \frac{(\sqrt{\lambda_1}+\sqrt{\lambda_2})^2 + 4(1-f)^2 a_k b_k}{4(1+a_k)} \,, \tag{B.62c}$$

with $\lambda_1 = 1 + a_k + b_k$ and $\lambda_2 = \lambda_1 + 4f(1-f)a_k b_k$.

Initial-Final: the map is given by

$$\bar{p}_i^\mu = a_i \tilde{p}_i^\mu + b_i \tilde{p}_j^\mu + f k_\perp^\mu \,, \tag{B.63a}$$

$$\bar{p}_j^\mu = a_j \tilde{p}_i^\mu + b_j \tilde{p}_j^\mu - (1-f) k_\perp^\mu \,, \tag{B.63b}$$

$$\bar{p}_k^\mu = a_k \tilde{p}_i^\mu + b_k \tilde{p}_j^\mu + k_\perp^\mu \,, \tag{B.63c}$$

with

$$a_k = \alpha_k \,, \qquad\qquad b_k = \beta_k (1+\alpha_k)^{\frac{2}{1+\beta_{\mathrm{PS}}}} \,, \tag{B.64a}$$

$$a_i = \frac{(\sqrt{\lambda_1}+\sqrt{\lambda_2})^2 - 4f^2 a_k b_k}{4(1-b_k)} \,, \qquad b_i = \frac{-(\sqrt{\lambda_1}-\sqrt{\lambda_2})^2 + 4f^2 a_k b_k}{4(1+a_k)} \,, \tag{B.64b}$$

$$a_j = \frac{-(\sqrt{\lambda_1}-\sqrt{\lambda_2})^2 + 4(1-f)^2 a_k b_k}{4(1-b_k)} \,, \quad b_j = \frac{(\sqrt{\lambda_1}+\sqrt{\lambda_2})^2 - 4(1-f)^2 a_k b_k}{4(1+a_k)} \,, \tag{B.64c}$$

and $\lambda_1 = 1 + a_k - b_k$ and $\lambda_2 = \lambda_1 - 4f(1-f)a_k b_k$. Since we are considering an antenna shower here, there is no need to have a separate treatment of a "final-initial" dipole.

Final-Final: the map is given by

$$p_i^\mu = a_i \tilde{p}_i^\mu + b_i \tilde{p}_j^\mu - f k_\perp^\mu \,, \tag{B.65a}$$

$$p_j^\mu = a_j \tilde{p}_i^\mu + b_j \tilde{p}_j^\mu - (1-f) k_\perp^\mu \,, \tag{B.65b}$$

$$p_k^\mu = a_k \tilde{p}_i^\mu + b_k \tilde{p}_j^\mu + k_\perp^\mu \,, \tag{B.65c}$$

and the coefficients read

$$a_k = \alpha_k \,, \qquad\qquad\qquad b_k = \beta_k \,, \tag{B.66a}$$

$$a_i = \frac{(\sqrt{\lambda_1} + \sqrt{\lambda_2})^2 + 4f^2 a_k b_k}{4(1-b_k)} \,, \qquad b_i = \frac{(\sqrt{\lambda_1} - \sqrt{\lambda_2})^2 + 4f^2 a_k b_k}{4(1-a_k)} \,, \tag{B.66b}$$

$$a_j = \frac{(\sqrt{\lambda_1} - \sqrt{\lambda_2})^2 + 4(1-f)^2 a_k b_k}{4(1-b_k)} \,, \quad b_j = \frac{(\sqrt{\lambda_1} + \sqrt{\lambda_2})^2 + 4(1-f)^2 a_k b_k}{4(1-a_k)} \,, \tag{B.66c}$$

with $\lambda_1 = 1 - a_k - b_k$ and $\lambda_2 = \lambda_1 + 4f(1-f)a_k b_k$.

C Analytics for sub-leading colour matrix element tests

Here, we provide all of the analytic ingredients needed to make the comparisons presented in section 5. The differential cross section for the emission of one additional soft gluon with momentum k and energy fraction z off an amplitude $\mathrm{d}\sigma_n$ can be written as

$$\mathrm{d}\sigma_{n+1} = \mathrm{d}\sigma_n \frac{\mathrm{d}z}{z} \frac{\mathrm{d}\Omega}{2\pi} \frac{\alpha_s}{2\pi} \sum_{i,j} C_{ij}(k|ij), \tag{C.1}$$

where $\mathrm{d}\Omega = \mathrm{d}\cos\theta \mathrm{d}\phi$ is the element of solid angle for the emitted gluon, C_{ij} the colour factor, and the eikonal factor $(k|ij)$ is given by

$$(k|ij) = \frac{1 - \cos\theta_{ij}}{(1 - \cos\theta_{ki})(1 - \cos\theta_{kj})}. \tag{C.2}$$

Starting from eq. (C.1) we now compute the differential matrix element and integrated rate for two and three emissions.

C.1 $q\bar{q} \to Z$

Let us begin with the $q\bar{q} \to Z$ case.

Two emissions. One of the two initial configurations is a $q\bar{q}g_1$ system from which we emit a second soft gluon. The $q\bar{q} \to Zg_1g_2$ amplitude is

$$\frac{|\mathcal{M}_{q\bar{q}g_1g_2}|^2}{|\mathcal{M}_{q\bar{q}g_1}|^2} = \frac{\alpha_s}{2\pi} \left[\frac{C_A}{2}(g_2|g_1q) + \frac{C_A}{2}(g_2|g_1\bar{q}) + (C_F - \frac{C_A}{2})(g_2|q\bar{q}) \right] , \tag{C.3}$$

The integrated emission rate, that we denote $I_{\mathrm{FC}}^{Zg_1}$, is obtained after integrating over the solid angle $\int \mathrm{d}\Omega = \int \mathrm{d}\cos\theta \, \mathrm{d}\phi$, defined with respect to the direction of the emitting line

i or j. The azimuthal integration results in the well known property of angular ordering, i.e.

$$\int \frac{\mathrm{d}\Omega}{2\pi}(k|ij) = \frac{1}{2}\left[\int_{\cos\theta_{ij}}^{\cos\theta_{\mathrm{cut},ik}} \frac{\mathrm{d}\cos\theta_{ik}}{1-\cos\theta_{ik}} + \int_{\cos\theta_{ij}}^{\cos\theta_{\mathrm{cut},jk}} \frac{\mathrm{d}\cos\theta_{jk}}{1-\cos\theta_{jk}}\right] \tag{C.4}$$

$$= \frac{1}{2}\left[-\ln\left(1-\cos\theta_{\mathrm{cut},ik}\right) - \ln\left(1-\cos\theta_{\mathrm{cut},jk}\right) + 2\ln\left(1-\cos\theta_{ij}\right)\right],$$

with θ_{cut} a collinear regulator that can be different for each of the terms. In what follows, we use θ_{cut} ($\theta_{\mathrm{cut},s}$) to denote the regulator for primary (secondary) emissions.

$$I_{\mathrm{FC}}^{Zg_1} \equiv \int \frac{\mathrm{d}\Omega}{2\pi} \frac{|\mathcal{M}_{q\bar{q}g_1g_2}|^2}{|\mathcal{M}_{q\bar{q}g_1}|^2}$$

$$= \frac{\alpha_s}{2\pi}\left\{\frac{C_A}{2}\left[\ln\left(1-\cos\theta_{1q}\right) + \ln(1-\cos\theta_{1\bar{q}}) - \ln(1-\cos\theta_{q\bar{q}}) - \ln(1-\cos\theta_{\mathrm{cut},s})\right]\right.$$

$$\left. + C_F\left[\ln(1-\cos\theta_{q\bar{q}}) - \ln(1-\cos\theta_{\mathrm{cut}})\right]\right\}, \tag{C.5}$$

Since the initial-state quarks are back-to-back we can replace $\cos\theta_{q\bar{q}} = -1$ and rewrite the angles in terms of rapidities using

$$\eta = \pm|\ln\tan\theta/2| \to 1 - \cos\theta = \frac{2}{1+\mathrm{e}^{2\eta}}. \tag{C.6}$$

We obtain

$$I_{\mathrm{FC}}^{Zg_1} = \frac{\alpha_s}{2\pi}\left\{\frac{C_A}{2}\left[\ln(1+\mathrm{e}^{2\eta_{\mathrm{cut},s}}) - \ln(1+\mathrm{e}^{2\Delta\eta_{1q}}) - \ln(1+\mathrm{e}^{2\Delta\eta_{1\bar{q}}})\right] + C_F\left[\ln(1+\mathrm{e}^{2\eta_{\mathrm{cut}}})\right]\right\}. \tag{C.7}$$

To arrive at our final result, we first use that η_{cut} and $\eta_{\mathrm{cut},s}$ correspond to small angles, such that $\ln(1+\mathrm{e}^{2\eta_{\mathrm{cut}(,s)}}) \simeq 2\eta_{\mathrm{cut}(,s)}$. Secondly, we write $\Delta\eta_{1q} = \eta_1$ and $\Delta\eta_{1\bar{q}} = -\eta_1$ (which holds as long as we do only one emission, and is not sensitive to the rapidity of the colour-singlet system). Consequently,

$$\ln(1+\mathrm{e}^{2\Delta\eta_{1q}}) + \ln(1+\mathrm{e}^{2\Delta\eta_{1\bar{q}}}) = 2\eta_1 + 2\ln(1+\mathrm{e}^{-2\eta_1}), \tag{C.8a}$$

$$\ln(1+\mathrm{e}^{2\Delta\eta_{1q}}) - \ln(1+\mathrm{e}^{2\Delta\eta_{1\bar{q}}}) = 2\eta_1. \tag{C.8b}$$

Inserting this result into eq. (C.7), we obtain the final expression:

$$I_{\mathrm{FC}}^{Zg_1} = \frac{\alpha_s}{2\pi}\left[C_A\left(\eta_{\mathrm{cut},f} - \eta_1 - \ln(1+\mathrm{e}^{-2\eta_1})\right) + 2C_F\eta_{\mathrm{cut}}\right]. \tag{C.9}$$

Starting from a $q\bar{q} \to Z$ configuration, we may also backward-evolve the quark into an initial-state gluon after emitting an anti-quark. We obtain

$$\frac{|\mathcal{M}_{g\bar{q}\bar{q}_1g_2}|^2}{|\mathcal{M}_{g\bar{q}\bar{q}_1}|^2} = \frac{\alpha_s}{2\pi}\left[\frac{C_A}{2}(g_2|\bar{q}g) + \frac{C_A}{2}(g_2|\bar{q}_1g) + (C_F - \frac{C_A}{2})(g_2|\bar{q}\bar{q}_1)\right], \tag{C.10}$$

and

$$I_{\mathrm{FC}}^{Zq_1} = \frac{\alpha_s}{2\pi}\left[C_F\left(\eta_{\mathrm{cut}} + \eta_{\mathrm{cut},f} - \ln\left(1+\mathrm{e}^{2\Delta\eta_{\bar{q}\bar{q}_1}}\right)\right)\right.$$

$$\left. + \frac{C_A}{2}\left(\eta_{\mathrm{cut}} + \ln\left(1+\mathrm{e}^{2\Delta\eta_{\bar{q}\bar{q}_1}}\right) - \ln\left(1+\mathrm{e}^{2\Delta\eta_{g\bar{q}_1}}\right)\right)\right], \tag{C.11a}$$

$$= \frac{\alpha_s}{2\pi}\left[C_F\left(\eta_{\mathrm{cut}} + \eta_{\mathrm{cut},f} - \ln\left(1+\mathrm{e}^{-2\eta_1}\right)\right) + C_A\left(\eta_{\mathrm{cut}} - \eta_1\right)\right]. \tag{C.11b}$$

Three emissions. Following the same steps as in the previous calculation, we can now consider the emission of a third parton either from a Zg_1g_2, Zg_1q_2, Zq_1g_2 or a Zq_1q_2 system. For simplicity, we take the soft and collinear limit. The integrated emissions rates are then given by

$$I_{\text{FC}}^{Zg_1g_2} = \frac{2\alpha_s}{\pi}\left[2C_F\eta_{\text{cut}} + 2C_A\eta_{\text{cut,s}}\right],\tag{C.12a}$$

$$I_{\text{FC}}^{Zg_1q_2} = \frac{2\alpha_s}{\pi}\left[C_F\left(\eta_{\text{cut}} - \eta_2 + \eta_{\text{cut,s}}\right) + C_A\left(\eta_{\text{cut}} + \eta_{\text{cut,s}} + \eta_2\right)\right],\tag{C.12b}$$

$$I_{\text{FC}}^{Zq_1g_2} = \frac{2\alpha_s}{\pi}\left[C_F\left(\eta_{\text{cut}} + \eta_1 + \eta_{\text{cut,s}}\right) + C_A\left(\eta_{\text{cut}} + \eta_{\text{cut,s}} - \eta_1\right)\right],\tag{C.12c}$$

$$I_{\text{FC}}^{Zq_1q_2} = \frac{2\alpha_s}{\pi}\left[C_F\left(2\eta_{\text{cut}} + \eta_1 - \eta_2\right) + C_A\left(2\eta_{\text{cut,s}} - \eta_1 + \eta_2\right)\right].\tag{C.12d}$$

C.2 $gg \to H$

Two emissions. For the $gg \to H$ cases we first consider the backwards splitting of a gluon into a gluon. Denoting the initial-state gluons with g_a and g_b we obtain

$$\frac{|\mathcal{M}_{g_ag_bg_1g_2}|^2}{|\mathcal{M}_{g_ag_bg_1}|^2} = \frac{\alpha_s}{2\pi}\left[\frac{C_A}{2}(g_2|g_1g_a) + \frac{C_A}{2}(g_2|g_1g_b) + \frac{C_A}{2}(g_2|g_ag_b)\right],\tag{C.13}$$

and

$$I_{\text{FC}}^{Hg_1} = \frac{\alpha_s}{2\pi}C_A\left[2\eta_{\text{cut}} + \eta_{\text{cut,s}} - \eta_1 - \ln\left(1 + e^{-2\eta_1}\right)\right].\tag{C.14}$$

The other possibility is a gluon backwards splitting to a quark, for which we obtain

$$\frac{|\mathcal{M}_{gqq_1g_2}|^2}{|\mathcal{M}_{gqq_1}|^2} = \frac{\alpha_s}{2\pi}\left[\frac{C_A}{2}(g_2|gq) + \frac{C_A}{2}(g_2|gq_1) + \left(C_F - \frac{C_A}{2}\right)(g_2|qq_1)\right],\tag{C.15}$$

and

$$I_{\text{FC}}^{Hq_1} = \frac{\alpha_s}{2\pi}\left[C_F\left(\eta_{\text{cut}} + \eta_{\text{cut,s}} - 2\eta_1 - \ln\left(1 + e^{-2\eta_1}\right)\right) + C_A\left(\eta_{\text{cut}} + \eta_1\right)\right].\tag{C.16}$$

Three emissions. Finally, we consider three emissions starting from a $gg \to H$ process. The integrated colour rates read

$$I_{\text{FC}}^{Hg_1g_2} = \frac{2\alpha_s}{\pi}\left[2C_A\left(\eta_{\text{cut}} + \eta_{\text{cut,s}}\right)\right],\tag{C.17a}$$

$$I_{\text{FC}}^{Hg_1q_2} = \frac{2\alpha_s}{\pi}\left[C_F\left(\eta_{\text{cut}} + \eta_2 + \eta_{\text{cut,s}}\right) + C_A\left(\eta_{\text{cut}} + \eta_{\text{cut,s}} - \eta_2\right)\right],\tag{C.17b}$$

$$I_{\text{FC}}^{Hq_1g_2} = \frac{2\alpha_s}{\pi}\left[C_F\left(\eta_{\text{cut}} - \eta_1 + \eta_{\text{cut,s}}\right) + C_A\left(\eta_{\text{cut}} + \eta_{\text{cut,s}} + \eta_1\right)\right],\tag{C.17c}$$

$$I_{\text{FC}}^{Hq_1q_2} = \frac{2\alpha_s}{\pi}\left[C_F\left(2\eta_{\text{cut}} + 2\eta_{\text{cut,s}} - \eta_1 + \eta_2\right) + C_A\left(\eta_1 - \eta_2\right)\right].\tag{C.17d}$$

D Deriving the branching amplitudes for spin correlations

Here we collect the branching amplitudes in terms for spinor products for initial-state splittings. The final-state expressions can be found in appendix A of ref. [45]. We first define the spinor product for two light-like momenta p_a and p_b

$$S_\lambda(p_a, p_b) = \bar{u}_\lambda(p_a)u_{-\lambda}(p_b),\tag{D.1}$$

where $\lambda = \pm 1$ is the Dirac spinor helicity. This spinor product satisfies $S_\lambda(p_a, p_b) = -S_\lambda(p_b, p_a)$. The polarisation vector of a gluon with momentum p can be written in terms of spinors by using a light-like reference vector r as

$$\epsilon_\lambda^*(p) = \frac{1}{\sqrt{2}} \frac{1}{S_{-\lambda}(r,p)} \bar{u}_\lambda(p) \gamma^\mu u_\lambda(r), \tag{D.2}$$

which obeys $\epsilon_\lambda^*(p) = -\epsilon_{-\lambda}(p)$. To perform the necessary calculations, the Chisholm identity is useful

$$\slashed{\epsilon}_\lambda^*(p) = \frac{\sqrt{2}}{S_{-\lambda}(r,p)} \left[u_\lambda(r)\bar{u}_\lambda(p) + u_{-\lambda}(p)\bar{u}_{-\lambda}(r) \right]. \tag{D.3}$$

We consider a collinear initial-state splitting with $p_i \to \tilde{p}_i + p_k$, such that $\tilde{p}_i = (1-z)p_i$ and $p_k = zp_i$ (i.e. we use the same convention as in eq. (2.2)). In this limit, any dependence of the branching amplitudes on the gauge vector r vanishes. The result can be written in terms of the single spinor product $S_\lambda(p_i, p_k)$ by using the identities

$$S_\lambda(p_i, \tilde{p}_i) = -\sqrt{\frac{z}{1-z}} S_\lambda(p_i, p_k), \quad S_\lambda(p_k, \tilde{p}_i) = -\sqrt{\frac{1}{1-z}} S_\lambda(p_i, p_k), \tag{D.4}$$

which are valid in the collinear limit. We now compute the relevant collinear branching amplitudes, stripped from any overall factors as they are not relevant in the spin correlation algorithm. The results are summarised in table 1 in section 6.1.

$q_I \to \tilde{q}_I g_F.$ The branching amplitude is

$$\mathcal{M}_{q_I(p_i) \to \tilde{q}_I(\tilde{p}_i) g_F(p_k)}^{\lambda_{\tilde{i}} \lambda_i \lambda_k} = \bar{u}_{\lambda_{\tilde{i}}}(\tilde{p}_i) \slashed{\epsilon}_{\lambda_k}^* u_{\lambda_i}(p_i) \tag{D.5}$$

$$= \frac{\sqrt{2}}{S_{-\lambda_k}(r, p_k)} \bar{u}_{\lambda_{\tilde{i}}}(\tilde{p}_i) \left[u_{\lambda_k}(r)\bar{u}_{\lambda_k}(p_k) + u_{-\lambda_k}(p_k)\bar{u}_{-\lambda_k}(r) \right] u_{\lambda_i}(p_i).$$

Recall that the order of the spin indices in the superscript differs from the order of the momenta in the subscript. The amplitude vanishes for $\lambda_{\tilde{i}} = -\lambda_i$, so we set $\lambda = \lambda_{\tilde{i}} = \lambda_i$. We find

$$\mathcal{M}_{q_I(p_i) \to \tilde{q}_I(\tilde{p}_i) g_F(p_k)}^{\lambda \lambda \lambda} = \frac{\sqrt{2}}{\sqrt{z(1-z)}} S_\lambda(p_i, p_k), \tag{D.6a}$$

$$\mathcal{M}_{q_I(p_i) \to \tilde{q}_I(\tilde{p}_i) g_F(p_k)}^{\lambda \lambda -\lambda} = \sqrt{2} \sqrt{\frac{1-z}{z}} S_{-\lambda}(p_i, p_k). \tag{D.6b}$$

$g_I \to \tilde{g}_I g_F.$ The branching amplitude reads

$$\mathcal{M}_{g_I(p_i) \to \tilde{g}_I(\tilde{p}_i) g_F(p_k)}^{\lambda_{\tilde{i}} \lambda_i, \lambda_k} = + \epsilon_{-\lambda_i}^*(p_i) \cdot \epsilon_{\lambda_k}^*(p_k)\, p_k \cdot \epsilon_{\lambda_{\tilde{i}}}^*(\tilde{p}_i) - \epsilon_{-\lambda_i}^*(p_i) \cdot \epsilon_{\lambda_{\tilde{i}}}^*(\tilde{p}_i)\, \tilde{p}_i \cdot \epsilon_{\lambda_k}^*(p_k)$$

$$- \epsilon_{\lambda_{\tilde{i}}}^*(\tilde{p}_i) \cdot \epsilon_{\lambda_k}^*(p_k)\, p_k \cdot \epsilon_{-\lambda_i}^*(p_i). \tag{D.7}$$

We take all gluons to have the same gauge vector r, in which case we find

$$\epsilon_\lambda^*(p_a) \cdot \epsilon_\lambda^*(p_b) = 0, \tag{D.8a}$$

$$\epsilon_\lambda^*(p_a) \cdot \epsilon_{-\lambda}^*(p_b) = 1, \tag{D.8b}$$

$$\epsilon_\lambda^*(p_a) \cdot p_b = \frac{1}{\sqrt{2}} \frac{S_{-\lambda}(p_b, r)}{S_{-\lambda}(r, p_a)} S_\lambda(p_a, p_b). \tag{D.8c}$$

We find that the only non-zero amplitudes are

$$\mathcal{M}^{\lambda\lambda\lambda}_{g_I(p_i)\to\tilde{g}_I(\tilde{p}_i)g_F(p_k)} = -\frac{\sqrt{2}}{\sqrt{z}(1-z)}S_\lambda(p_i,p_k)\,, \tag{D.9a}$$

$$\mathcal{M}^{\lambda\lambda-\lambda}_{g_I(p_i)\to\tilde{g}_I(\tilde{p}_i)g_F(p_k)} = -\sqrt{2}\frac{1-z}{\sqrt{z}}S_{-\lambda}(p_i,p_k)\,, \tag{D.9b}$$

$$\mathcal{M}^{\lambda-\lambda-\lambda}_{g_I(p_i)\to\tilde{g}_I(\tilde{p}_i)g_F(p_k)} = -\sqrt{2}\frac{z^{3/2}}{1-z}S_\lambda(p_i,p_k)\,. \tag{D.9c}$$

$q_I \to \tilde{g}_I q_F$. The branching amplitude is

$$\mathcal{M}^{\lambda_{\tilde{\imath}}\lambda_i\lambda_k}_{q_I(p_i)\to\tilde{g}_I(\tilde{p}_i)q_F(p_k)} = \bar{u}_{\lambda_k}(p_k)\not{\epsilon}^*_{\lambda_{\tilde{\imath}}}u_{\lambda_i}(p_i) \tag{D.10}$$

$$= \frac{\sqrt{2}}{S_{-\lambda_{\tilde{\imath}}}(r,\tilde{p}_i)}\bar{u}_{\lambda_k}(p_k)\Big[u_{\lambda_{\tilde{\imath}}}(r)\bar{u}_{\lambda_{\tilde{\imath}}}(\tilde{p}_i) + u_{-\lambda_{\tilde{\imath}}}(\tilde{p}_i)\bar{u}_{-\lambda_{\tilde{\imath}}}(r)\Big]u_{\lambda_i}(p_i).$$

Note that the polarisation vector is complex conjugated, since the gluon is in the final state in terms of the $1\to 2$ splitting. The amplitude vanishes for $\lambda_k = -\lambda_i$. Setting to $\lambda_{\tilde{\imath}} = \lambda$, we find the non-vanishing contributions

$$\mathcal{M}^{\lambda\lambda\lambda}_{q_I(p_i)\to\tilde{g}_I(\tilde{p}_i)q_F(p_k)} = -\frac{\sqrt{2}}{1-z}S_\lambda(p_i,p_k)\,, \tag{D.11a}$$

$$\mathcal{M}^{\lambda-\lambda-\lambda}_{q_I(p_i)\to\tilde{g}_I(\tilde{p}_i)q_F(p_k)} = -\sqrt{2}\frac{z}{1-z}S_\lambda(p_i,p_k)\,. \tag{D.11b}$$

$g_I \to \tilde{q}_I \bar{q}_F$. The branching amplitude reads

$$\mathcal{M}^{\lambda_{\tilde{\imath}}\lambda_i\lambda_k}_{g_I(p_i)\to\tilde{q}_I(\tilde{p}_i)\bar{q}_F(p_k)} = \bar{u}_{\lambda_{\tilde{\imath}}}(\tilde{p}_i)\not{\epsilon}_{\lambda_i}u_{-\lambda_k}(p_k) \tag{D.12}$$

$$= -\bar{u}_{\lambda_{\tilde{\imath}}}(\tilde{p}_i)\not{\epsilon}^*_{-\lambda_i}u_{-\lambda_k}(p_k)$$

$$= -\frac{\sqrt{2}}{S_{\lambda_i}(r,p_i)}\bar{u}_{\lambda_{\tilde{\imath}}}(\tilde{p}_i)\Big[u_{-\lambda_i}(r)\bar{u}_{-\lambda_i}(p_i) + u_{\lambda_i}(p_i)\bar{u}_{\lambda_i}(r)\Big]u_{-\lambda_k}(p_k).$$

Note the $-\lambda_k$, because the final state is an antiquark, and the absence of a complex conjugate on the polarisation, because it is now truly in the initial state of the splitting. The amplitude vanishes for $\lambda_{\tilde{\imath}} = \lambda_k$. We set $\lambda = \lambda_{\tilde{\imath}} = -\lambda_k$ and find the following non-vanishing amplitudes

$$\mathcal{M}^{\lambda\lambda-\lambda}_{g_I(p_i)\to\tilde{q}_I(\tilde{p}_i)\bar{q}_F(p_k)} = \sqrt{2}\sqrt{1-z}S_{-\lambda}(p_i,p_k), \tag{D.13a}$$

$$\mathcal{M}^{\lambda-\lambda-\lambda}_{g_I(p_i)\to\tilde{q}_I(\tilde{p}_i)\bar{q}_F(p_k)} = -\sqrt{2}\frac{z}{\sqrt{1-z}}S_\lambda(p_i,p_k)\,. \tag{D.13b}$$

References

[1] M. van Beekveld, S. Ferrario Ravasio, K. Hamilton, G.P. Salam, A. Soto-Ontoso, G. Soyez et al., *PanScales showers for hadron collisions: all-order validation*, *JHEP* **11** (2022) 020 [arXiv:2207.09467] [INSPIRE].

[2] G. Heinrich, *Collider Physics at the Precision Frontier*, *Phys. Rept.* **922** (2021) 1 [arXiv:2009.00516] [INSPIRE].

[3] S. Frixione and B.R. Webber, *Matching NLO QCD computations and parton shower simulations*, *JHEP* **06** (2002) 029 [hep-ph/0204244] [INSPIRE].

[4] P. Nason, *A New method for combining NLO QCD with shower Monte Carlo algorithms*, *JHEP* **11** (2004) 040 [hep-ph/0409146] [INSPIRE].

[5] S. Jadach, W. Płaczek, S. Sapeta, A. Siódmok and M. Skrzypek, *Matching NLO QCD with parton shower in Monte Carlo scheme — the KrkNLO method*, *JHEP* **10** (2015) 052 [arXiv:1503.06849] [INSPIRE].

[6] K. Hamilton, P. Nason, C. Oleari and G. Zanderighi, *Merging H/W/Z + 0 and 1 jet at NLO with no merging scale: a path to parton shower + NNLO matching*, *JHEP* **05** (2013) 082 [arXiv:1212.4504] [INSPIRE].

[7] S. Alioli, C.W. Bauer, C. Berggren, F.J. Tackmann, J.R. Walsh and S. Zuberi, *Matching Fully Differential NNLO Calculations and Parton Showers*, *JHEP* **06** (2014) 089 [arXiv:1311.0286] [INSPIRE].

[8] S. Höche, Y. Li and S. Prestel, *Higgs-boson production through gluon fusion at NNLO QCD with parton showers*, *Phys. Rev. D* **90** (2014) 054011 [arXiv:1407.3773] [INSPIRE].

[9] P.F. Monni, P. Nason, E. Re, M. Wiesemann and G. Zanderighi, *MiNNLO$_{PS}$: a new method to match NNLO QCD to parton showers*, *JHEP* **05** (2020) 143 [*Erratum ibid.* **02** (2022) 031] [arXiv:1908.06987] [INSPIRE].

[10] J.M. Campbell, S. Höche, H.T. Li, C.T. Preuss and P. Skands, *Towards NNLO+PS Matching with Sector Showers*, arXiv:2108.07133 [INSPIRE].

[11] S. Prestel, *Matching N3LO QCD calculations to parton showers*, *JHEP* **11** (2021) 041 [arXiv:2106.03206] [INSPIRE].

[12] S. Catani, F. Krauss, R. Kuhn and B.R. Webber, *QCD matrix elements + parton showers*, *JHEP* **11** (2001) 063 [hep-ph/0109231] [INSPIRE].

[13] M.L. Mangano, M. Moretti and R. Pittau, *Multijet matrix elements and shower evolution in hadronic collisions: $Wb\bar{b} + n$ jets as a case study*, *Nucl. Phys. B* **632** (2002) 343 [hep-ph/0108069] [INSPIRE].

[14] F. Krauss, *Matrix elements and parton showers in hadronic interactions*, *JHEP* **08** (2002) 015 [hep-ph/0205283] [INSPIRE].

[15] N. Lavesson and L. Lönnblad, *Extending CKKW-merging to One-Loop Matrix Elements*, *JHEP* **12** (2008) 070 [arXiv:0811.2912] [INSPIRE].

[16] S. Hoeche, F. Krauss, S. Schumann and F. Siegert, *QCD matrix elements and truncated showers*, *JHEP* **05** (2009) 053 [arXiv:0903.1219] [INSPIRE].

[17] K. Hamilton, P. Richardson and J. Tully, *A Modified CKKW matrix element merging approach to angular-ordered parton showers*, *JHEP* **11** (2009) 038 [arXiv:0905.3072] [INSPIRE].

[18] W.T. Giele, D.A. Kosower and P.Z. Skands, *Higher-Order Corrections to Timelike Jets*, *Phys. Rev. D* **84** (2011) 054003 [`arXiv:1102.2126`] [InSPIRE].

[19] S. Plätzer, *Controlling inclusive cross sections in parton shower + matrix element merging*, *JHEP* **08** (2013) 114 [`arXiv:1211.5467`] [InSPIRE].

[20] L. Lönnblad and S. Prestel, *Merging Multi-leg NLO Matrix Elements with Parton Showers*, *JHEP* **03** (2013) 166 [`arXiv:1211.7278`] [InSPIRE].

[21] R. Frederix and S. Frixione, *Merging meets matching in MC@NLO*, *JHEP* **12** (2012) 061 [`arXiv:1209.6215`] [InSPIRE].

[22] L. Lönnblad and S. Prestel, *Unitarising Matrix Element + Parton Shower merging*, *JHEP* **02** (2013) 094 [`arXiv:1211.4827`] [InSPIRE].

[23] J. Bellm, S. Gieseke and S. Plätzer, *Merging NLO Multi-jet Calculations with Improved Unitarization*, *Eur. Phys. J. C* **78** (2018) 244 [`arXiv:1705.06700`] [InSPIRE].

[24] H. Brooks and C.T. Preuss, *Efficient multi-jet merging with the Vincia sector shower*, *Comput. Phys. Commun.* **264** (2021) 107985 [`arXiv:2008.09468`].

[25] A.B. Martinez, F. Hautmann and M.L. Mangano, *TMD evolution and multi-jet merging*, *Phys. Lett. B* **822** (2021) 136700 [`arXiv:2107.01224`].

[26] T. Sjöstrand, S. Mrenna and P.Z. Skands, *PYTHIA 6.4 Physics and Manual*, *JHEP* **05** (2006) 026 [`hep-ph/0603175`] [InSPIRE].

[27] W.T. Giele, D.A. Kosower and P.Z. Skands, *A simple shower and matching algorithm*, *Phys. Rev. D* **78** (2008) 014026 [`arXiv:0707.3652`] [InSPIRE].

[28] S. Schumann and F. Krauss, *A Parton shower algorithm based on Catani-Seymour dipole factorisation*, *JHEP* **03** (2008) 038 [`arXiv:0709.1027`] [InSPIRE].

[29] S. Platzer and S. Gieseke, *Coherent Parton Showers with Local Recoils*, *JHEP* **01** (2011) 024 [`arXiv:0909.5593`] [InSPIRE].

[30] S. Höche and S. Prestel, *The midpoint between dipole and parton showers*, *Eur. Phys. J. C* **75** (2015) 461 [`arXiv:1506.05057`] [InSPIRE].

[31] B. Cabouat and T. Sjöstrand, *Some Dipole Shower Studies*, *Eur. Phys. J. C* **78** (2018) 226 [`arXiv:1710.00391`] [InSPIRE].

[32] T. Sjöstrand et al., *An introduction to PYTHIA 8.2*, *Comput. Phys. Commun.* **191** (2015) 159 [`arXiv:1410.3012`] [InSPIRE].

[33] M. Bahr et al., *HERWIG++ Physics and Manual*, *Eur. Phys. J. C* **58** (2008) 639 [`arXiv:0803.0883`] [InSPIRE].

[34] J. Bellm et al., *HERWIG 7.2 release note*, *Eur. Phys. J. C* **80** (2020) 452 [`arXiv:1912.06509`] [InSPIRE].

[35] T. Gleisberg et al., *Event generation with SHERPA 1.1*, *JHEP* **02** (2009) 007 [`arXiv:0811.4622`] [InSPIRE].

[36] SHERPA collaboration, *Event Generation with Sherpa 2.2*, *SciPost Phys.* **7** (2019) 034 [`arXiv:1905.09127`] [InSPIRE].

[37] S. Gieseke, P. Stephens and B. Webber, *New formalism for QCD parton showers*, *JHEP* **12** (2003) 045 [`hep-ph/0310083`] [InSPIRE].

[38] S. Catani, B.R. Webber and G. Marchesini, *QCD coherent branching and semiinclusive processes at large x*, *Nucl. Phys. B* **349** (1991) 635 [INSPIRE].

[39] S. Catani, L. Trentadue, G. Turnock and B.R. Webber, *Resummation of large logarithms in e^+e^- event shape distributions*, *Nucl. Phys. B* **407** (1993) 3 [INSPIRE].

[40] A. Banfi, G. Corcella and M. Dasgupta, *Angular ordering and parton showers for non-global QCD observables*, *JHEP* **03** (2007) 050 [hep-ph/0612282] [INSPIRE].

[41] M. Dasgupta and G.P. Salam, *Resummation of nonglobal QCD observables*, *Phys. Lett. B* **512** (2001) 323 [hep-ph/0104277] [INSPIRE].

[42] M. Dasgupta, F.A. Dreyer, K. Hamilton, P.F. Monni and G.P. Salam, *Logarithmic accuracy of parton showers: a fixed-order study*, *JHEP* **09** (2018) 033 [*Erratum ibid.* **03** (2020) 083] [arXiv:1805.09327] [INSPIRE].

[43] M. Dasgupta, F.A. Dreyer, K. Hamilton, P.F. Monni, G.P. Salam and G. Soyez, *Parton showers beyond leading logarithmic accuracy*, *Phys. Rev. Lett.* **125** (2020) 052002 [arXiv:2002.11114] [INSPIRE].

[44] K. Hamilton, R. Medves, G.P. Salam, L. Scyboz and G. Soyez, *Colour and logarithmic accuracy in final-state parton showers*, *JHEP* **03** (2021) 041 [arXiv:2011.10054] [INSPIRE].

[45] A. Karlberg, G.P. Salam, L. Scyboz and R. Verheyen, *Spin correlations in final-state parton showers and jet observables*, *Eur. Phys. J. C* **81** (2021) 681 [arXiv:2103.16526] [INSPIRE].

[46] K. Hamilton, A. Karlberg, G.P. Salam, L. Scyboz and R. Verheyen, *Soft spin correlations in final-state parton showers*, *JHEP* **03** (2022) 193 [arXiv:2111.01161] [INSPIRE].

[47] G. Bewick, S. Ferrario Ravasio, P. Richardson and M.H. Seymour, *Logarithmic accuracy of angular-ordered parton showers*, *JHEP* **04** (2020) 019 [arXiv:1904.11866] [INSPIRE].

[48] G. Bewick, S. Ferrario Ravasio, P. Richardson and M.H. Seymour, *Initial state radiation in the HERWIG 7 angular-ordered parton shower*, *JHEP* **01** (2022) 026 [arXiv:2107.04051] [INSPIRE].

[49] J.R. Forshaw, J. Holguin and S. Plätzer, *Building a consistent parton shower*, *JHEP* **09** (2020) 014 [arXiv:2003.06400] [INSPIRE].

[50] J. Holguin, J.R. Forshaw and S. Plätzer, *Improvements on dipole shower colour*, *Eur. Phys. J. C* **81** (2021) 364 [arXiv:2011.15087] [INSPIRE].

[51] Z. Nagy and D.E. Soper, *Summations by parton showers of large logarithms in electron-positron annihilation*, arXiv:2011.04777 [INSPIRE].

[52] G. Parisi and R. Petronzio, *Small Transverse Momentum Distributions in Hard Processes*, *Nucl. Phys. B* **154** (1979) 427 [INSPIRE].

[53] J.C. Collins, D.E. Soper and G.F. Sterman, *Transverse Momentum Distribution in Drell-Yan Pair and W and Z Boson Production*, *Nucl. Phys. B* **250** (1985) 199 [INSPIRE].

[54] Z. Nagy and D.E. Soper, *On the transverse momentum in Z-boson production in a virtuality ordered parton shower*, *JHEP* **03** (2010) 097 [arXiv:0912.4534] [INSPIRE].

[55] T. Sjöstrand, *A Model for Initial State Parton Showers*, *Phys. Lett. B* **157** (1985) 321 [INSPIRE].

[56] G. Gustafson and U. Pettersson, *Dipole Formulation of QCD Cascades*, *Nucl. Phys. B* **306** (1988) 746 [INSPIRE].

[57] S. Catani and M.H. Seymour, *A General algorithm for calculating jet cross-sections in NLO QCD*, *Nucl. Phys. B* **485** (1997) 291 [*Erratum ibid.* **510** (1998) 503] [`hep-ph/9605323`] [ɪɴSPIRE].

[58] T. Sjöstrand and P.Z. Skands, *Transverse-momentum-ordered showers and interleaved multiple interactions*, *Eur. Phys. J. C* **39** (2005) 129 [`hep-ph/0408302`] [ɪɴSPIRE].

[59] B. Jäger, A. Karlberg, S. Plätzer, J. Scheller and M. Zaro, *Parton-shower effects in Higgs production via Vector-Boson Fusion*, *Eur. Phys. J. C* **80** (2020) 756 [`arXiv:2003.12435`] [ɪɴSPIRE].

[60] S. Höche, S. Mrenna, S. Payne, C.T. Preuss and P. Skands, *A Study of QCD Radiation in VBF Higgs Production with Vincia and PYTHIA*, *SciPost Phys.* **12** (2022) 010 [`arXiv:2106.10987`] [ɪɴSPIRE].

[61] N. Fischer, S. Prestel, M. Ritzmann and P. Skands, *Vincia for Hadron Colliders*, *Eur. Phys. J. C* **76** (2016) 589 [`arXiv:1605.06142`] [ɪɴSPIRE].

[62] H. Brooks, C.T. Preuss and P. Skands, *Sector Showers for Hadron Collisions*, *JHEP* **07** (2020) 032 [`arXiv:2003.00702`] [ɪɴSPIRE].

[63] B. Andersson, G. Gustafson, L. Lönnblad and U. Pettersson, *Coherence Effects in Deep Inelastic Scattering*, *Z. Phys. C* **43** (1989) 625 [ɪɴSPIRE].

[64] E.A. Kuraev, L.N. Lipatov and V.S. Fadin, *The Pomeranchuk Singularity in Nonabelian Gauge Theories*, *Sov. Phys. JETP* **45** (1977) 199 [ɪɴSPIRE].

[65] I.I. Balitsky and L.N. Lipatov, *The Pomeranchuk Singularity in Quantum Chromodynamics*, *Sov. J. Nucl. Phys.* **28** (1978) 822 [ɪɴSPIRE].

[66] R. Kirschner and L.n. Lipatov, *Double Logarithmic Asymptotics and Regge Singularities of Quark Amplitudes with Flavor Exchange*, *Nucl. Phys. B* **213** (1983) 122 [ɪɴSPIRE].

[67] H. Jung et al., *The CCFM Monte Carlo generator CASCADE version 2.2.03*, *Eur. Phys. J. C* **70** (2010) 1237 [`arXiv:1008.0152`] [ɪɴSPIRE].

[68] S. Baranov et al., *CASCADE3 A Monte Carlo event generator based on TMDs*, *Eur. Phys. J. C* **81** (2021) 425 [`arXiv:2101.10221`] [ɪɴSPIRE].

[69] J.R. Andersen and J.M. Smillie, *Constructing All-Order Corrections to Multi-Jet Rates*, *JHEP* **01** (2010) 039 [`arXiv:0908.2786`] [ɪɴSPIRE].

[70] J.R. Andersen and J.M. Smillie, *The Factorisation of the t-channel Pole in Quark-Gluon Scattering*, *Phys. Rev. D* **81** (2010) 114021 [`arXiv:0910.5113`] [ɪɴSPIRE].

[71] J.R. Andersen and J.M. Smillie, *Multiple Jets at the LHC with High Energy Jets*, *JHEP* **06** (2011) 010 [`arXiv:1101.5394`] [ɪɴSPIRE].

[72] L. Hartgring, E. Laenen and P. Skands, *Antenna Showers with One-Loop Matrix Elements*, *JHEP* **10** (2013) 127 [`arXiv:1303.4974`] [ɪɴSPIRE].

[73] Z. Nagy and D.E. Soper, *Ordering variable for parton showers*, *JHEP* **06** (2014) 178 [`arXiv:1401.6366`] [ɪɴSPIRE].

[74] Z. Nagy and D.E. Soper, *Jets and threshold summation in Deductor*, *Phys. Rev. D* **98** (2018) 014035 [`arXiv:1711.02369`] [ɪɴSPIRE].

[75] G. Gustafson, *Multiplicity distributions in QCD cascades*, *Nucl. Phys. B* **392** (1993) 251 [ɪɴSPIRE].

[76] A. Banfi, G.P. Salam and G. Zanderighi, *Principles of general final-state resummation and automated implementation*, *JHEP* **03** (2005) 073 [hep-ph/0407286] [INSPIRE].

[77] C. Friberg, G. Gustafson and J. Hakkinen, *Color connections in e^+e^- annihilation*, *Nucl. Phys. B* **490** (1997) 289 [hep-ph/9604347] [INSPIRE].

[78] Z. Nagy and D.E. Soper, *Effects of subleading color in a parton shower*, *JHEP* **07** (2015) 119 [arXiv:1501.00778] [INSPIRE].

[79] S. Plätzer, M. Sjodahl and J. Thorén, *Color matrix element corrections for parton showers*, *JHEP* **11** (2018) 009 [arXiv:1808.00332] [INSPIRE].

[80] Z. Nagy and D.E. Soper, *Parton showers with more exact color evolution*, *Phys. Rev. D* **99** (2019) 054009 [arXiv:1902.02105] [INSPIRE].

[81] M. De Angelis, J.R. Forshaw and S. Plätzer, *Resummation and Simulation of Soft Gluon Effects beyond Leading Color*, *Phys. Rev. Lett.* **126** (2021) 112001 [arXiv:2007.09648] [INSPIRE].

[82] J.R. Forshaw, J. Holguin and S. Plätzer, *Rings and strings: a basis for understanding subleading colour and QCD coherence beyond the two-jet limit*, *JHEP* **05** (2022) 190 [arXiv:2112.13124] [INSPIRE].

[83] S. Platzer and M. Sjodahl, *Subleading N_c improved Parton Showers*, *JHEP* **07** (2012) 042 [arXiv:1201.0260] [INSPIRE].

[84] S. Höche and D. Reichelt, *Numerical resummation at subleading color in the strongly ordered soft gluon limit*, *Phys. Rev. D* **104** (2021) 034006 [arXiv:2001.11492] [INSPIRE].

[85] S. Frixione and B.R. Webber, *The role of colour flows in matrix element computations and Monte Carlo simulations*, *JHEP* **11** (2021) 045 [arXiv:2106.13471] [INSPIRE].

[86] J.R. Forshaw, A. Kyrieleis and M.H. Seymour, *Super-leading logarithms in non-global observables in QCD*, *JHEP* **08** (2006) 059 [hep-ph/0604094] [INSPIRE].

[87] S. Catani, D. de Florian and G. Rodrigo, *Space-like (versus time-like) collinear limits in QCD: Is factorization violated?*, *JHEP* **07** (2012) 026 [arXiv:1112.4405] [INSPIRE].

[88] Z. Nagy and D.E. Soper, *Exponentiating virtual imaginary contributions in a parton shower*, *Phys. Rev. D* **100** (2019) 074005 [arXiv:1908.11420] [INSPIRE].

[89] T. Becher, M. Neubert and D.Y. Shao, *Resummation of Super-Leading Logarithms*, *Phys. Rev. Lett.* **127** (2021) 212002 [arXiv:2107.01212] [INSPIRE].

[90] A. Banfi, G.P. Salam and G. Zanderighi, *Phenomenology of event shapes at hadron colliders*, *JHEP* **06** (2010) 038 [arXiv:1001.4082] [INSPIRE].

[91] J.R. Forshaw and J. Holguin, *Coulomb gluons will generally destroy coherence*, *JHEP* **12** (2021) 084 [arXiv:2109.03665] [INSPIRE].

[92] Y.L. Dokshitzer, G.D. Leder, S. Moretti and B.R. Webber, *Better jet clustering algorithms*, *JHEP* **08** (1997) 001 [hep-ph/9707323] [INSPIRE].

[93] M. Wobisch and T. Wengler, *Hadronization corrections to jet cross-sections in deep inelastic scattering*, in *Workshop on Monte Carlo Generators for HERA Physics (Plenary Starting Meeting)*, pp. 270–279, 4, 1998 [hep-ph/9907280] [INSPIRE].

[94] J.C. Collins, *Spin Correlations in Monte Carlo Event Generators*, *Nucl. Phys. B* **304** (1988) 794 [INSPIRE].

[95] I.G. Knowles, *Angular Correlations in QCD*, *Nucl. Phys. B* **304** (1988) 767 [ɪɴSPIRE].

[96] I.G. Knowles, *Spin Correlations in Parton - Parton Scattering*, *Nucl. Phys. B* **310** (1988) 571 [ɪɴSPIRE].

[97] I.G. Knowles, *A Linear Algorithm for Calculating Spin Correlations in Hadronic Collisions*, *Comput. Phys. Commun.* **58** (1990) 271 [ɪɴSPIRE].

[98] R. Kleiss and W.J. Stirling, *Spinor Techniques for Calculating $p\bar{p} \longrightarrow W+-/Z0 + Jets$*, *Nucl. Phys. B* **262** (1985) 235 [ɪɴSPIRE].

[99] M. Dinsdale, M. Ternick and S. Weinzierl, *Parton showers from the dipole formalism*, *Phys. Rev. D* **76** (2007) 094003 [arXiv:0709.1026] [ɪɴSPIRE].

[100] S. Hoeche, S. Schumann and F. Siegert, *Hard photon production and matrix-element parton-shower merging*, *Phys. Rev. D* **81** (2010) 034026 [arXiv:0912.3501] [ɪɴSPIRE].

[101] T. Carli, T. Gehrmann and S. Hoeche, *Hadronic final states in deep-inelastic scattering with Sherpa*, *Eur. Phys. J. C* **67** (2010) 73 [arXiv:0912.3715] [ɪɴSPIRE].